

ISSN 1881-7831 Online ISSN 1881-784X

DD & T

Drug Discoveries & Therapeutics

Volume 13, Number 6
December 2019



www.ddtjournal.com

DD & T

Drug Discoveries & Therapeutics



ISSN: 1881-7831
Online ISSN: 1881-784X
CODEN: DDTRBX
Issues/Year: 6
Language: English
Publisher: IACMHR Co., Ltd.

Drug Discoveries & Therapeutics is one of a series of peer-reviewed journals of the International Research and Cooperation Association for Bio & Socio-Sciences Advancement (IRCA-BSSA) Group and is published bimonthly by the International Advancement Center for Medicine & Health Research Co., Ltd. (IACMHR Co., Ltd.) and supported by the IRCA-BSSA and Shandong University China-Japan Cooperation Center for Drug Discovery & Screening (SDU-DDSC).

Drug Discoveries & Therapeutics publishes contributions in all fields of pharmaceutical and therapeutic research such as medicinal chemistry, pharmacology, pharmaceutical analysis, pharmaceuticals, pharmaceutical administration, and experimental and clinical studies of effects, mechanisms, or uses of various treatments. Studies in drug-related fields such as biology, biochemistry, physiology, microbiology, and immunology are also within the scope of this journal.

Drug Discoveries & Therapeutics publishes Original Articles, Brief Reports, Reviews, Policy Forum articles, Case Reports, News, and Letters on all aspects of the field of pharmaceutical research. All contributions should seek to promote international collaboration in pharmaceutical science.

Editorial Board

Editor-in-Chief:

Kazuhisa SEKIMIZU
Teikyo University, Tokyo, Japan

Co-Editors-in-Chief:

Xishan HAO
Tianjin Medical University, Tianjin, China
Munehiro NAKATA
Tokai University, Hiratsuka, Japan

Chief Director & Executive Editor:

Wei TANG
National Center for Global Health and Medicine, Tokyo, Japan

Senior Editors:

Guanhua DU
Chinese Academy of Medical Science and Peking Union Medical College, Beijing, China
Xiao-Kang LI
National Research Institute for Child Health and Development, Tokyo, Japan
Masahiro MURAKAMI
Osaka Ohtani University, Osaka, Japan
Yutaka ORIHARA
The University of Tokyo, Tokyo, Japan
Tomofumi SANTA
The University of Tokyo, Tokyo, Japan
Hongbin SUN
China Pharmaceutical University, Nanjing, China

Fengshan WANG
Shandong University, Ji'nan, China

Managing Editor:

Hiroshi HAMAMOTO
Teikyo University, Tokyo, Japan

Web Editor:

Yu CHEN
The University of Tokyo, Tokyo, Japan

Proofreaders:

Curtis BENTLEY
Roswell, GA, USA
Thomas R. LEBON
Los Angeles, CA, USA

Editorial and Head Office:

Pearl City Koishikawa 603,
2-4-5 Kasuga, Bunkyo-ku,
Tokyo 112-0003, Japan
Tel.: +81-3-5840-9697
Fax: +81-3-5840-9698
E-mail: office@ddtjournal.com

Drug Discoveries & Therapeutics

Editorial and Head Office

Pearl City Koishikawa 603, 2-4-5 Kasuga, Bunkyo-ku,
Tokyo 112-0003, Japan

Tel: +81-3-5840-9697, Fax: +81-3-5840-9698
E-mail: office@ddtjournal.com
URL: www.ddtjournal.com

Editorial Board Members

Alex ALMASAN <i>(Cleveland, OH)</i>	Rodney J. Y. HO <i>(Seattle, WA)</i>	Ken-ichi MAFUNE <i>(Tokyo)</i>	Quanxing WANG <i>(Shanghai)</i>
John K. BUOLAMWINI <i>(Memphis, TN)</i>	Hsing-Pang HSIEH <i>(Zhunan, Miaoli)</i>	Sridhar MANI <i>(Bronx, NY)</i>	Stephen G. WARD <i>(Bath)</i>
Jianping CAO <i>(Shanghai)</i>	Yongzhou HU <i>(Hangzhou, Zhejiang)</i>	Tohru MIZUSHIMA <i>(Tokyo)</i>	Yuhong XU <i>(Shanghai)</i>
Shousong CAO <i>(Buffalo, NY)</i>	Yu HUANG <i>(Hong Kong)</i>	Abdulla M. MOLOKHIA <i>(Alexandria)</i>	Bing YAN <i>(Ji'nan, Shandong)</i>
Jang-Yang CHANG <i>(Tainan)</i>	Amrit B. KARMARKAR <i>(Karad, Maharashtra)</i>	Yoshinobu NAKANISHI <i>(Kanazawa, Ishikawa)</i>	Chunyan YAN <i>(Guangzhou Guangdong)</i>
Fen-Er CHEN <i>(Shanghai)</i>	Toshiaki KATADA <i>(Tokyo)</i>	Siriporn OKONOGI <i>(Chiang Mai)</i>	Xiao-Long YANG <i>(Chongqing)</i>
Zhe-Sheng CHEN <i>(Queens, NY)</i>	Gagan KAUSHAL <i>(Philadelphia, PA)</i>	Weisan PAN <i>(Shenyang, Liaoning)</i>	Yun YEN <i>(Duarte, CA)</i>
Zilin CHEN <i>(Wuhan, Hubei)</i>	Ibrahim S. KHATTAB <i>(Kuwait)</i>	Chan Hum PARK <i>(Eumseong)</i>	Yasuko YOKOTA <i>(Tokyo)</i>
Xiaolan CUI <i>(Beijing)</i>	Shiroh KISHIOKA <i>(Wakayama, Wakayama)</i>	Rakesh P. PATEL <i>(Mehsana, Gujarat)</i>	Takako YOKOZAWA <i>(Toyama, Toyama)</i>
Shaofeng DUAN <i>(Lawrence, KS)</i>	Robert Kam-Ming KO <i>(Hong Kong)</i>	Shivanand P. PUTHLI <i>(Mumbai, Maharashtra)</i>	Rongmin YU <i>(Guangzhou, Guangdong)</i>
Mohamed F. EL-MILIGI <i>(6th of October City)</i>	Nobuyuki KOBAYASHI <i>(Nagasaki, Nagasaki)</i>	Shafiqur RAHMAN <i>(Brookings, SD)</i>	Guangxi ZHAI <i>(Ji'nan, Shandong)</i>
Hao FANG <i>(Ji'nan, Shandong)</i>	Norihiko KOKUDO <i>(Tokyo, Japan)</i>	Adel SAKR <i>(Cairo)</i>	Liangren ZHANG <i>(Beijing)</i>
Marcus L. FORREST <i>(Lawrence, KS)</i>	Toshiro KONISHI <i>(Tokyo)</i>	Gary K. SCHWARTZ <i>(New York, NY)</i>	Lining ZHANG <i>(Ji'nan, Shandong)</i>
Takeshi FUKUSHIMA <i>(Funabashi, Chiba)</i>	Chun-Guang LI <i>(Melbourne)</i>	Yuemao SHEN <i>(Ji'nan, Shandong)</i>	Na ZHANG <i>(Ji'nan, Shandong)</i>
Harald HAMACHER <i>(Tübingen, Baden-Württemberg)</i>	Minyong LI <i>(Ji'nan, Shandong)</i>	Brahma N. SINGH <i>(New York, NY)</i>	Ruiwen ZHANG <i>(Houston, TX)</i>
Kenji HAMASE <i>(Fukuoka, Fukuoka)</i>	Xun LI <i>(Ji'nan, Shandong)</i>	Tianqiang SONG <i>(Tianjin)</i>	Xiu-Mei ZHANG <i>(Ji'nan, Shandong)</i>
Junqing HAN <i>(Ji'nan, Shandong)</i>	Jikai LIU <i>(Wuhan, Hubei)</i>	Sanjay K. SRIVASTAVA <i>(Abilene, TX)</i>	Yongxiang ZHANG <i>(Beijing)</i>
Xiaojiang HAO <i>(Kunming, Yunnan)</i>	Xinyong LIU <i>(Ji'nan, Shandong)</i>	Chandan M. THOMAS <i>(Bradenton, FL)</i>	Jian-hua ZHU <i>(Guangzhou, Guangdong)</i>
Kiyoshi HASEGAWA <i>(Tokyo)</i>	Yuxiu LIU <i>(Nanjing, Jiangsu)</i>	Li TONG <i>(Xining, Qinghai)</i>	
Waseem HASSAN <i>(Rio de Janeiro)</i>	Hongxiang LOU <i>(Jinan, Shandong)</i>	Murat TURKOGLU <i>(Istanbul)</i>	<i>(As of February 2019)</i>
Langchong HE <i>(Xi'an, Shaanxi)</i>	Xingyuan MA <i>(Shanghai)</i>	Hui WANG <i>(Shanghai)</i>	

Original Article

- 299 - 305 **Different activities of antitumor immunomodulators to induce neutrophil adherence response.**
Motoharu Tanaka, Shigeru Abe
- 306 - 313 **Gene disruption of ribosomal protein L5 (RPL5) decreased the sensitivity of CHO-K1 cells to uncoupler carbonylcyanide-3-chlorophenylhydrazone.**
Makoto Araki, Takuya Ishibashi, Masahiro Munesue, Kazuaki Ohashi, Yoshitaka Nobukuni, Masatomo Maeda
- 314 - 321 **Inhibitions of human parainfluenza virus type 2 replication by ribavirin and mycophenolate mofetil are restored by guanosine and S-(4-nitrobenzyl)-6-thioinosine.**
Jun Uematsu, Kae Sakai-Sugino, Sahoko Kihira-Nakanishi, Hidetaka Yamamoto, Kazuyuki Hirai, Mitsuo Kawano, Miwako Nishio, Masato Tsurudome, Myles O'Brien, Hiroshi Komada
- 322 - 327 **Investigation of efficacy and safety of low-dose sodium glucose transporter 2 inhibitors and differences between two agents, canagliflozin and ipragliflozin, in patients with type 2 diabetes mellitus.**
Kaoru Sugimoto, Ichiro Abe, Midori Minezaki, Yuichi Takashi, Kentaro Ochi, Hideyuki Fujii, Hanako Ohishi, Yuka Yamao, Tadachika Kudo, Kenji Ohe, Makiko Abe, Yasushi Ohnishi, Tomohiro Shinagawa, Shigeaki Mukoubara, Kunihisa Kobayashi
- 328 - 334 **Safflower seed extract synergizes the therapeutic effect of cisplatin and reduces cisplatin-induced nephrotoxicity in human colorectal carcinoma RKO cells and RKO-transplanted mice.**
Chan Hum Park, Min Jo Kim, Chang Yeol Yang, Takako Yokozawa, Yu Su Shin
- 335 - 342 **Methanol extract of *Lonicera caerulea* var. *emphylocalyx* fruit has anti-motility and anti-biofilm activity against enteropathogenic *Escherichia coli*.**
Masaaki Minami, Hiroshi Takase, Mineo Nakamura, Toshiaki Makino
- 343 - 353 **Janus microspheres for enhanced enteral drug delivery: Preparation and orientated attachment to a Caco-2 monolayer.**
Akihiro Matsumoto, Chie Watanabe, Masahiro Murakami

Brief Report

- 354 - 359 **FADS2 and ELOVL6 mutation frequencies in Japanese Crohn's disease patients.**
Yutaro Motoi, Zensho Ito, Shizuka Suzuki, Shinichiro Takami, Kaori Matsuo, Mio Sato, Yuki Ota, Mizuki Tsuruta, Masahiro Kojima, Mitsutaka Noguchi, Kan Uchiyama, Takahiro Kubota

CONTENTS

(Continued)

- 360 - 364** **Feasibility of microbial sample collection on the skin from people in Yaoundé, Cameroonin.**
Nana C. Benderli, Kazuhiro Ogai, Yukie M. Lloyd, John Paul Arios, Boonyanudh Jiyarom, A. Honore Awanakam, Livo Forgu Esemu, Aki Hori, Rosette Megnekou, Rose G.F. Leke, Takayuki Kuraishi, Shigefumi Okamoto, Gabriel Loni Ekali

Communication

- 365 - 369** **"4+7" city drug volume-based purchasing and using pilot program in China and its impact.**
Mi Tang, Jiangjiang He, Minxing Chen, Lixuan Cong, Yuan Xu, Yan Yang, Zhiying Hou, Peipei Song, Chunlin Jin

Guide for Authors

Copyright

Different activities of antitumor immunomodulators to induce neutrophil adherence response

Motoharu Tanaka¹, Shigeru Abe^{2,3,*}

¹Department of Health and Nutrition, Faculty of Human Science, Tokiwa University, Mito, Ibaraki, Japan;

²Teikyo University Institute of Medical Mycology, Tokyo, Japan;

³Department of Sport and Medical Science, Faculty of Medical Technology, Teikyo University, Tokyo, Japan.

Summary

Functions of neutrophils, major participant in host defense mechanisms, are known to be regulated by various types of immunomodulators. Capacity of immunomodulators which are reported to show antitumor effect *in vivo* to induce neutrophil adherence response *in vitro* was investigated. Several bacterial immunomodulators (OK-432, *Corynebacterium parvum*, B.C.G.) and components of bacteria cell walls (lipopolysaccharide (LPS), lipid A, lipoteichoic acid, N-cell wall skeleton (N-CWS), muramyl dipeptide (MDP)) and fungal polysaccharides (lentinan, zymosan A, etc.) were tested. Neutrophils prepared from peripheral blood of healthy men were incubated with each immunomodulator at 37°C for 60 min in 96 well plastic plates, then neutrophils adherent to substratum were stained by crystal violet and their optical density at 570 nm was measured as a parameter of neutrophil adherence. Although purified polysaccharides mainly prepared from fungi did not induce the adherent response, not only bacterial bodies and their components but also tumor necrosis factor- α (TNF- α) clearly induced it. On the base of these results, functional classification and typing of immunomodulators by different activities in neutrophil adherence was discussed.

Keywords: Immunomodulator, neutrophil adherence, tumor necrosis factor- α , bacterial components, fungal polysaccharide

1. Introduction

Many types of immunomodulators are conceived to have antitumor activities mainly through activation of various leukocytes, such as macrophage, natural killer cells and T, and B-lymphocytes. Neutrophils have been also recognized to participate in antitumor action by bacterial immunomodulators (OK-432, etc.) and β -1,3-glucans (1-3). We reported that intraperitoneal administration of various types of antitumor immunomodulators rapidly induce neutrophils into the peritoneal cavity of mice (4). This suggested that many types of antitumor immunomodulators activate neutrophils *in vivo*. Neutrophils, responding to stimulus at the earliest phase in inflammatory cellular reaction, affect the following cellular reactions with host defence

functions.

Clarification of antitumor immunomodulators based on neutrophil activation is important to understand their antitumor action, but it has not been studied systemically. So, we examined here the capacity of immunomodulators to activate neutrophils *in vitro*.

There are many parameters of neutrophil activation, such as chemotaxis, increased adherence, release of lysosomal enzymes, production of active oxygens and so on. Here, we used a neutrophil adherence assay to measure activation of human peripheral blood neutrophils because adherence to plastic plates is reported to be a reliable method for testing phagocytotic activity of neutrophils (5,6).

2. Materials and Methods

2.1. Materials

Samples were kindly donated as follows. Recombinant-human tumor necrosis factor (rhTNF); Asahi Chemical

*Address correspondence to:

Dr. Shigeru Abe, Teikyo University Institute of Medical Mycology; 359 Otsuka, Hachioji, Tokyo 192-0395, Japan.

E-mail: sabe@main.teikyo-u.ac.jp

Ind.(Tokyo, Japan), anti-recombinant human TNF- α monoclonal antibody (anti-rhTNF antibody); Prof. D. Mizuno of Biotechnol. Res. Center, Teikyo Univ. (Kawasaki, Japan), OK-432; Chugai Pharmaceutical Ltd. (Tokyo, Japan), muramyl dipeptide (MDP) and purified mannoglucan polyalcohol (MGA); Daiichi Seiyaku Co. Ltd. (Tokyo, Japan) (currently, Daiichi-Sankyo Company, Limited, Tokyo, Japan), TAK (linear β -1,3 glucan); Takeda Chemical Industries (Tokyo, Japan), lentinan; Ajinomoto Co. (Kanagawa, Japan), lipoteicoic acid; Funakoshi (Tokyo, Japan), N-cell wall skelton (N-CWS); Fujisawa Pharm. Ind. Ltd.(Osaka, Japan) (currently, Astellas Pharma Inc. Tokyo, Japan), levamisole; Kyowa Hakko, Co. (Kanagawa, Japan) (currently, Kyowa Kirin Co., Ltd., Tokyo, Japan). Another samples were purchased as follows. *Escherichia coli* derived lipid A (lipid A); Daiichi Chemical Ltd. (Tokyo, Japan), killed *Bordetella pertussis*; Chiba Serum Institute (Chiba, Japan), killed *Corynebacterium parvum*; Ribi Immunochem. Res. Inc. (Hamilton, Mont., USA), B.C.G.; Japan B.C.G. Ind. (Tokyo, Japan), *E. coli*-lipopolysaccharide (*E.coli*-LPS); Difco Laboratories (Detroit, Mich., USA), and lambda-carrageenan, dextran sulfate, zymosan A and poly(I)-poly(C); Sigma Chemicals (St. Lous, Mo., USA). Dextran 70, Ficoll-paque solution and 96-well flat-bottom culture plates were purchased from Midori-juji Ltd. (Osaka, Japan) (currently, Mitsubishi Tanabe Pharma, Osaka, Japan), Pharmacia Fine Chemicals INC. (Uppsala, Sweden) (currently, GE Health HyClone, USA) and Falcon Ltd. (Franklin Lakes, NJ, USA), respectively.

2.2. Neutrophil preparation

Neutrophil was prepared according to the method of Yakuwa *et al.* (5). Heparinized venous blood obtained from healthy male volunteers was mixed with an equal volume of 6% dextran/saline and kept at room temperature approximately for 30 min to allow the erythrocytes to sediment. Separated plasma fraction was layered on Ficoll soln., and centrifuged at 1,400 rpm (200 \times g) for 30 min at room temperature.

Neutrophils and red blood cells sedimented at the bottom of the tube were washed with phosphate buffer saline (PBS(-)), and residual erythrocytes were lysed at first by the addition of hypotonic PBS(-) (one third of isotonic) and next by the addition of Gey's solution. The residual neutrophils were suspended with medium (10% FCS-20mM HEPES RPMI 1640).

2.3. Neutrophil adherence Assay

Assay was done in accordance with the method of Yakuwa *et al.* (5). In brief, a 10² μ L of samples (TNF for control) was placed in a well of 96 well flat bottom culture plates, and an equal volume of neutrophil

suspension (ca. 2.5 \times 10⁶ cells/mL) was added there.

After incubating at 37°C for scheduled times, non-adherent cells were removed by washing with saline. Then, each well was dried and stained with 2 \times 10² μ L of distilled water containing 0.5% crystal violet, 12% formalin and 10% ethanol solution. After washing the wells, attached cells stained with crystal violet were solubilized with 1% SDS and the absorbance of optical density at 570 nm with the use of a Titertek Multiskan MTP-100 (Thermo Fisher Scientific K.K., Tokyo, Japan) was measured.

2.4. Statistics

Each data represents the mean of 3 values. Neutrophil adherence was observed as the absorbance at 588 nm after being stained with crystal violet, and expressed as percent value of that observed with 1 U/mL of rhTNF in the same assay plate in order to compare independent experiments.

3. Results

3.1. Time course change of LPS-induced adherence

We examined the adherence inducing ability of various biological response modifiers (BRMs) preliminary, then found that rhTNF and *E.coli*-LPS have potent activity on neutrophil adherence (5,6). Concentration dependency and time course change of neutrophil adherence induced by *E.coli*-LPS and rhTNF are indicated in Figures 1 and 2, respectively. Concentration dependent adherence was observed at 1-10³ ng/mL by *E.coli*-LPS and most potent activity was seen at 60 min. On the other hand, concentration dependent adherence was observed at 10⁻¹-10² U/mL in the case of rhTNF. Adherence reached almost plateau level at 10 U/mL. One U/mL of rhTNF was used as the internal standard

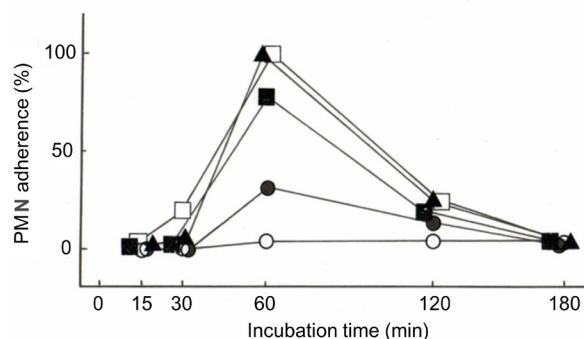


Figure 1. Time course change of neutrophil adherence to 96 well plastic plates induced by *E. coli*-LPS. Neutrophils (2.5 \times 10³ cells/well) were incubated with 1-10³ ng/mL of LPS at 37°C for several time intervals. Adherent neutrophils were stained and adherence activities were measured at O.D. 588 nm. Neutrophil adherence was expressed as % of the maximum O.D. induced by 10² U/mL of rhTNF. Each point represents the mean of 3 values. ○, control; ●, LPS 1 ng/mL; ■, LPS 10 ng/mL; ▲, LPS 10² ng/mL; □, LPS 10³ ng/mL.

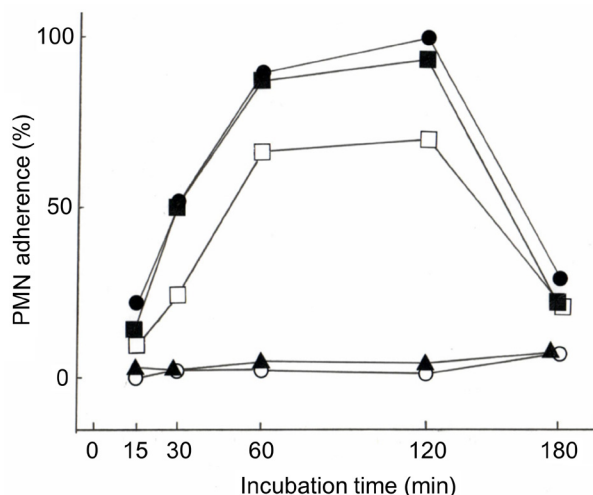


Figure 2. Time course change of neutrophil adherence to 96 well plastic plates induced by rhTNF. Neutrophil (2.5×10^5 cells/well) were incubated with 10^{-1} - 10^2 U/mL of rhTNF at 37°C for several time intervals. Adherent neutrophils were stained and adherence activities were measured at O.D. 588 nm. Neutrophil adherence was expressed as % of the maximum O.D. induced by 100 U/mL of rhTNF. Each point represents the mean of 3 values. ○, control; ▲, rhTNF 10^{-1} U/mL; □, rhTNF 1 U/mL; ■, rhTNF 10 U/mL; ●, rhTNF 10^2 U/mL.

for all the experiments, because 1 U/mL of rhTNF induced significant neutrophil adherence constantly at submaximum level in several independent experiments (data not shown) and purified TNF can be supplied. On the incubation period, although maximum effect was seen at 120 min, submaximum effect was already obtained even at 60 min at rhTNF and maximum effect was observed at 60 min for LPS. Then, we adopted 60 min for incubation period for all the plenary studies to keep the consistency throughout the experiments.

3.2. Induction of neutrophil adherence by bacteria and its components

Neutrophil adherence activity was examined for bacteria-derived BRMs which were reported to be effective for tumor models in animals (7-15). All the tested bacteria BRMs (*C. parvum*, OK-432, B.C.G.) showed neutrophil adherence activities (Figure 3A).

Adherence activities of cell wall components of bacteria were indicated in Figure 3B. LPS derived from gram-negative *E. coli* (*E. coli*-LPS) induced adherence activity in a dose dependent manner. Although the adherence response by 10^{-2} $\mu\text{g}/\text{mL}$ of LPS varied in each experiment tested, responses induced by it at more than 10^{-1} $\mu\text{g}/\text{mL}$ seems to show relatively constant values. In the following experiments, we tested the effect of several samples for 3 concentrations or more (10 fold difference in the adjacent 2 concentrations) which had been thought to be effective in *in vitro* experiments.

Lipid A, which is thought to be the active center of LPS, shows a prominent effect on neutrophil even

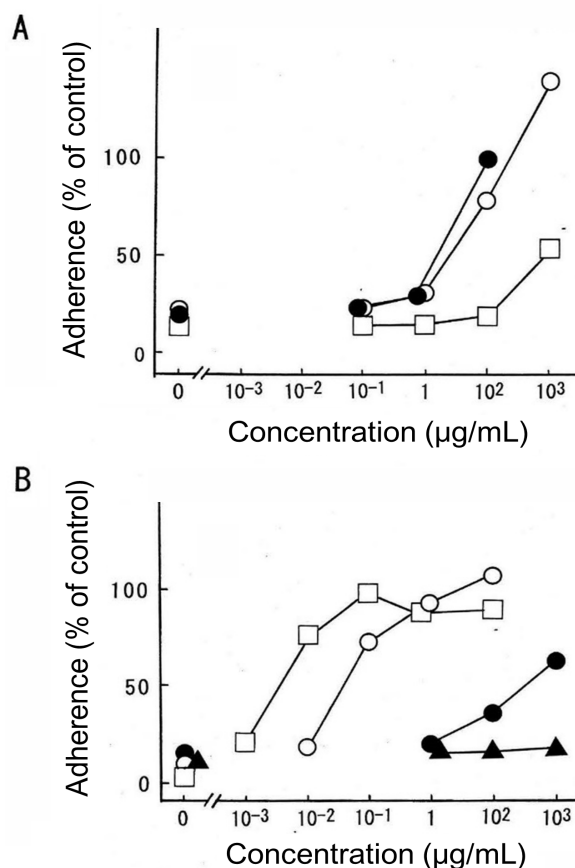


Figure 3. Neutrophil adherence activities of bacteria-BRMs (A) and cell wall components of bacteria (B). Activities was expressed as % of that of rhTNF 1 U/mL. Neutrophil (2.5×10^5 cells/well) were incubated with each sample at 37°C for 60 min. Adherent neutrophils were stained and adherence activities were measured at O.D. 588 nm. Each point represents the mean of 3 values. A: ●, *C. parvum*; ○, OK-432; □, B.C.G. B: □, lipid A; ○, *E. coli*-LPS; ●, lipoteicoic acid; ▲, MDP.

at a dose of 10^{-2} $\mu\text{g}/\text{mL}$ which is about one tenth of that of LPS. These concentrations of lipid A and LPS on adherence correspond well with that of migrating activity which is reported by Kotani *et al.* (24). Although a dose dependent increase of adherence activity was also observed in a component of gram-positive bacteria cell wall lipoteicoic acid, high concentration was necessary to show a prominent effect. Any activity was not observed in MDP even at a high dose of 10^2 $\mu\text{g}/\text{mL}$.

3.3. Effects of polysaccharides on neutrophil adherence

Neutrophil adherence activity was tested for polysaccharide-derived BRMs and some others which have been reported to be effective against tumors in animal models already (16-23) (Figure 4). Glucans such as zymosan and lentinan shows little activity even at a high dose of 10^2 $\mu\text{g}/\text{mL}$. MGA has no effect on PMN adherence also. Furthermore, TAK (linear β -1,3-glucan), which we reported to have an activating effect on neutrophil exudated in peritoneal fluid *in vitro* (1), did not induce adherence activity on neutrophil

in this condition (data not shown). Levamisole, a low molecular weight chemical immunomodulatory did not demonstrate any adherence activity.

3.4. Effect of anti-rhTNF antibody on neutrophil adherence activity

Neutrophil adherence induced by bacteria and its component might be caused by some kinds of cytokines secreted from neutrophil. In such cytokines, TNF is the most probable candidates since interleukin-1 (IL-1) and platelet activating factor (PAF), which are also

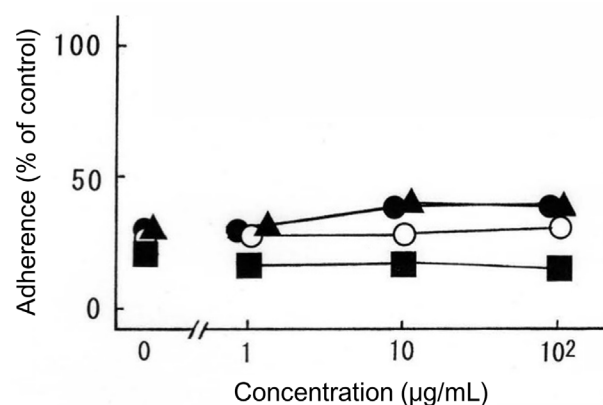


Figure 4. Neutrophil adherence activities of polysaccharide-BRMs. Activity was expressed as % of that of rhTNF 1 U/mL. Neutrophil (2.5×10^5 cells/well) were incubated with each sample at 37°C for 60 min. Adherent neutrophils were stained and adherence activities were measured at O.D. 588nm. Each point represents the mean of 3 values. ○, lentinan; ▲, C. zymosan; ■, MGA; ●, levamisole.

secreted from neutrophil when stimulated (25,26), did not show any significant adherence activities on neutrophil even at high doses (IL-1 10^3 U/mL: 18.3%, PAF 10^{-4} M: 25.5%, when compared with the activity of control), then we examined whether adherence activity of BRMs might be affected by the anti-rhTNF antibodies or not. Anti-rhTNF antibody (2×10^4 fold dilution) suppress the activity of 1 U/mL of rhTNF almost completely (2.1%, when compared with the activity of control). However, the antibody did not have any effect on the activities of 0.1 KE/mL OK-432 (without antibody: 52.5%, with antibody: 51.1%, when compared with the activity of control), 1 µg/mL *E.coli*-LPS (without antibody: 52.5%, with antibody: 51.1%, when compared with the activity of control) and 100 ng/mL lipid A (without antibody: 99.0%, with antibody: 98.2%, when compared with the activity of control). These data suggest that PMN adherence induced by bacteria-derived BRMs such as OK-432, *E. coli*-LPS and lipid A are not mediated by the TNF secreted exogenously from neutrophil.

3.5. Classification of various BRMs according to neutrophil adherence properly

General classification of BRMs according to their origin are shown in Table 1. On the right column, global classification based on the quantity of neutrophil exudate into the peritoneal cavity after injecting BRMs into mice intraperitoneally, which was reported by Morikawa *et al.* (4), is demonstrated. This data suggests that although most bacteria and cell wall components

Table 1. Summary of neutrophil adherence activities and neutrophil-inducing pattern of various BRMs

Category	BRM	Neutrophil Adherence (A)	Neutrophil induction (B) <i>In vivo</i>
Bacteria			
G (-)	<i>B pertussis</i> (7)	-	
G (+)	<i>C. parvum</i> (8)	+	++
	OK-432 (9)	+	++
	BCG (10)	+	++
Component of bacteria			
G (-)	<i>E.coli</i> -LPS (11)	+	+
	Lipid A (12)	+	
G (+)	MDP (13)	-	+
	N-CWS (14)	++	
	Lipoteicoic acid (15)	+	
Polysaccharide			
	MGA (16)	-	
	Carrageenan (17)	-	++
	Dextran sulfate (18)	-	-
	Lentinan (19)	-	++
	β-1,3glucan (20)	-	++
	Zymosan A (21)	-	++
Others			
	Levamisol (22)	-	-
	Poly(I)-poly(C) (23)	-	+

BRMs showing *in vivo* antitumor effect are categorized based on their origin, and neutrophil inductive activity *in vivo* and neutrophil adherence activity *in vitro* are indicated. G(-); gram negative, G(+); gram positive. (A) Relative activities of neutrophil adherence were classified according to their potencies. +, adherence more than 50% of that of rhTNF 1 U/mL was observed at 10^2 µg/mL, and dose dependency was observed. -, No adherence activity was observed even at 10^2 µg/mL or 10^5 cell/mL. (B) Quoted from the paper of K. Morikawa *et al.* (4). ++, Highly potent type inducing more than 6×10^6 neutrophil/mouse, +, Relatively low neutrophil-inducing type inducing less than 6×10^6 neutrophil/mouse, -, No neutrophil-inducing activity. *In vivo* antitumor activities on each BRM are shown below.

of bacteria-derived BRMs have neutrophil adherence activity, polysaccharide and another BRMs (levamisole, poly (I)-poly (C), ET-18-OMe) do not have any such property *in vitro* although induction of PMN into peritoneal cavity are observed *in vivo* (16-23).

4. Discussion

In this report, we examined direct neutrophil adherence inducing properties of various antitumor BRMs. All the BRMs tested in this study are reported to have antitumor effect *in vivo* (7-23). Adherence activities of neutrophil to plastic plates were found in *E. coli*-LPS, N-CWS, bacteria and its components such as lipid A and lipoteichoic acid. In summary, bacteria-derived BRMs have direct activating properties on neutrophil. On the other hand, antitumor polysaccharide such as lentinan, zymosan and β -1,3-glucan, which show antitumor activity, did not show adherence induction on neutrophil at all.

We reported already that all of the BRMs tested in this paper (except levamisole, dextran sulfate) induce neutrophil more than 10^6 cells/mouse into peritoneal cavity within 6 h after injection (4). These data suggest that these BRMs must have some influence on neutrophil in the body. Considering from these data and our new data that most bacteria-derived BRMs except *B. pertussis* and MDP can induce the adherence of neutrophil and polysaccharide do not effect on neutrophil adherence at all, bacteria-derived BRMs must have an effect on neutrophil directly, but another ones (polysaccharides) must accumulate neutrophil indirectly through the activation of complements or macrophage *in vivo*. For example, zymosan is well known to activate neutrophil prominently by activating complement of alternative pathway (27). However, in this system, complement system does not work, because only inactivated bovine serum was used. Lack of complement system must be the reason why zymosan did not induce neutrophil adherence.

Another different point is such BRMs that directly activate the neutrophil have local antitumor effects generally (12,28). In other words, such BRMs are effective prominently, if they are injected locally to contact with tumor tissue. On the other hand, such agents as polysaccharides and poly(I)-poly(C), which did not induce neutrophil adherence directly, are not reported to have local antitumor activity (28). This relationship suggests that local antitumor effect of bacteria-derived BRM might be connected with direct activation of neutrophil and systemic antitumor effect of polysaccharide might be connected with indirect activation of neutrophil through the activation of complements or macrophages.

If TNF producing ability of BRMs are classified into 2 groups (priming agents and triggering agents), BRMs that induce the adherence of neutrophil directly

(OK-432, LPS, lipoteichoic acid *et al.*) are known to be TNF triggering agents (29-32). On the other hand, another BRMs such as MDP, glucan and zymosan are reported to have priming activity of TNF release (30,33). Considering from these facts and the report that neutrophil can produce TNF in certain condition (34), direct induction of PMN adherence by bacteria-derived BRMs is considered to be caused by TNF released from neutrophil. Then, we tested the effect of rhTNF antibody on neutrophil adherence induced by BRMs. However, induction of neutrophil adherence by LPS, lipid A and OK-432 were not influenced at all. Then it is improbable that TNF secreted from neutrophil by BRM mediate the adherence of neutrophil.

It is reported that increased activity of neutrophil by LPS depends on the increased expression of CD11b/CD18 *via* TLR-4 (35,36). On the other hand, TLR-2 is thought to mediate responses to Gram-positive bacterial protein (37). TLR-2 as well as TLR-4 are expressed in neutrophils in addition to macrophages (38). Then, stimulated adherence by *E. coli* LPS, lipid A and OK-432 may be explained by the increased expression of CD11b/CD18 through TLR4 and the increased adherence by N-CWS and lipoteichoic acid may be mediated by TLR-2 expressed in neutrophils in addition to macrophages. As activation of TLR4 and TLR2 are reported to be tumoricidal (11,39), antitumor mechanism of bacterial BRMs may depend on the activation of TLR4 and/or TLR2 expressed in neutrophil in addition to macrophage. So far, the mechanism of antitumor effect of BRM was explained mainly through the activation of macrophage (40). However, neutrophils and macrophages are considered to coordinate in immune response in several diseases (41). Therefore, neutrophils activated by bacterial BRMs may attack tumors directly and/or indirectly in cooperation with macrophages.

In conclusion, direct activation of neutrophil may be related with the local antitumor effect of bacteria-derived BRM to some extent.

References

1. Morikawa K, Takeda R, Yamazaki M, Mizuno D. Induction of tumoricidal activity of polymorphonuclear leukocytes by a linear 1,3-glucan and other immunomodulators in murine cells. *Cancer Res.* 1985; 45:1496-1501.
2. Ikenami M, Yamazaki M. Participation of polymorphonuclear leukocyte-derived factor in murine tumour cell killing. *Br J Cancer.* 1985; 52:575-581.
3. Morikawa K, Kageyama S, Yamazaki M, Mizuno D. Hydrogen peroxide as a tumoricidal mediator of murine polymorphonuclear leukocytes induced by a linear 1,3-D-glucan and some other immunomodulators. *Cancer Res.* 1985; 45:3482-3486.
4. Morikawa M, Kikuchi Y, Abe S, Yamazaki M, Mizuno D. Early cellular responses in the peritoneal cavity of mice to anti-tumor immunomodulators. *Gan.* 1984; 75:370-378.

5. Yakuwa N, Inoue T, Watanabe T, Sendo F. A nobel neutrophil adherence test that well reflects the activating state of neutrophils. *Microbial Immunol.* 1989; 33:843-852.
6. Abe S, Ohnishi M, Kimura S, Yamazaki M, Oshima H, Mizuno D, Yamaguchi H. In: BRM activities of low-toxic *Bordetella pertussis* lipopolysaccharides. *Microbial Infect.* (H. Friedman eds.), Plenum Press, NY, 1992; pp. 69-76.
7. Ohnishi M, Kimura S, Yamazaki M, Oshima H, Mizuno D, Abe S, Yamaguchi H. Anti-tumor activity of low-toxicity lipopolysaccharide of *Bordetella pertussis*. *Br J Cancer.* 1994; 69:1038-1042.
8. Talib WH, Saleh S. Propionibacterium acnes augments antitumor, anti-angiogenesis and immunomodulatory effects of melatonin on breast cancer implanted in mice. *Plos One.* 2015; 10:e0124384.
9. Ishii Y, Yamaoka H, Toh K, Kikuchi K. Inhibition of tumor growth *in vivo* and *in vitro* by macrophages from rats treated with a streptococcal preparation, OK-432. *Gan.* 1976; 67:115-119.
10. Ruitenberg EJ, Steerenberg PA, van Noorle Jansen LM. Effect of BCG and *C. parvum* on *in vivo* Lieteria clearance and tumor growth. Comparative studies in normal and congenitally athymic (nude) mice. *Dev Biol Stand.* 1977; 38:103-107.
11. Okuyama H, Tominaga A, Fukuoka S, Taguchi T, Kusumoto Y, Ono S. Spirulina lipopolysaccharides inhibit tumor growth in a Toll-like receptor 4-dependent manner by altering the cytokine milieu from interleukin-17/interleukin-23 to interferon- γ . *Oncology Rep.* 2017; 37:684-694.
12. Martin A, Seignez C, Racoeu C, Isambert N, Mabrouk N, Scagliarini A, Reveneau S, Arnould L, Bettaieb A, Jeannin JF, Paul C. Tumor-derived granzyme B-expressing neutrophils acquire antitumor potential after lipid A treatment. *Oncotarget.* 2018; 9:28364-28378.
13. Brodt P, Blore J, Phillips NC, Munzer JS, Rioux JD. Inhibition of murine hepatic growth by liposomes containing a lipophilic muramyl dipeptides. *Cancer Immunol Immunother.* 1989; 28:54-58.
14. Inamura N, Fujitsu T, Nakahara K, Abiko M, Horii Y, Mashimoto S, Aoki H. Potentiation of tumoricidal properties of murine macrophages by *Nocardia rubra* cell wall skeleton (N-CWS). *J Antibiotics.* 1984; 37:244-252.
15. Okamoto M, Ohe G, Oshikawa T, Furuichi S, Nishikawa H, Tano T, Ahmed SU, Yoshida H, Moriya Y, Saito M, Sato M. Enhancement of anti-cancer immunity by a lipoteichoic-acid-related molecule isolated from a penicillin-killed group A *Streptococcus*. *Cancer Immunol Immunother.* 2001; 50:408-416.
16. Abe S, Takahashi K, Tsubouchi J, Aida K, Yamazaki M, Mizuno D. Different local therapeutic effects of various polysaccharides on MH134 hepatoma in mice and its relation to inflammation induced by the polysaccharides. *Gan.* 1984; 75:459-465.
17. Zhou G, Sheng W, Yao W, Wang C. Effect of low molecular λ -carrageenan from *Chondrus ocellatus* on antitumor H-22 activity of 5-Fu. *Pharmacol Res.* 2006; 53:129-134.
18. Xu Y, Huang Y, Wang J, Wang X, Wang H. Dextran sulfate inhibition on human gastric cancer cells invasion, migration and epithelial-mesenchymal transformation. *Oncology Lett.* 2018; 16:5041-5049.
19. Sasaki T, Takasuka N, Chihara G, Maeda Y. Antitumor activity of degraded products of lentinan: its correlation with molecular weight. *Gan.* 1976; 67:191-195.
20. Kasai S, Fujimoto S, Nitta K, Baba H, Kunimoto T. Antitumor activity of polymorphonuclear leukocytes activated by a beta-1,3-D-glucan. *J Pharmacobiodyn.* 1991; 14:519-525.
21. Taghavi M, Mortaz E, Khosravi A, Vahedi G, Folkerts G, Varahram M, Kazempour-Dizaji M, Garssen J, Adcock M. Zymosan attenuates melanoma growth progression, increases splenocyte proliferation and induces TLR-2/4 and TNF- α expression in mice. *J Inflamm (Lond).* 2018; 15:5.
22. Sampson D. Immunopotential and tumor inhibition with levamisole. *Cancer Treat Rep.* 1978; 62:1623-1625.
23. Hirabayashi K, Yano J, Inoue T, Yamaguchi T, Tanigawara K, Smyth GE, Ishiyama K, Ohgi T, Kimura K, Irimura T. Inhibition of cancer cell growth by polyinosinic-polycytidylic acid/cationic liposome complex: a new biological activity. *Cancer Res.* 1999; 59:4325-4333.
24. Kotani S, Takada H, Tsujimoto M. Synthetic lipid A with endotoxic and related biological activities comparable to those of a natural lipid A from an *Escherichia coli* Re-mutant. *Infect Immun.* 1985; 49:225-237.
25. Tiku K, Tiku ML, Skosey JL. Interleukin 1 production by human polymorphonuclear neutrophils. *J Immunol.* 1986; 136:3677-3685.
26. Bussolino F, Sironi M, Bocchietto E, Mantovani A. Synthesis of platelet-activating factor by polymorphonuclear neutrophils stimulated with interleukin-8. *J Biol Chem.* 1992; 267:4598-14603.
27. Oda T, Kojima Y, Akaike T, Ijiri S, Molla A, Maeda H. Inactivation of chemotactic activity of C5a by the serratal 56-kilodalton protease. *Infect Immun.* 1990; 58:1269-1272.
28. Ebina T, Murata K. Differences of antitumor effect of various BRMs by intratumoral administration. *Gan To Kagaku Ryoho.* 1992; 19:1429-1432. (*in Japanese*)
29. Yamamoto A, Nagamuta M, Usami H, Sugawara Y, Watanabe N, Niitsu Y, Urushizaki I. Release of tumor necrosis factor (TNF) into peritoneal fluids by OK-432, a streptococcal preparation. *Immunopharmacology.* 1986; 11:79-86.
30. Okutomi T, Inagawa H, Nishizawa T, Oshima H, Soma G, Mizuno D. Priming effect of orally administered muramyl dipeptide on induction of endogenous tumor necrosis factor. *J Biol Response Mod.* 1990; 9:564-569.
31. Takahashi K, Kisugi J, Gatanaga T, Yamazaki M, Mizuno D, Abe S. Induction of cytotoxic activity in sera by immunomodulators. *Yakugaku Zasshi.* 1985; 105:862-865. (*in Japanese*)
32. Majcherczyk PA, Rubli E, Heumann D, Glauser MP, Moreillon P. Teichoic acids are not required for *Streptococcus pneumoniae* and *Staphylococcus aureus* cell walls to trigger the release of tumor necrosis factor by peripheral blood monocytes. *Infect Immun.* 2003; 71:3707-3713.
33. Ohno N, Asada N, Adachi Y, Yadomae T. Enhancement of LPS triggered TNF- α (tumor necrosis factor- α) production by (1->3)- β -D-glucans in mice. *Biol Pharm Bull.* 1995; 18:126-133.
34. Finsterbusch M, Voisin MB, Beyrau M, Williams TJ, Nourshargh S. Neutrophils recruited by chemoattractants *in vivo* induce microvascular plasma protein leakage through secretion of TNF. *J Exp Med.* 2014; 211:1307-1314.
35. Zhou X, Gao XP, Fan J, Liu Q, Anwar KN, Frey RS,

- Malik AB. LPS activation of Toll-like receptor 4 signals CD11b/CD18 expression in neutrophils. *Am J Physiol Lung Cell Mol Physiol.* 2005; 288:L655-L662.
36. Maruyama N, Tansho-Nagakawa S, Miyazaki C, Shimomura K, Ono Y, Abe S. Inhibition of neutrophil adhesion and antimicrobial activity by diluted hydrosol prepared from *Rosa damascene*. *Biol Pharm Bull.* 2017; 40:161-168.
37. Calkins CM, Barsness K, Bensard DD, Vasquez-Torres A, Raeburn CD, Meng X, McIntyre RC Jr. Toll-like receptor-4 signaling mediates pulmonary neutrophil sequestration in response to gram-positive bacterial enterotoxin. *J Surg Res.* 2002; 104:124-130.
38. Bonfim C, Mamoni RL, Blotta MH. TLR-2, TLR-4 and dectin-I expression in human monocytes and neutrophils stimulated by *Paracoccidioides brasiliensis*. *Med Mycol.* 2009; 47:722-733.
39. Feng Y, Mu R, Wang Z, Xing P, Zhang J, Dong L, Wang C. A toll-like receptor agonist mimicking signal to generate tumor-suppressive macrophages. *Nat Commun.* 2019; 10:2272.
40. Brunda MJ, Sulich V, Wright RB, Palleroni AV. Tumoricidal activity and cytokine secretion by tumor-infiltrating macrophages. *Int J Cancer.* 1991; 48:704-708.
41. Prame Kumar K, Nicholls AJ, Wong CHY. Partners in crime: neutrophils and monocytes/macrophages in inflammation and disease. *Cell Tissue Res.* 2018; 371:551-565.
- (Received September 11, 2019; Revised October 26, 2019; Accepted December 22, 2019)

Gene disruption of ribosomal protein L5 (RPL5) decreased the sensitivity of CHO-K1 cells to uncoupler carbonylcyanide-3-chlorophenylhydrazone

Makoto Araki¹, Takuya Ishibashi², Masahiro Munesue^{3,§}, Kazuaki Ohashi⁴, Yoshitaka Nobukuni⁵, Masatomo Maeda^{6,*}

¹ Meiji Pharmaceutical University, Tokyo, Japan;

² Ritsumeikan-Global Innovation Research Organization, Ritsumeikan University, Kyoto, Japan;

³ Graduate School of Pharmaceutical Sciences, Osaka University, Suita, Osaka, Japan;

⁴ School of Pharmacy, Iwate Medical University, Iwate, Japan;

⁵ Research Institute for Radiation Biology and Medicine, Hiroshima University, Hiroshima, Japan;

⁶ Faculty of Pharmaceutical Sciences, Niigata University of Pharmacy and Applied Life Sciences, Niigata, Japan.

Summary

Protonophoric uncoupler carbonylcyanide-3-chlorophenylhydrazone (CCCP) decreases the proton motive force (ΔP) of the mitochondrial inner membrane and results in inhibition of oxidative phosphorylation. In this study, a CCCP-resistant clone was isolated from a random gene trap insertional mutant library of Chinese hamster ovary (CHO)-K1 cells which was constructed by infecting a retrovirus vector, ROSA β geo. Although we expected the isolation of the mutants defective in nuclear genes responsible for mitochondrial functions, the disrupted gene of the isolated mutant that we named R1 cells was identified as one of the alleles for ribosomal protein 5 of large subunit (RPL5). The R1 cells express as much as 80% RPL5 protein compared with the parental CHO-K1 cells, possibly due to enhanced transcription from a remaining wild-type RPL5 allele in R1 cells. Furthermore, the protein amount is not decreased by CCCP in R1 cells, in contrast to its clear reduction by CCCP in parental cells. Since mutations of RPL5 and other ribosomal proteins are responsible for the ribosomopathies and cancer, the present mutant may be a useful cellular model of such human diseases from a viewpoint of energy metabolism as well as a tool for the study of ribosome biogenesis and extra-ribosomal function of the RPL5 protein.

Keywords: Ribosomopathies, Diamond-Blackfan anemia, random gene trap mutagenesis, uncoupler, mitochondria

1. Introduction

Mitochondria play vital roles in aerobic energy production and homeostasis in living cells (1). The respiratory chain, through which electrons are transferred, produces an electrochemical gradient of H⁺ across the mitochondrial inner membrane. This proton motive force (ΔP) drives the synthesis of cellular energy currency, ATP, by ATP synthase (2). Furthermore, more

than 1,200 nuclear genes are believed to maintain and regulate the mitochondrial structure and function (3), although mammalian mitochondrial DNA retains 37 genes (1). Thus, it is not surprising that mitochondrial dysfunction would be induced by various mutations in both the nuclear and mitochondrial genomes (4), which results in health problems (1,3).

Uncouplers are compounds that translocate H⁺ across a membrane passively and dissipate ΔP (5). Carbonylcyanide-3-chlorophenylhydrazone (CCCP) is an example of such protonophoric uncouplers (6), and is known to be an apoptotic inducer (7). Inhibition of oxidative phosphorylation due to a decrease in ΔP would induce reactive oxygen species, and finally lead to apoptosis of the cells (8). In this study, we attempted

[§]Present Address: Santen Pharmaceutical Co., Ltd., Japan.

*Address correspondence to:

Dr. Masatomo Maeda. Laboratory of Gene Therapy, Faculty of Pharmaceutical Sciences, Niigata University of Pharmacy and Applied Life Sciences, Niigata 956-8603, Japan.
E-mail: mmaeda@nupals.ac.jp

to isolate CCCP-resistant clones of mammalian cultured cells since mutations of nuclear genes would reduce the toxic effect of CCCP. Phenotypic studies of the mutants will not only clarify gene functions but also give an idea of treatments for mitochondrial or mitochondrial-like disorders (3).

In this study, we adopted gene trap mutagenesis, a technique generating loss-of-function mutations randomly (9). We screened a random gene trap insertional mutant library of Chinese hamster ovary (CHO)-K1 cells (10) constructed by infection with the retrovirus gene trap vector ROSA β geo (11). The isolated CCCP-resistant clone exhibited haploinsufficiency of the gene for ribosomal protein 5 of large subunit (RPL5). We characterized this clone, and discussed its properties from the viewpoints of energy metabolism and roles of RPL5.

2. Materials and Methods

2.1. Cell culture

CHO-K1 cells (12) and the random gene trap insertional mutant library (10) were cultured in Ham's F-12 medium (Sigma, MO, USA) supplemented with 10% (v/v) fetal bovine serum (Biowest, Nuaille France) in a CO₂ incubator at 37°C. CCCP (Nacalai, Kyoto, Japan) dissolved in dimethyl sulfoxide (DMSO) (10 mM) was added at the indicated concentration in the medium. Control culture medium without CCCP contained a similar amount of DMSO. The cell cycle was analyzed with a Muse Cell Analyzer (Merck Millipore, MA, USA) according to the manufacturer's protocol using a Muse Cell Cycle Kit (13). The sensitivity to CCCP and colchicine (Calbiochem, CA, USA) was examined by colony formation at 37°C (14).

2.2. Identification of the disrupted gene

Total RNA of R1 cells was prepared with an RNeasy Mini Kit (Qiagen, Hilden, Germany) according to the manufacturer's protocol, and reverse transcribed with phosphorylated primer LacZr 005 and single-stranded cDNA was circularized. The product was subjected to polymerase chain reaction (PCR) with primer pairs LacZf 003/LacZr 002 and LacZf 004/LacZr 001 (Table 1) and *GoTaq*[®] (Promega, WI, USA) successively; preheating (96°C, 5 min), followed by 30 cycles of denaturation (96°C, 0.5 min), annealing (55°C, 0.5 min), and extension (72°C, 1 min), and then post-incubation (72°C, 7 min) in a GeneAmp PCR System 2400 (PerkinElmer, MA, USA). The DNA fragments separated by 2% agarose gel-electrophoresis were ligated into the pGEM-T easy vector (Promega) and then introduced into *Escherichia coli* TOP-10F'. The DNA sequence was determined by the dideoxy chain-termination method with *Ampli Taq* (Roche, Basel,

Table 1. List of PCR primers used in this study

LacZr 001:	5'-TTCCCAGTCACGACGTTGTA-3'
LacZr 002:	5'-GTGCTGCAAGGCGATTAAGT-3'
LacZf 003:	5'-GTTGATGAAAAGCTGGCTACA-3'
LacZf 004:	5'-TGATGGCGTTAACTCGGCGT-3'
LacZr 005:	5'-ATGCGCTCAGGTCAAATTC-3'
P1:	5'-GACGGTGTCTGTTCCGCAGGATG-3'
P2:	5'-GACCTTTAGCTCTCAGCAGCCCG-3'
P3:	5'-AGGAAGCGGTCAGCCCATTCG-3'
RPL5f:	5'-TGTCTGTTCCGCAGGATGGG-3'
RPL5r:	5'-CAGTTTTACCCTCTCGCCGCC-3'
actin-f:	5'-AGAGCTATGAGCTGCCTGATG-3'
actin-r:	5'-CGTGGATGCCACAGGATTC-3'
T7 primer:	5'-TAATACGACTCACTATA-3'
M13R primer:	5'-GGAAACAGCTATGACCATG-3'

Switzerland) and a sequence primer (T7 or M13R) (15). The molecular biological techniques were performed by published methods (16).

2.3. SDS-polyacrylamide gel-electrophoresis and Western blotting

Cells treated with or without 5 μ M CCCP for 24 h were collected in 1 mL (3×10^5 cells) of ice-cold 20 mM tris(hydroxymethyl)aminomethane (Tris)-HCl (pH 7.5), 150 mM NaCl, 2 mM ethylenediaminetetraacetic acid, 10 μ g/ μ L leupeptin, 10 μ g/ μ L pepstatin (TNE) containing 1% (w/v) NP-40 and then kept on ice for 30 min. After sheering of the suspension 10 times through a 25G needle, a supernatant (12,000 \times g, 30 min) was obtained. The resulting cell extract was subjected to sodium dodecyl sulfate (SDS)-polyacrylamide gel-electrophoresis (17), and then electro-blotted onto a Hybond-P PVDF membrane (GE Healthcare, IL, USA) (18).

The membrane was blocked overnight at 4°C with 10 mM sodium phosphate buffer (pH 7.2), 137 mM NaCl, 3 mM KCl (PBS) containing 0.1% (v/v) Tween-20 and 3% (w/v) skim milk (Wako, Osaka, Japan). Rabbit and mouse polyclonal antibodies recognizing human RPL5 (Abcam, Cambridge, UK) and glyceraldehyde-3-phosphate dehydrogenase (GAPDH) (Wako), respectively, were reacted for 1 h as the first antibodies [$\times 5000$ dilution in 25 mM Tris-HCl (pH 7.6), 150 mM NaCl containing 0.1% (w/w) Tween-20 (TBS-T)]. The membrane was washed in TBS-T for 5 min (3 times). Horseradish peroxidase-linked goat anti-rabbit and anti-mouse immunoglobulins ($\times 5000$ diluted) (Jackson, PA, USA) were used as the second antibodies with ECL Prime Western Blotting Detection Reagent (GE Healthcare). The RPL5 and GAPDH were visualized with a LAS-3000 (Fuji Film, Tokyo, Japan). To detect GAPDH the membrane was re-probed after analysis of RPL5 (19).

2.4. Quantitative analysis of RPL5 mRNA

Total RNA of R1 and CHO-K1 cells was reverse transcribed with a PrimeScript RT reagent kit (TaKaRa, Shiga, Japan) with a random 6 mer primer. Real time PCR was performed on an Eco Real Time PCR System (Illumina, CA, USA) and SYBR Premix Ex Taq II (TaKaRa) with primer pair RPL5f/RPL5r or β Actin-f/ β Actin-r. The data were analyzed by the $\Delta\Delta$ Ct method.

2.5. Staining of mitochondria

Cells cultured for 24 h on poly-L-lysine-coated chamber slides (Iwaki, Shizuoka, Japan) were further treated with 5 μ M CCCP or DMSO for 8 h. The treated cells were incubated for 15 min in medium containing 100 nM MitoTracker Red CMX Ros (Molecular Probes, OR, USA) and then washed with fresh medium. The cells were fixed with 4% formaldehyde. The fluorescence of fixed cells was detected under an Olympus confocal microscopy system FV1000 (IX81), the excitation and detection conditions were adjusted to the channel for AlexaFluor 568 (Invitrogen, CA, USA).

2.6. Chemicals

Restriction enzymes were purchased from NEB (MA, USA) and Toyobo (Osaka, Japan). RNaseH, T4 DNA ligase (Ligation Kit Ver.2.1), and a 5'-Full RACE Core Set were obtained from TaKaRa. Oligonucleotides were supplied by Invitrogen. A GENECLAN III Kit was obtained from BIO101 (CA, USA). All other chemicals used were of the highest grade commercially available.

3. Results

3.1. Isolation of a CCCP-resistant clone

Since more than 3 μ M CCCP inhibited the colony formation of parent CHO-K1 cells, we selected the CCCP-resistant cells in the presence of 5 μ M CCCP. Three colonies were formed from a culture of 3.4×10^7 cells after 14 days. However, only one clone showed partial resistance to CCCP and other two clones did not grow in the presence of CCCP after colony isolation. We named this clone R1, and further characterized its properties and identified a disrupted gene.

R1 cells formed colonies in the presence of 3 μ M CCCP. However, the resistance phenotype was not significant, colony formation decreasing in parallel with the wild type and not being detected under the isolation conditions (5 μ M) (Figure 1A). Interestingly, R1 cells that had been treated with 5 μ M CCCP in Figure 1A formed a significant number of colonies (as much as 700 colonies) in the fresh medium without CCCP while none grew on the plate of wild type. Thus, the R1 cells were still resistant and alive in the presence of 5 μ M

CCCP without growth although wild type CHO-K1 cells were completely killed under the same conditions.

Furthermore, as evident from Figure 1B, the R1 clone was not resistant to colchicine, suggesting that the resistance of R1 cells to CCCP could not be ascribed to the multidrug resistance phenotype (20).

3.2. Identification of a disrupted gene

We first cloned the exon moiety of the disrupted gene preceding the inserted β geo. The 5'-rapid amplification of cDNA ends technique amplified a 290 bp DNA fragment which had an upstream additional sequence, as indicated by the capital letters in the "Trapped sequence" in Figure 2A. This sequence corresponds to a component of a large 60S ribosomal subunit, RPL5, essentially identical to those of Chinese hamster, human and rodents. All the published sequence data except pROSA β geo (Figure 2A) were obtained from National Center for Biotechnology Information (<https://www.ncbi.nlm.nih.gov>, accessed September 30, 2016).

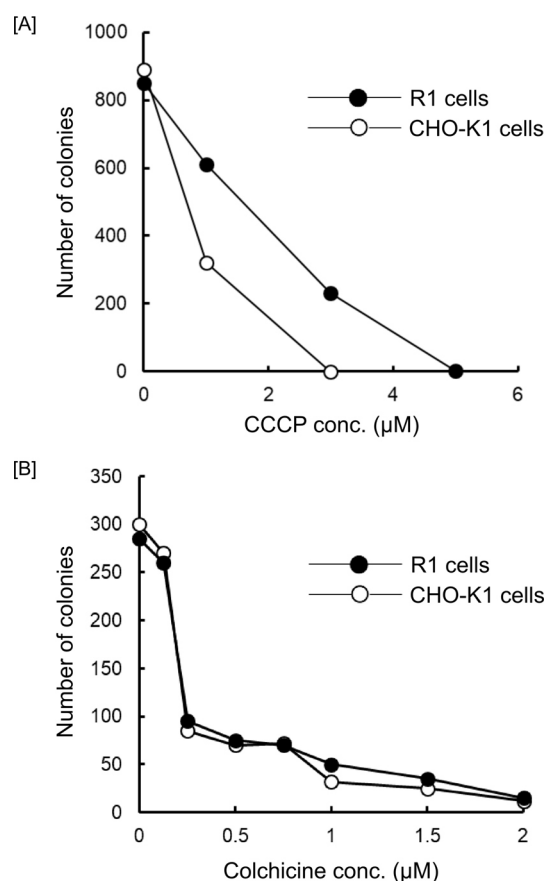


Figure 1. Colony formation of the CCCP-resistant clone in the presence of CCCP and colchicine. [A] Cells (10^4 cells) were seeded in 6 cm diameter dishes. CCCP was added on the following day. Then the cells further cultured for 9 days were stained and colonies were counted. Each point represents the mean \pm standard deviation of duplicate sample dishes. [B] Cells (2,000 cells) were seeded in each well of a 24 well-plate. Various concentrations of colchicine were added at 5 h after inoculation. On the 6th day, the cells were stained and colonies were counted.

site "ag" in the vector sequence was used (Figure 3B), consisting with the finding that a retrovirus vector tends to insert into the 5' portion of the gene (9).

3.3. Properties of R1 cells

We next determined the expression levels of RPL5 protein and mRNA under the steady state culture

conditions by Western blotting analysis and quantitative PCR, respectively. In the absence of CCCP, the amount of RPL5 protein in R1 cells was about 80% of that in the parental CHO-K1 cells in spite of that the normal *RPL5* gene in the former cells comprised one half of the latter (Figure 4A, lanes 1 and 3). Such observation could be partly explained by the increased transcription from the remaining wild-type allele (22). Actually, the mRNA

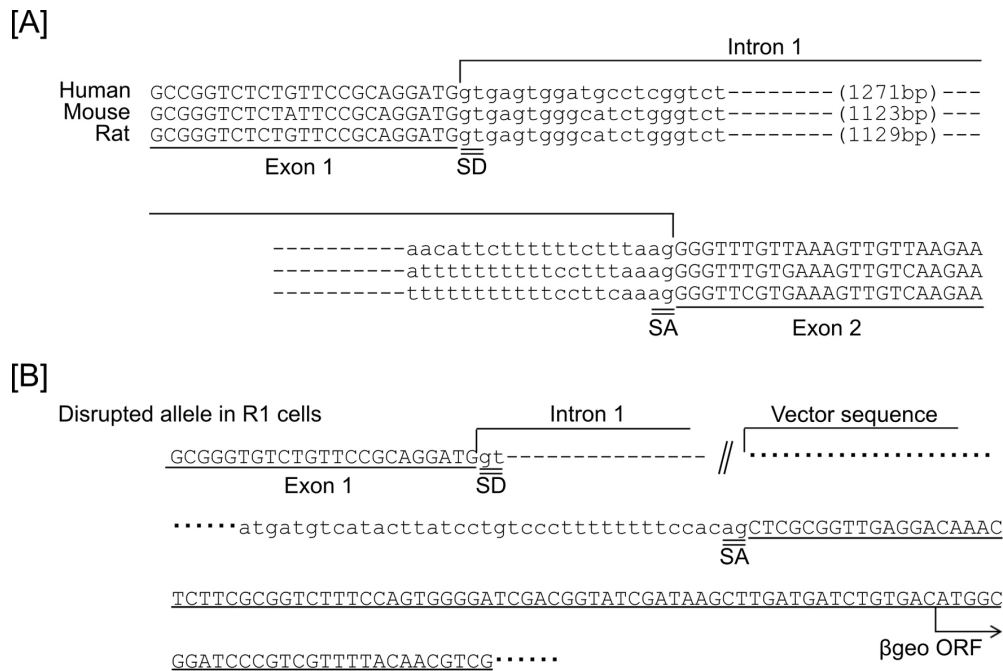


Figure 3. Comparison of the genomic sequences and splicing sites of *RPL5* of various species. [A] The nucleotide sequences of downstream of exon 1, upstream of exon 2 and both ends of intron 1 for the human (NG_011779) and rodents (NC_000071 for mouse and NC_005113 for rat) *RPL5* genes were aligned. The nucleotide residues of introns are indicated by lowercase letters. Splicing donor site "gt" and acceptor site "ag" (32) are double-underlined, and denoted by SD and SA, respectively. [B] The gene disruption event that occurred in the R1 cell is explained: the retrovirus vector was inserted into intron 1 of the *RPL5* gene. The splicing donor site (SD) of intron 1 of the *RPL5* gene and the splicing acceptor site (SA) of the *βgeo* gene in the retrovirus vector are indicated by double underlines. Canonical splicing (32) occurred during transcription of the fusion gene, and both underlined sequences in capital letters were connected, as is evident from the trapped sequence shown in Figure 2A.

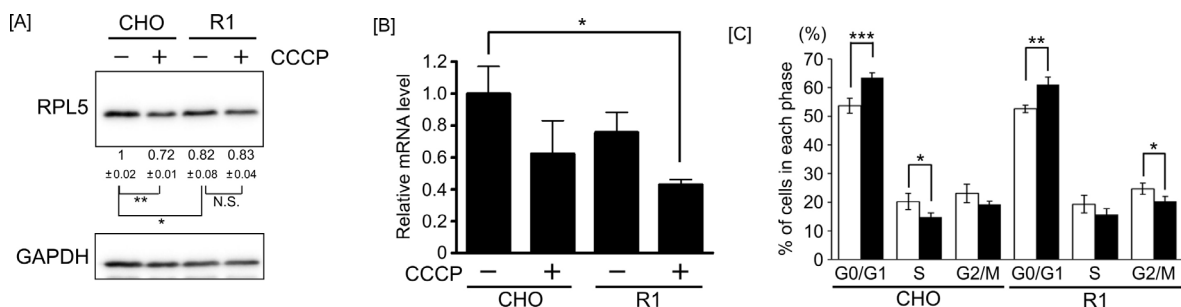


Figure 4. Expression levels of protein and mRNA for *RPL5*, and cell cycle analyses. [A] Cell lysates (15 μg) were separated by SDS-polyacrylamide gel-electrophoresis. RPL5 and GAPDH were detected by means of Western blotting with anti-RPL5 (upper) and anti-GAPDH (lower) antibodies, respectively. The numerical values at the bottom of blot are the relative amounts of RPL5 protein normalized as to those of housekeeping GAPDH protein. The standard deviations of band intensity ($n = 3$) were determined with ImageJ software [<http://imagej.nih.gov/ij/> (accessed August 20, 2019)]. The data were analyzed by means of Tukey-Kramer test. * p -values < 0.05 and ** p < 0.01 were considered statistically significant. N.S.; Not Significant. This experiment was repeated twice and a similar tendency was observed. [B] Total cellular RNA was prepared, and the mRNA expression level of RPL5 was determined by real-time PCR. The expression level was normalized as to that of β -actin mRNA. The results of triplicate samples are presented as mean values \pm standard deviation ($n = 3$). Tukey-Kramer test was performed as in [A]. * (p -values < 0.05). [C] The R1 and CHO-K1 cells that had been cultured with (closed bar) or without 5 μM CCCP (open bar) for 24 h were analyzed. The percentage of each phase in the culture was shown. Each bar represents the mean \pm standard deviation of three independent experiments. The data were analyzed by means of 2-tailed unpaired Student's t -test. * p -values < 0.05, ** p < 0.01 and *** p < 0.001 were considered statistically significant.

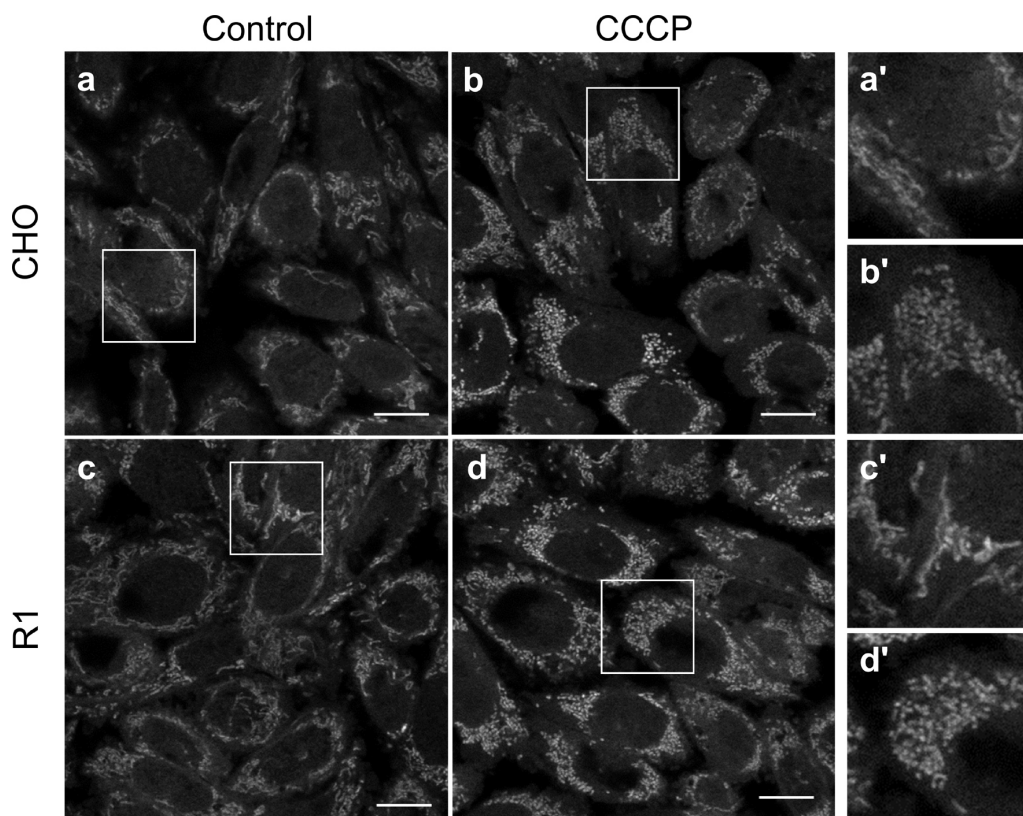


Figure 5. Morphology of mitochondria in R1 and CHO-K1 cells treated with or without CCCP. Cells cultured on poly-L-lysine-coated chamber slides for 24 h were treated with or without 5 μ M CCCP for 8 h, and then further incubated in fresh medium containing 100 nM MitoTracker Red CMX Ros without CCCP. The fluorescence of the fixed cells was observed under a confocal microscope. Magnification bars, 10 μ m. Three independent experiments gave essentially the same results. The boxed areas in a - d were enlarged (a'-d', respectively). We further examined mitochondrial images in the presence of CCCP for 24 h. However, they were indistinguishable from those with 8 h (not shown). The mitochondrial numbers in the presence of CCCP were calculated for total 135 cells in three different images from CHO-K1 and R1 cells, respectively. Although relative amounts of R1 cells were about 1.52-fold of those of CHO-K1 cells, the difference between CHO-K1 and R1 cells was not significant (p -value = 0.07).

level of R1 cells was more than half of CHO-K1 cells (Figure 4B, without CCCP), as was suggested by protein levels at steady state being primarily determined by mRNA levels (23).

The mRNA levels of both R1 and CHO-K1 cells further decreased in the presence of CCCP (Figure 4B). Concomitantly, the amount of RPL5 protein decreased in CHO-K1 cells in the presence of CCCP (Figure 4A, lanes 1 and 2). However, it remained constant in R1 cells (Figure 4A, lanes 3 and 4). It seems likely that the stability of RPL5 protein may increase in R1 cells upon adding CCCP to save energy required for transcriptional and translational processes.

Cell cycle analyses demonstrated that the distribution of cells in the G0/G1, S and G2/M phases was essentially the same between R1 and CHO-K1 cells in the presence and absence of CCCP although the presence of CCCP for 24 h slightly increased the population in G0/G1 for both cell types. Thus, the effect of CCCP on cell cycle progression was essentially the same in resistant and sensitive cells (Figure 4C).

We further observed mitochondrial images of both R1 and CHO-K1 cells in the presence of CCCP for 8 h on staining with a fluorescent organelle marker,

MitoTracker Red CMX Ros (Figure 5). Both cells without CCCP showed essentially the same filamentous mitochondrial structure (Figures 5a and 5c). In the presence of CCCP, mitochondria became shortened and vesicular (Figures 5b and 5d) as indicated by the enlarged figures (Figures 5a'-5d'). However, we could not detect significant difference between mitochondrial morphology and numbers for R1 and CHO-K1 cells in the presence of CCCP (Figure 5).

4. Discussion

The isolated R1 cells showed partial resistance to CCCP, which could be explained by that R1 cells are more resistant to a low-energy supply and survive under the energetic stress conditions in the presence of CCCP, although they would be difficult to grow under a higher concentration of CCCP due to an extremely low energy level or a toxic effect of CCCP other than uncoupling (6).

Haploinsufficiency of ribosomal proteins essential for cell growth may impair functional ribosomal biogenesis in general (24). Ribosomopathies are human disorders associated with defects of ribosomal subunit genes and ribosome biogenesis (25). A typical example

is Diamond-Blackfan anemia: about 60-70% of the patients are heterozygotes for mutations and deletions of various ribosomal subunit genes (26). Furthermore, the genes for ribosomal protein 19 of small subunit and RPL5 are most often altered (27). If we consider that RPL5 stabilizes p53 (28) and cooperatively inactivates c-Myc (29), such tumor suppressor functions of RPL5 are consistent with the finding that heterozygous inactivation of *RPL5* associates with the most common somatic ribosomal defect in human cancer (30).

Cancer cells are known to depend on the aerobic glycolysis for continued growth and survival (31). Since our culture condition is aerobic, it seems likely that such survival of R1 cells must be supported by aerobic metabolism even without mitochondrial energetic functions under oxidative stress condition. Thus, the CCCP-resistant R1 cells with a heterozygous mutation of *RPL5* will become a tool for the study of not only cellular regulatory mechanisms concerning ribosomal biogenesis and extra-ribosomal functions of the RPL5 protein but also ribosomopathies, cancer etiology and therapy.

Acknowledgements

We thank Dr. Philippe Soriano (Department of Developmental and Regenerative Biology, Icahn School of Medicine at Mt. Sinai) for kindly providing the plasmid construct, pROSA β geo.

References

- Kagawa Y, Cha SH, Hasegawa K, Hamamoto T, Endo H. Regulation of energy metabolism in human cells in aging and diabetes: FoF1, mtDNA, UCP, and ROS. *Biochem Biophys Res Commun.* 1999; 266:662-676.
- Mitchell P. Keilin's respiratory chain concept and its chemiosmotic consequences. *Science.* 1979; 206:1148-1159.
- Suomalainen A. Mitochondrial roles in disease: a box full of surprises. *EMBO Mol Med.* 2015; 7:1245-1247.
- Angelini C, Bello L, Spinazzi M, Ferrati C. Mitochondrial disorders of the nuclear genome. *Acta Myol.* 2009; 28:16-23.
- Terada H. Uncouplers of oxidative phosphorylation. *Environ Health Perspect.* 1990; 87:213-218.
- Newell KJ, Tannock IF. Reduction of intracellular pH as a possible mechanism for killing cells in acidic regions of solid tumors: effects of carbonylcyanide-3-chlorophenylhydrazone. *Cancer Res.* 1989; 49:4477-4482.
- Arena G, Gelmetti V, Torosantucci L, Vignone D, Lamorte G, De Rosa P, Cilia E, Jonas EA, Valente EM. PINK1 protects against cell death induced by mitochondrial depolarization, by phosphorylating Bcl-xL and impairing its pro-apoptotic cleavage. *Cell Death Differ.* 2013; 20:920-930.
- Wallace DC. Mitochondrial diseases in man and mouse. *Science.* 1999; 283:1482-1488.
- Stanford WL, Cohn JB, Cordes SP. Gene-trap mutagenesis: past, present and beyond. *Nature Rev Genetics.* 2001; 2:756-768.
- Nobukuni Y, Kohno K, Miyagawa K. Gene Trap mutagenesis-based forward genetic approach reveals that the tumor suppressor OVCA1 is a component of the biosynthetic pathway of diphthamide on elongation factor 2. *J Biol Chem.* 2005; 280:10572-10577.
- Friedrich G, Soriano P. Promoter traps in embryonic stem cells: a genetic screen to identify and mutate developmental genes in mice. *Genes Dev.* 1991; 5:1513-1523.
- Maeda M, Nishijima M, Akamatsu Y, Sakakibara Y. Alteration in the characters of CDP-choline synthetase and phospholipid-choline exchange enzyme upon choline starvation in Chinese hamster ovary cells. *J Biol Chem.* 1985; 260:5925-5930.
- Ushijima H, Horyozaki A, Maeda M. Anisomycin-induced GATA-6 degradation accompanying a decrease of proliferation of colorectal cancer cells. *Biochem Biophys Res Commun.* 2016; 478:481-485.
- Maeda M, Ishida A, Ni L, Kobayashi A. Isolation of CHO-K1 clones defective in cAMP-dependent proteolysis, as determined by the stability of exogenously expressed GATA-6. *Biochem Biophys Res Commun.* 2005; 329:140-146.
- Sanger F, Coulson AR, Barrell BG, Smith AJH, Roe BA. Cloning in single-stranded bacteriophage as an aid to rapid DNA sequencing. *J Mol Biol.* 1980; 143:161-178.
- Sambrook J, Fritsch EF, Maniatis T. *Molecular Cloning: A Laboratory Manual*, 2nd ed. Cold Spring Harbor Laboratory, Cold Spring Harbor. 1989.
- Laemmli UK. Cleavage of structural proteins during the assembly of the bacteriophage T4. *Nature.* 1970; 227:680-685.
- Towbin H, Staehelin T, Gordon J. Electrophoretic transfer of proteins from polyacrylamide gels to nitrocellulose sheets: procedure and some applications. *Proc Natl Acad Sci U S A.* 1979; 76:4350-4354.
- Mehra-Chaudhary R, Matsui H, Raghow R. Msx3 protein recruits deacetylase to down-regulate the Msx1 promoter. *Biochem J.* 2001; 353:13-22.
- Sharma RC, Inoue S, Roitelman J, Schimke RT, Simoni RD. Peptide transport by the multidrug resistance pump. *J Biol Chem.* 1992; 267:5731-5734.
- Kremkow BG, Baik JY, MacDonald ML, Lee KH. CHOgenome.org 2.0: Genome resources and website updates. *Biotechnol J.* 2015; 10:931-938.
- Mills EW, Green R. Ribosomopathies: There's strength in numbers. *Science.* 2017; 358:eaan2755.
- Liu Y, Beyer A, Aebersold R. On the dependency of cellular protein levels on mRNA abundance. *Cell.* 2016; 165:535-550.
- Teng T, Mercer CA, Thomas G, Fumagalli S. Loss of tumor suppressor RPL5/RPL11 does not induce cell cycle arrest but impedes proliferation due to reduced ribosome content and translation capacity. *Mol Cell Biol.* 2013; 33:4660-4671.
- Narla A, Ebert BL. Ribosomopathies: human disorders of ribosome dysfunction. *Blood.* 2010; 115:3196-3205.
- Farrar JE, Vlachos A, Atsidaftos E, Carlson-Donohoe H, Markello TC, Arceci RJ, Ellis SR, Lipton JM, Bodine DM. Ribosomal protein gene deletions in Diamond-Blackfan anemia. *Blood.* 2011; 118:6943-6951.
- Kuramitsu M, Sato-Otsubo A, Morio T, *et al.* Extensive gene deletions in Japanese patients with Diamond-Blackfan anemia. *Blood.* 2012; 119:2376-2384.

28. Sloan K, Bohnsack MT, Watkins NJ. The 5S RNP couples p53 homeostasis to ribosome biogenesis and nuclear stress. *Cell Report.* 2013; 5:237-247.
29. Liao JM, Zhou X, Gatignol A, Lu H. Ribosomal proteins L5 and L11 cooperatively inactivate c-Myc via RNA-induced silencing complex. *Oncogene.* 2015; 33:4916-4923.
30. Fancello L, Kampen KR, Hofman IJF, Verbeeck J, De Keersmaecker K. The ribosomal protein gene *RPL5* is a haploinsufficient tumor suppressor in multiple cancer types. *Oncotarget.* 2017; 8:14462-14478.
31. Vander Heiden MG, Cantley LC, Thompson CB. Understanding the Warburg effect: the metabolic requirements of cell proliferation. *Science.* 2009; 324:1029-1033.
32. Shapiro MB, Senapathy P. RNA splice junctions of different classes of eukaryotes: sequence statistics and functional implications in gene expression. *Nucl Acids Res.* 1987; 15:7155-7174.

(Received October 21, 2019; Revised December 14, 2019; Accepted December 21, 2019)

Inhibitions of human parainfluenza virus type 2 replication by ribavirin and mycophenolate mofetil are restored by guanosine and *S*-(4-nitrobenzyl)-6-thioinosine

Jun Uematsu^{1,§,*}, Kae Sakai-Sugino^{2,§,a}, Sahoko Kihira-Nakanishi^{2,§}, Hidetaka Yamamoto³, Kazuyuki Hirai³, Mitsuo Kawano⁴, Miwako Nishio⁴, Masato Tsurudome⁴, Myles O'Brien⁵, Hiroshi Komada^{1,b}

¹ Microbiology and Immunology Section, Department of Clinical Nutrition, Graduate School of Health Science, Suzuka University of Medical Science, Suzuka, Mie, Japan;

² Department of Clinical Nutrition, Faculty of Health Science, Suzuka University of Medical Science, Suzuka, Mie, Japan;

³ Faculty of Pharmaceutical Sciences, Suzuka University of Medical Science, Suzuka, Mie, Japan;

⁴ Department of Microbiology, Mie University Graduate School of Medicine, Tsu, Mie, Japan;

⁵ Graduate School of Mie Prefectural College of Nursing, Tsu, Mie, Japan.

Summary

The antiviral activities of a nucleoside analog antiviral drug (ribavirin) and a non-nucleoside drug (mycophenolate mofetil) against human parainfluenza virus type 2 (hPIV-2) were investigated, and the restoration of the inhibition by guanosine and *S*-(4-nitrobenzyl)-6-thioinosine (NBTI: equilibrative nucleoside transporter 1 inhibitor) were also investigated. Ribavirin (RBV) and mycophenolate mofetil (MMF) inhibited cell fusion induced by hPIV-2. Both RBV and MMF considerably reduced the number of viruses released from the cells. Virus genome synthesis was inhibited by RBV and MMF as determined by polymerase chain reaction (PCR) and real time PCR. mRNA syntheses were also reduced. An indirect immunofluorescence study showed that RBV and MMF largely inhibited viral protein syntheses. Using a recombinant green fluorescence protein (GFP)-expressing hPIV-2 without matrix protein (rhPIV-2ΔMGFP), it was found that virus entry into the cells and multinucleated giant cell formation were almost completely blocked by RBV and MMF. RBV and MMF did not disrupt actin microfilaments or microtubules. Both guanosine and NBTI completely or partially reversed the inhibition by RBV and MMF in the viral replication, syntheses of genome RNA, mRNA and protein, and multinucleated giant cell formation. NBTI caused a little damage in actin microfilaments, but had no effect on microtubules. Both RBV and MMF inhibited the replication of hPIV-2, mainly by inhibiting viral genome RNA, mRNA and protein syntheses. The inhibition was almost completely recovered by guanosine. These results indicate that the major mechanism of the inhibition is the depletion of intracellular GTP pools.

Keywords: Human respiratory tract pathogen, antiviral drug, mycophenolic acid, recovery of virus replication inhibition, a recombinant green fluorescence protein expressing hPIV-2 without matrix protein

1. Introduction

Human parainfluenza virus type 2 (hPIV-2) is one of the major human respiratory tract pathogens of infants and children. hPIV-2 is a member of the genus *Rubulavirus* in the family *Paramyxoviridae*, and it possesses a single-stranded, non-segmented, negative stranded RNA genome of 15,654 nucleotides (1). hPIV-2 has 7

structural proteins, NP, V, phospho (P), matrix (M), F, HN and large (L) proteins. The gene order of hPIV-2 is 3'-(leader)-NP-V/P-M-F-HN-L-(trailer)-5'. All genes of hPIV-2 were sequenced by our group (2-7). Monoclonal antibodies (mAbs) were made, and antigenic diversity of clinical isolates was investigated by Tsurudome *et al.* (8). The infectious hPIV-2 from cDNA clone was constructed by Kawano *et al.*, and it was shown that its

growth property was the same as that of control natural hPIV-2 (9).

Ribavirin (RBV) is a synthesized nucleoside analog that has broad antiviral activities against many DNA and RNA viruses. RBV was reported to be effective in the treatment of hepatitis C virus in combination with interferon (10,11), and of respiratory syncytial virus (12). It was shown that its antiviral activity *in vitro* is mediated mainly by inhibition of inosine monophosphate dehydrogenase (IMPDH) (13), inhibition of RNA-dependent RNA polymerase, and incorporation into viral RNA and induces point mutation of RNA virus, but the precise mechanism is still not fully understood. Our previous study showed that only RBV out of eight nucleoside analog antiviral drugs inhibited replication of hPIV-2 *in vitro*, but mechanism of inhibition is unclear (14). Mycophenolate mofetil (MMF) has been used as an immunosuppressive agent especially in organ transplanted patients. MMF is a nonnucleoside IMPDH inhibitor. Mycophenolic acid (MPA) is a hydrolyzed material of MMF, binds to IMPDH, induces depletion of intracellular GTP pools, and inhibits replication of some viruses such as hepatitis C virus (15) and reovirus (16).

The present investigation aimed at ascertaining the inhibitory capacity of RBV and MMF for hPIV-2 replication and, furthermore, elucidating the inhibitory mechanism of the drugs. To investigate the effects of the drugs on viral genome synthesis, virus RNA was prepared and analyzed by polymerase chain reaction (PCR) and real time PCR. To elucidate the effects of the two drugs on mRNA synthesis, cDNA was synthesized using oligo dT primer, and PCR was carried out. Virus protein expression was observed by indirect immunofluorescence study using mAbs against NP, F and HN proteins of hPIV-2 (8). The inhibitory effects of RBV and MMF on cell-to-cell spreading of hPIV-2 were analyzed using a recombinant green fluorescence protein-expressing hPIV-2 without matrix protein (rhPIV-2ΔMGFP) (9,17,18). The number of viruses released from infected cells was determined. Cytoskeleton was reported to have an important role in paramyxovirus replication. Actin microfilaments are important in the human parainfluenza virus type 3 life cycle, specifically at the level of viral transport and replication (19). Tubulin also acts as a positive

transcription factor for *in vitro* RNA synthesis by Sendai virus (20). The effects of RBV and MMF on actin microfilaments and microtubules were analyzed using rhodamine phalloidin and anti-tubulin α mAb, respectively.

2. Materials and Methods

2.1. Drugs used in this study

Antiviral drugs, RBV and mycophenolate mofetil (MMF) were purchased from Wako Chemicals (Osaka, Japan). They were dissolved at 1 mg/mL in 10 mM phosphate buffered saline, pH 7.2 (PBS), and sterilized by filtration. MMF, a prodrug of mycophenolic acid (MPA), is rapidly hydrolyzed to MPA in aqueous solution. Guanosine was from Wako Chemicals, and dissolved at 1 mg/mL in dimethyl sulfoxide, and *S*-(4-nitrobenzyl)-6-thioinosine (NBTI) also from Wako Chemicals, dissolved at 1 mg/mL in PBS and sterilized by filtration.

2.2. Virus and recombinant virus

The virus and the recombinant virus were approved by the relevant biosafety committees of Suzuka University of Medical Science. hPIV-2 (Toshiba strain) was used. rhPIV-2ΔMGFP was constructed according to the method described previously (9,17,18), and it was shown that it did not produce infectious virus particles without addition of M protein gene *in trans* (data not shown). The virus titer was determined using Vero cells and the titer was about 1×10^5 TCID₅₀/mL.

2.3. Cell line and cultivation of cells

LLCMK₂ cells (rhesus monkey kidney cell line) were cultured in a flat-bottomed 24-well plate in 1 mL culture medium. Minimum essential medium α (MEM α : Wako Chemicals), supplemented with 2% fetal calf serum (FCS) and 0.1 mg/mL kanamycin, was used. The cells were cultured at 37°C in a humidified atmosphere with 5% CO₂. After 3 days, when the cells became confluent (5×10^5 cells), the medium was changed to MEM α with 0.5% FCS and 0.1 mg/mL kanamycin. The antiviral drugs were added to the cells, and the cells were infected with hPIV-2 (3×10^2 TCID₅₀).

2.4. Cytopathogenic assay

Cell fusion was observed at 4 days post infection under cell culture microscope (Olympus, Tokyo, Japan).

2.5. RNA preparation, cDNA synthesis and real time PCR

RNA was extracted from the cells (2×10^6 cells) cultured in a flat-bottomed 6-well plate using TRIZOL

[§]These authors contributed equally to this work.

*Address correspondence to:

Dr. Jun Uematsu, Microbiology and Immunology Section, Department of Clinical Nutrition, Graduate School of Health Science, Suzuka University of Medical Science, 1001-1 Kishioka, Suzuka, Mie 510-0293, Japan.
E-mail: uematsu@suzuka-u.ac.jp

Present address:

^aDepartment of Life and Environmental Science, Tsu City College, Tsu, Mie, Japan.

^bDepartment of Microbiology, Mie University Graduate School of Medicine, Tsu, Mie, Japan.

reagent (Invitrogen, Carlsbad, CA, USA) according to the manufacturer's method. cDNA was synthesized with 1 µg RNA using Reverse Tra Ace qPCR RT Master Mix (TOYOBO, Osaka, Japan) and NP gene specific primer (nucleotide number 1661-1679: 5'-CAACATTCAATGAATCAGT-3'). Real time PCR was performed on the ABI PRISM 7700 Sequence Detection System (Life Technologies Japan, Tokyo, Japan) using TaqMan Probe (1932-1956: 5'-FAM-AAGCACCGGATTCTAACCCGTCCTG-TAMRA-3'), forward primer (1851-1875: 5'-ACACACTCATCCAG ACAAATCAAAC-3'), and reverse primer (1958-1980: 5'-TGTGGAGGTTATCTGATCACGAA-3').

2.6. Detection of messenger RNA (mRNA)

cDNA was synthesized with 1 µg RNA using oligo dT primer and superscript II reverse transcriptase (Invitrogen), and PCR was carried out with forward primers for NP (nucleotide number 1,081-1,100: 5'-CATGGCCAAGTACATGGCTC-3'), F (5,821-5,840: 5'-CCCTATCCCTGAATCACAAT-3') and HN (7,741-7,760: 5'-ATTTCCTGTATATGGTGGTC-3') genes of hPIV-2 (18), and reverse primers for NP (1,466-1,489: 5'-CCTCCGAGTATCGATTGGATTGAA-3'), F (6,661-6,681: 5'-TGTCACGAGACGTTACGGACA-3') and HN (8,481-8,500: 5'-GAACTCCCCTAAAAGAGATG-3') genes and Ex Taq (Takara Bio, Kusatsu, Japan).

2.7. Immunofluorescence study

To detect virus proteins in the infected cells, the cells were fixed with 3.7% formaldehyde solution in PBS at room temperature for 15 min. The cells were further incubated with 0.05% Tween 20 in PBS at room temperature for 15 min to detect NP protein that exists mainly in the cytoplasm, or 3 min to detect F and HN proteins that are both in the cytoplasm and in the cell membrane, washed with PBS, and incubated with mouse mAbs against NP, F and HN proteins of hPIV-2 at room temperature for 30 min. After washing with PBS, the cells were incubated with Alexa 488 conjugated secondary antibody to mouse IgGs (Invitrogen) at room temperature for 30 min, and observed under a fluorescence microscope (Olympus, Tokyo, Japan).

Actin microfilaments was detected using rhodamine phalloidin (Invitrogen) and microtubules were observed using anti-tubulin α mAb against sea urchin tubulin α (clone B-5-1-2, Sigma-Aldrich, St Louis, MO, USA) at 4 days of cultivation. The cells were fixed with 3.7% formaldehyde solution in PBS at 37°C for 15 min, washed with PBS, and the cells were further incubated with 0.05% Tween 20 in PBS at 37°C for 3 min to detect actin and for 15 min to detect microtubules.

2.8. Cell-to-cell spreading of hPIV-2

The drugs were added to the cells, and immediately after the addition, the cells were infected with rhPIV-2ΔMGFP (1×10^4 TCID₅₀), and cultured for 4 days. They were then fixed with 1.2% formaldehyde solution in PBS at room temperature for 15 min and observed under a fluorescence microscope.

3. Results

3.1. Inhibitory effects of RBV and MMF

The inhibitory effects of RBV and MMF were observed at 4 days post infection. RBV and MMF had a dose dependent inhibitory effect on cell fusion (data not shown). RBV (20 µg/mL) and MMF (2 µg/mL, 1.48 µg/mL as MPA) completely inhibited the cell fusion, indicating that lower concentration of MMF can inhibit hPIV-2 replication. The inhibitions of cell fusion by RBV and MMF were recovered with the addition of guanosine and NBTI (data not shown).

3.2. Titration of virus released from the infected cells and RBV or MMF treated cells, and restoration of the inhibitory effect by guanosine and NBTI

The titers of virus released from cells cultured with and without RBV (20 µg/mL) and MMF (2 µg/mL) at 4 days post infection were determined. Without the drugs, the virus titer was about 5×10^6 TCID₅₀/mL, and it was reduced to less than 10 TCID₅₀/mL by RBV and MMF dose dependently (data not shown), indicating that both drugs largely prevented the virus replication and the release of virus from the infected cells. However, the inhibitions were dose dependently recovered (more than 10^6 TCID₅₀/mL) by guanosine and NBTI (Figure 1). Guanosine fully recovered the inhibition by RBV (Figure 1A) and MMF (Figure 1C), and NBTI could recover the inhibition by RBV to about 10^5 TCID₅₀/mL (Figure 1B), and the inhibition by MMF only to about 10^3 TCID₅₀/mL (Figure 1D).

We carried out the restoration experiment using 20 µg/mL of RBV, 2 µg/mL of MMF, 50 µg/mL of guanosine and 70 µg/mL of NBTI. Figures 2A and 2B are the results of 5 independent experiments, showing that guanosine fully restored the inhibition by RBV and MMF, and that NBTI partially restored it.

3.3. Viral genome RNA synthesis and mRNA synthesis

RNA was prepared from the infected cells at 4 days post infection, and the viral genome RNA was analyzed by real time PCR. Figures 2C and 2D show that RBV and MMF inhibited viral genome RNA synthesis, and guanosine and NBTI almost fully restored the inhibitions by RBV and MMF. There are some discrepancies between the results of virus titers and the result of real time PCR.

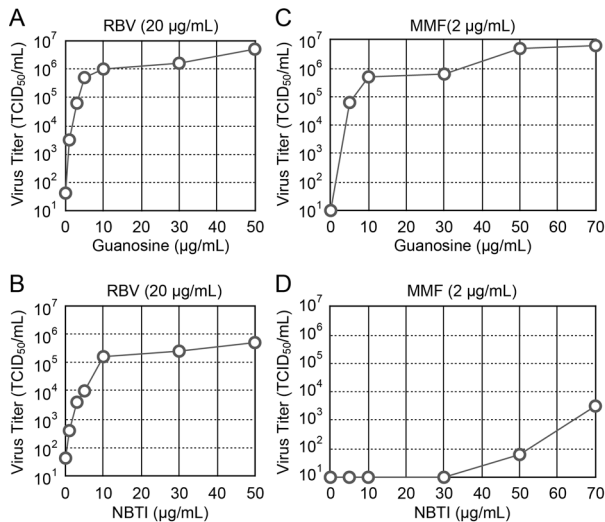


Figure 1. The inhibitions by RBV and MMF were dose dependently recovered by guanosine and NBTI. Guanosine fully recovered the inhibition by RBV and MMF (about 10^6 TCID₅₀/mL) (A and C), NBTI recovered the inhibition by RBV to about 10^5 TCID₅₀/mL (B) and the inhibition by MMF only to about 10^3 TCID₅₀/mL (D).

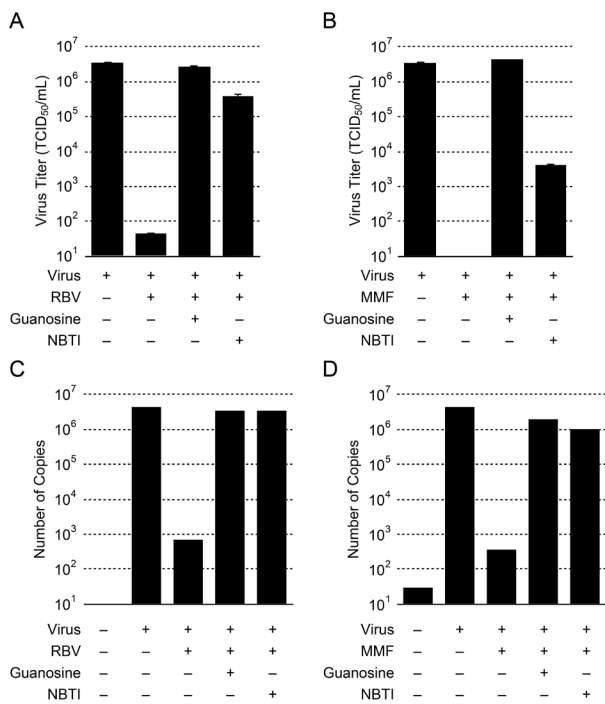


Figure 2. The results of virus titration and real time PCR. RBV and MMF inhibited virus release and viral genome RNA synthesis. Guanosine fully restored the virus release, while NBTI partially restored it (A and B). (mean \pm SEM, $n = 5$). RBV and MMF inhibited viral genome RNA syntheses, guanosine and NBTI fully recovered the inhibition by RBV and MMF (C and D).

In the following experiment, genome RNA synthesis was analyzed by PCR. PCR was carried out using hPIV-2 specific primers for NP, F and HN genes (Figures 3A and 4A). The number of base pairs between forward and reverse primers of NP, F and HN genes was about 400, 860 and 760, respectively.

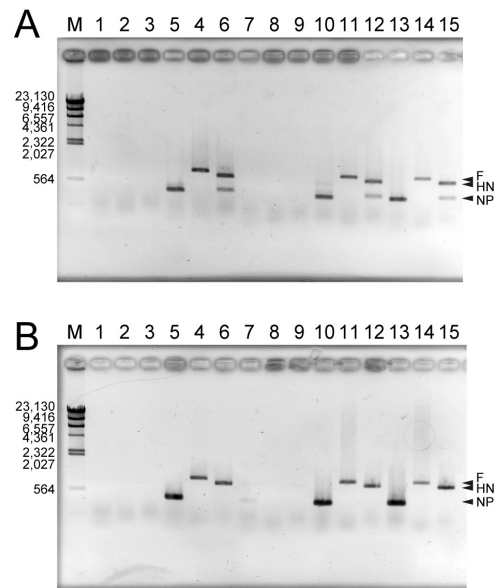


Figure 3. Inhibition of viral genome RNA and mRNA syntheses by RBV and restoration of the inhibition by guanosine and NBTI. (A) shows that NP (lane 4), F (lane 5) and HN (lane 6) gene were detected in the virus-infected cells, but not in the RBV-treated infected cells (NP: lane 7, F: lane 8 and HN: lane 9). Guanosine (NP: lane 10, F: lane 11, HN: lane 12), and NBTI (NP: lane 13, F: lane 14, HN: lane 15) restored the genome RNA syntheses. Lanes 1, 2 and 3: negative control of NP, F and HN gene, respectively. (B) shows that viral mRNA was detected in the infected cells (NP: lane 4, F: lane 5, HN: lane 6), but not in the RBV-treated cells (NP: lane 7, F: lane 8, HN: lane 9), and that the inhibition was restored by guanosine (NP: lane 10, F: lane 11, HN: lane 12) and NBTI (NP: lane 13, F: lane 14, HN: lane 15). Lane M is a size marker.

To detect mRNAs of the three viral proteins, cDNA was synthesized using oligo dT primer, and PCR was carried out using hPIV-2 specific primers for NP, F and HN genes (Figures 3B and 4B). Figure 3A shows that NP (lane 4), F (lane 5) and HN (lane 6) genome RNA were detected in the virus-infected cells, but not in the RBV-treated infected cells (NP: lane 7, F: lane 8 and HN: lane 9). Figure 3A also shows that guanosine (NP: lane 10, F: lane 11, HN: lane 12), and NBTI (NP: lane 13, F: lane 14, HN: lane 15) restored the genome RNA syntheses. Figure 3B shows that viral mRNA was detected in the infected cells, but not in RBV-treated cells, and that the inhibition was restored by guanosine and NBTI.

MMF inhibited both genome RNA and mRNA syntheses, and the inhibitions were also restored by guanosine, but not by NBTI (Figures 4A and 4B).

3.4. Viral protein synthesis

Indirect immunofluorescence study was performed to investigate the effects of the two antiviral drugs on hPIV-2 protein synthesis, and restoration by guanosine and NBTI. The drugs were added to the cells and they were infected with hPIV-2. At 4 days post infection, the cells were fixed and stained with the mAbs against NP, F and HN proteins of hPIV-2.

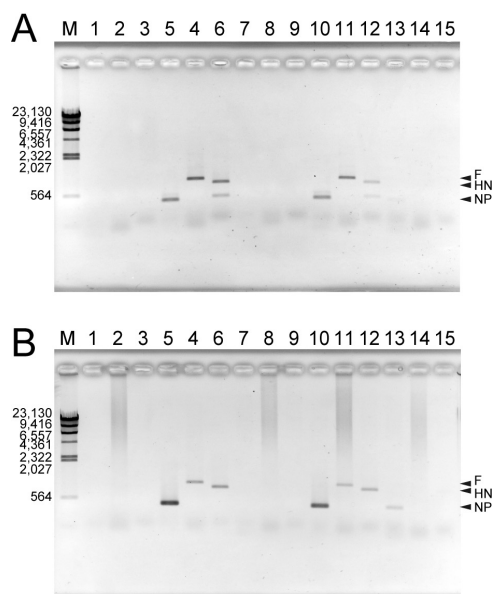


Figure 4. Inhibition of viral genome RNA and mRNA by MMF and the restoration of the inhibition by guanosine and NBTI. (A) shows that NP (lane 4), F (lane 5) and HN (lane 6) gene were detected in the virus-infected cells, but not in the MMF-treated infected cells (NP: lane 7, F: lane 8 and HN: lane 9). Guanosine restored the genome RNA syntheses (NP: lane 10, F: lane 11, HN: lane 12), but NBTI did not (NP: lane 13, F: lane 14, HN: lane 15). Lanes 1, 2 and 3: negative control of NP, F and HN gene, respectively. (B) shows that viral mRNA was detected in the infected cells (NP: lane 4, F: lane 5, HN: lane 6), but not in the MMF-treated cells (NP: lane 7, F: lane 8, HN: lane 9), and that the inhibition was restored by guanosine (NP: lane 10, F: lane 11, HN: lane 12), but not by NBTI (NP: lane 13, F: lane 14, HN: lane 15). Lane M is a size marker.

In Figure 5, Figures 5A, 5B, and 5C show the NP, F and HN protein expression in hPIV-2 infected cells, respectively. In hPIV-2 infected cells, NP, F and HN proteins were observed in almost all the cells: NP protein was observed in many strong fluorescent dots mainly in the cytoplasm, while F and HN proteins were in small dots in the cytoplasm and on the cell surface. RBV almost completely inhibited the expression of NP (Figure 5D), F (Figure 5E), and HN (Figure 5F) proteins. However, the expressions of the NP, F and HN proteins were recovered by guanosine (Figures 5G, 5H, and 5I, respectively), and by NBTI (Figures 5J, 5K, and 5L, respectively). Figures 5M to 5U show MMF also inhibited the syntheses of viral proteins (NP: Figure 5M, F: 5N, and HN: 5O). The restoration of the syntheses by guanosine (NP: Figure 5P, F: 5Q, and HN: 5R), and partial restoration by NBTI (NP: Figure 5S, F: 5T, and HN: 5U) were observed.

3.5. Cell-to-cell spreading of hPIV-2

The above results showed that RBV and MMF inhibited viral genome RNA, mRNA and protein syntheses, and the inhibitions were almost completely or partially recovered by guanosine and NBTI. In the following experiment, we determined the effect of the drugs on the cell-to-cell spreading of hPIV-2 using rhPIV-

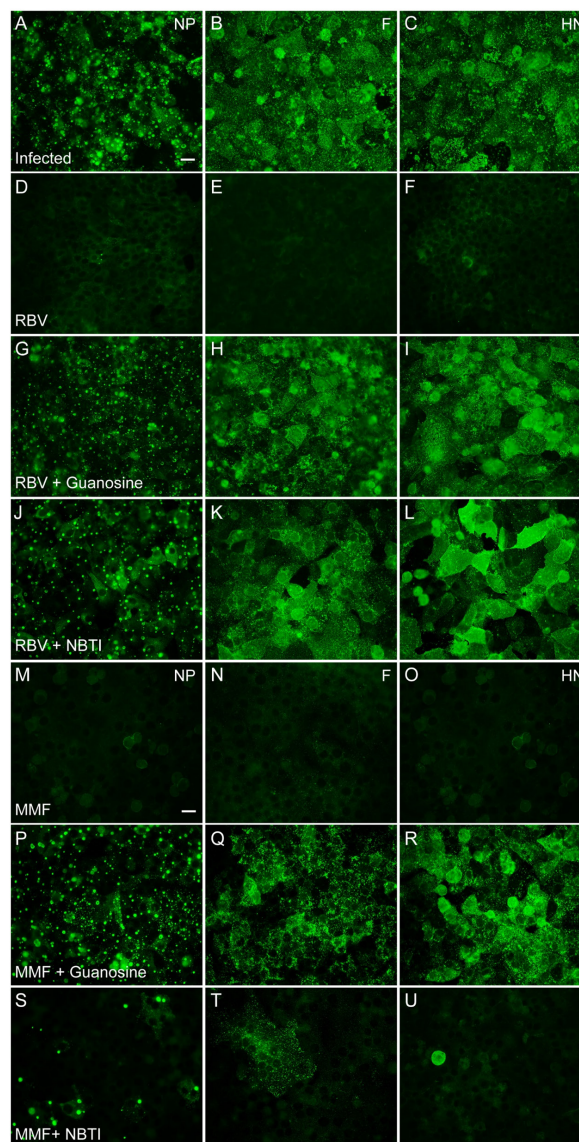


Figure 5. Protein expression in hPIV-2 infected cells, the inhibition by RBV and MMF, and the restoration by guanosine and NBTI. In hPIV-2 infected cells NP (A), F (B) and HN (C) proteins were expressed. RBV almost completely inhibited the expression of NP (D), F (E), and HN (F) proteins. However, the expressions of the NP, F and HN proteins were recovered by guanosine (G, H and I, respectively) and by NBTI (J, K and L, respectively). MMF also inhibited the syntheses of viral proteins (NP: M, F: N, and HN: O) and restoration of the syntheses by guanosine (NP: P, F: Q, and HN: R) and partial restoration by NBTI (NP: S, F: T, and HN: U). Bars in A and M: 100 μ m.

2 Δ MGFP (Figure 6).

Figure 6A is a positive control: there are multinucleated giant cells with strong fluorescence. Figures 6B, 6C, and 6D show the infected cells cultured with RBV, RBV plus guanosine, and RBV plus NBTI, respectively. In Figure 6B, RBV inhibited multinucleated giant cell formation. In Figure 6C, guanosine restored the multinucleated giant cell formation, and in the cells with RBV plus NBTI, relatively small sized fused cells with strong fluorescence were observed (Figure 6D).

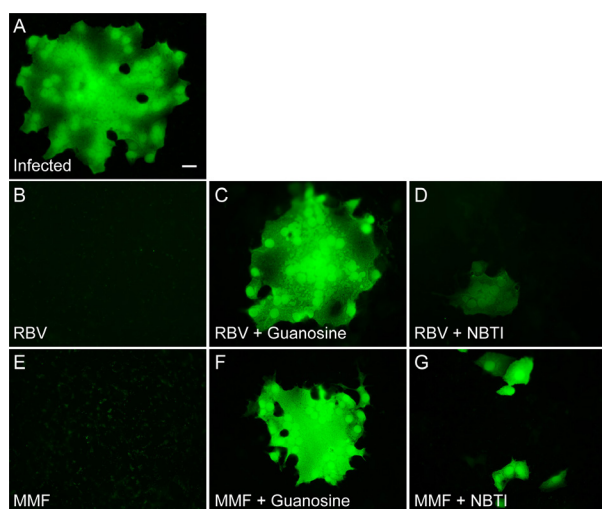


Figure 6. Inhibition of multinucleated giant cell formation by RBV and MMF, and restoration by guanosine and NBTI. (A) is the positive control. (B, C, and D) show the infected cells cultured with RBV, RBV plus guanosine, and RBV plus NBTI, respectively. Guanosine and NBTI restored giant cell formation (however, the size of fused cells restored by NBTI was relatively small). (E, F, and G) show the infected cells with MMF, MMF plus guanosine, and MMF plus NBTI, respectively. MMF also inhibited giant cell formation (E). Guanosine (F) recovered the giant cell formation. NBTI (G) could not fully recover the inhibition by MMF. Bar: 100 μ m.

Figures 6E, 6F, and 6G show the infected cells with MMF, MMF plus guanosine, and MMF plus NBTI, respectively. MMF also inhibited giant cell formation (Figure 6E). Guanosine recovered the giant cell formation but the sizes were relatively small (Figure 6F). However, NBTI could not recover the inhibition by MMF: a few fluorescent cells were observed (Figure 6G).

3.6. The effects of the drugs on actin microfilaments and microtubules

The drugs were added to the cells, and actin microfilaments and microtubules were observed under a fluorescence microscope at 4 days of cultivation without virus infection.

Figure 7A shows actin microfilaments in LLCMK₂ cells. As shown in Figures 7B and 7C, RBV and RBV plus guanosine did not disrupt actin microfilaments. However, RBV plus NBTI caused slight damage (Figure 7D). MMF (Figure 7E) and MMF plus guanosine (Figure 7F) did not cause actin microfilament damage, but MMF plus NBTI (Figure 7G) caused damage in actin microfilaments. These results indicated that one of the causes of the partial restoration by NBTI was due to the actin microfilament damage.

Figure 8A shows microtubules in the cells. As shown in Figures 8B, 8C and 8D, respectively, RBV, RBV plus guanosine, and RBV plus NBTI, did not induce damage in microtubules. MMF (Figure 8F), MMF plus guanosine (Figure 8F), and MMF plus NBTI (Figure 8G) also caused no damage.

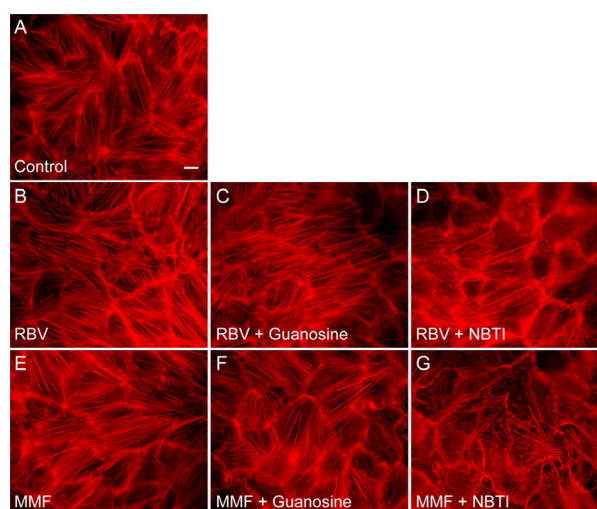


Figure 7. The effects of RBV and MMF on actin microfilaments. (A) is the positive control. (B and C) show that RBV and RBV plus guanosine did not disrupt actin microfilaments. However, RBV plus NBTI caused slight damage (D). Similar results were obtained in MMF (E-G). MMF (E) and MMF plus guanosine (F) did not cause actin microfilament damage, but MMF plus NBTI caused damage in actin microfilaments (G). Bar: 100 μ m.

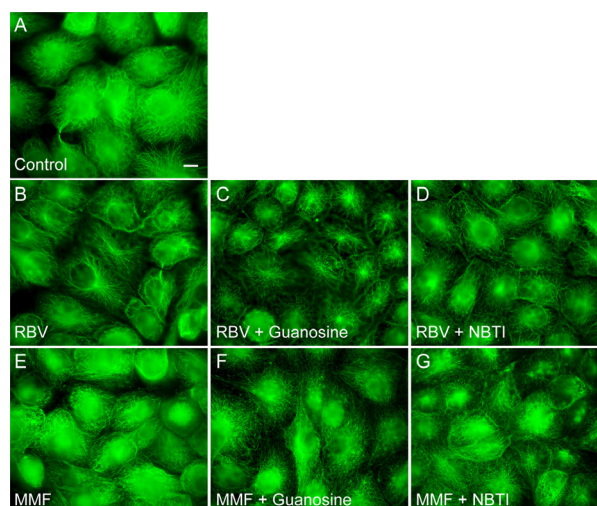


Figure 8. No inhibitory effect of RBV, MMF, guanosine and NBTI on microtubules. (A) is the positive control. (B, C and D) show RBV, RBV plus guanosine, and RBV plus NBTI, respectively. (E, F and G) show MMF, MMF plus guanosine and MMF plus NBTI, respectively. Bar: 100 μ m.

4. Discussion

The present study showed that RBV and MMF had inhibitory effects on hPIV-2 replication in LLCMK₂ cells and that the inhibition was restored by guanosine or NBTI. Almost no virus was found in the culture medium of RBV- or MMF-treated cells infected with hPIV-2. Viral genome RNA and mRNA were not detected in the RBV- or MMF-treated infected cells. In addition, viral proteins were not observed in the drug-treated infected cells. Using rhPIV-2 Δ MGFP, it was shown that both RBV and MMF completely inhibited

multinucleated giant cell formation. The inhibitory effects of RBV and MMF were not due to the disruption of actin microfilaments or microtubules. Guanosine and NBTI almost fully restored the inhibition of genome RNA, mRNA and protein syntheses by the two drugs. Multinucleated giant cell formation was also restored by guanosine or NBTI. However, guanosine is more effective than NBTI, one reason being that NBTI caused some damage in actin microfilaments. The discrepancy between the result of virus titer and the result of real time PCR were in part due to a little disruption of actin microfilaments, resulting in the partial inhibition of virus budding.

RBV is a synthesized nucleoside analog that has broad antiviral activities against many RNA viruses. RBV has been reported to be effective in the treatments of hepatitis C virus in combination with interferon (10,11), of respiratory syncytial virus (12) and of Lassa fever virus (21), yellow fever virus (22), Andes virus (23), flaviviruses and paramyxoviruses (13). Shah *et al.* examined the ability of RBV against vesicular stomatitis virus and Sendai virus using different cell types, and they found RBV exhibited its inhibitory action only on the cells that could uptake RBV (24). Upon uptake, RBV is phosphorylated into mono-, di- and tri-phosphate by cellular kinases. Several mechanisms are proposed (13,21,24), but the mechanism of RBV action on the viruses is still not fully elucidated. RBV inhibits the host enzyme inosine monophosphate dehydrogenase (IMPDH) essential for the *de novo* synthesis of GTP. Phosphorylated RBV directly inhibits viral RNA polymerase. RNA chain elongation is terminated by the incorporation of ribavirin tri-phosphate into viral RNA. Ribavirin tri-phosphate incorporation as a substitute for guanosine or adenosine leads to lethal mutagenesis. In this experiment, a sufficient amount of guanosine might competitively block RBV tri-phosphate incorporation into viral RNA, resulting the restoration from the inhibition. NBTI (a nucleoside transporter inhibitor) could block the incorporation of RBV tri-phosphate into viral RNA, and also partly recovered the inhibition. However, NBTI caused partial disruption of actin microfilaments, so the restoration may be partial.

MMF has been used as an immunosuppressive agent (10 µg/mL or greater), and inhibits replication of some viruses such as Dengue virus (25), hepatitis B virus (26), human immunodeficiency virus (27), and Japanese encephalitis virus (28). In the present study, 2 µg/mL of MMF (1.48 µg/mL as MPA) had an inhibitory effect on hPIV-2 replication, and Hermann *et al.* reported that 3 µg/mL MMF inhibited Type 2 Winnipeg, a cerebrospinal fluid-derived reovirus isolate (16). In addition, MMF had an inhibitory effect at 1/10 the dose of RBV (present experiment). From these results, MMF may be a promising agent for the treatment of human parainfluenza viruses which cause recurrent infection in infants and children.

MMF is a nonnucleoside inhibitor of IMPDH. Its hydrolytic product MPA binds to IMPDH and finally causes depletion of the GTP pool. Therefore, it is reasonable that a sufficient amount of guanosine could recover the inhibition by MMF. Though NBTI is a nucleoside transporter inhibitor, it also could partly restore the inhibition by MMF: viral RNA was fully restored and virus titer and viral protein were partly restored. The mechanism of restoration by NBTI remains to be elucidated.

References

1. Lamb RA, Parks GP. Paramyxoviridae: The viruses and their replication. In: Fields Virology, 5th ed. (Knipe DM, Howley PM, eds.). Lippincott Williams & Wilkins, Philadelphia, PA, USA, 2008; pp. 1449-1496.
2. Yuasa T, Bando H, Kawano M, Tsurudome M, Nishio M, Kondo K, Komada H, Ito Y. Sequence analysis of the 3' genome end and NP gene of human parainfluenza type 2 virus: sequence variation of the gene-starting signal and the conserved 3' end. *Virology*. 1990; 179:777-784.
3. Ohgimoto S, Bando H, Kawano M, Okamoto K, Kondo K, Tsurudome M, Nishio M, Ito Y. Sequence analysis of P gene of human parainfluenza type 2 virus; P and cysteine-rich proteins are translated by two mRNAs that differ by two non-templated G residues. *Virology*. 1990; 177:116-123.
4. Kawano M, Bando H, Ohgimoto S, Okamoto K, Kondo K, Tsurudome M, Nishio M, Ito Y. Complete nucleotide sequence of the matrix gene of human parainfluenza type 2 virus and expression of the M protein in bacteria. *Virology*. 1990; 179:857-861.
5. Kawano M, Bando H, Ohgimoto S, Okamoto K, Kondo K, Tsurudome M, Nishio M, Ito Y. Sequence of the fusion protein gene of human parainfluenza type 2 virus and its 3' intergenic region: lack of small hydrophobic (SH) gene. *Virology*. 1990; 178:289-292.
6. Kawano M, Bando H, Yuasa T, Kondo K, Tsurudome M, Komada H, Nishio M, Ito Y. Sequence determination of the hemagglutinin-neuraminidase (HN) gene of human parainfluenza type 2 virus and the construction of a phylogenetic tree for HN proteins of all the paramyxoviruses that are infectious to humans. *Virology*. 1990; 174:308-313.
7. Kawano M, Okamoto K, Bando H, Kondo K, Tsurudome M, Komada H, Nishio M, Ito Y. Characterizations of the human parainfluenza type 2 virus gene encoding the L protein and the intergenic sequences. *Nucleic Acids Res*. 1991; 19:2739-2746.
8. Tsurudome M, Nishio M, Komada H, Bando H, Ito Y. Extensive antigenic diversity among human parainfluenza type 2 virus isolates and immunological relationships among paramyxoviruses revealed by monoclonal antibodies. *Virology*. 1989; 171:38-48.
9. Kawano M, Kaito M, Kozuka Y, Komada H, Noda N, Namba K, Tsurudome M, Ito M, Nishio M, Ito Y. Recovery of infectious human parainfluenza type 2 virus from cDNA clones and properties of the defective virus without V-specific cysteine-rich domain. *Virology*. 2001; 284:99-112.
10. Dixit NM, Perelson AS. The metabolism, pharmacokinetics and mechanisms of antiviral activity of ribavirin against

- hepatitis C virus. *Cell Mol Life Sci.* 2006; 63:832-842.
11. Martin P, Jensen DM. Ribavirin in the treatment of chronic hepatitis C. *J Gastroenterol Hepatol.* 2008; 23:844-855.
 12. Smee DF, Matthews TR. Metabolism of ribavirin in respiratory syncytial virus-infected and uninfected cells. *Antimicrob Agents Chemother.* 1986; 30:117-121.
 13. Leyssen P, Balzarini J, De Clercq E, Neyts J. The predominant mechanism by which ribavirin exerts its antiviral activity *in vitro* against flaviviruses and paramyxoviruses is mediated by inhibition of IMP dehydrogenase. *J Virol.* 2005; 79:1943-1947.
 14. Kihira S, Uematsu J, Kawano M, Itoh A, Ookohchi A, Satoh S, Maeda Y, Sakai K, Yamamoto H, Tsurudome M, O'Brien M, Komada H. Ribavirin inhibits human parainfluenza virus type 2 replication *in vitro*. *Microbiol Immunol.* 2014; 58:628-635.
 15. Ye L, Li J, Zhang T, Wang X, Zhou Y, Liu J, Parekh HK, Ho W. Mycophenolate mofetil inhibits hepatitis C virus replication in human hepatic cells. *Virus Res.* 2012; 168:33-40.
 16. Hermann LL, Coombs KM. Mycophenolic acid inhibits replication of Type 2 Winnipeg, a cerebrospinal fluid-derived reovirus isolate. *Can J Infect Dis Med Microbiol.* 2004; 15:261-265.
 17. Uematsu J, Koyama A, Takano S, Ura Y, Tanemura M, Kihira S, Yamamoto H, Kawano M, Tsurudome M, O'Brien M, Komada H. Legume lectins inhibit human parainfluenza virus type 2 infection by interfering with the entry. *Viruses.* 2012; 4:1104-1115.
 18. Kitagawa H, Kawano M, Yamanaka K, Kakeda M, Tsuda K, Inada H, Yoneda M, Sakaguchi T, Nigi A, Nishimura K, Komada H, Tsurudome M, Yasutomi Y, Nosaka T, Mizutani H. Intranasally administered antigen 85B gene vaccine in none-replacing human parainfluenza type 2 virus vector ameliorates mouse atopic dermatitis. *Plos One.* 2013; 8:e66614.
 19. De BP, Banerjee AK. Involvement of actin microfilaments in the transcription/replication of human parainfluenza virus type 3: possible role of actin in other viruses. *Microsc Res Tech.* 1999; 47:114-123.
 20. Moyer SA, Baker SC, Lessard JL. Tubulin: a factor necessary for the synthesis of both Sendai virus and vesicular stomatitis virus RNAs. *Proc Natl Acad Sci U S A.* 1986; 83:5405-5409.
 21. Olschlager S, Neyts J, Gunther S. Depletion of GTP pool is not the predominant mechanism by which ribavirin exerts its antiviral effect on Lassa virus. *Antiviral Res.* 2011; 91:89-93.
 22. Leyssen P, De Clercq E, Neyts J. The anti-yellow fever virus activity of ribavirin is independent of error-prone replication. *Mol Pharmacol.* 2006; 69:1461-1467.
 23. Safronetz D, Haddock E, Feldmann F, Ebihara H, Feldmann H. *In vitro* and *in vivo* activity of ribavirin against Andes virus infection. *Plos One.* 2011; 6:e23560.
 24. Shah NR, Sunderland A, Grdzelishvili VZ. Cell type mediated resistance of vesicular stomatitis virus and Sendai virus to ribavirin. *Plos One.* 2010; 5:e11265.
 25. Diamond MS, Zachariah M, Harris E. Mycophenolic acid inhibits dengue virus infection by preventing replication of viral RNA. *Virology.* 2002; 304:211-221.
 26. Gong ZJ, De Meyer S, Clarysse C, Verslyte C, Neyts J, De Clercq E, Yap SH. Mycophenolic acid, an immunosuppressive agent, inhibits HBV replication *in vitro*. *J Viral Hepat.* 1999; 6:229-236.
 27. Hossain MM, Coull J, Drusano GL, Margolis DM. Dose proportional inhibition of HIV-1 replication by mycophenolic acid and synergistic inhibition in combination with abacavir, didanosine, and tenofovir. *Antiviral Res.* 2002; 55:41-52.
 28. Sebastian L, Madhusudana SN, Ravi V, Desai A. Mycophenolic acid inhibits replication of Japanese encephalitis virus. *Chemotherapy.* 2011; 57:56-61.

(Received November 8, 2019; Revised December 23, 2019; Accepted December 28, 2019)

Investigation of efficacy and safety of low-dose sodium glucose transporter 2 inhibitors and differences between two agents, canagliflozin and ipragliflozin, in patients with type 2 diabetes mellitus

Kaoru Sugimoto^{1,§}, Ichiro Abe^{1,2,3,§,*}, Midori Minezaki^{1,2}, Yuichi Takashi^{1,2}, Kentaro Ochi^{1,2}, Hideyuki Fujii^{1,2,3}, Hanako Ohishi¹, Yuka Yamao¹, Tadachika Kudo¹, Kenji Ohe⁴, Makiko Abe⁵, Yasushi Ohnishi², Tomohiro Shinagawa³, Shigeaki Mukoubara², Kunihisa Kobayashi¹

¹ Department of Endocrinology and Diabetes Mellitus, Fukuoka University Chikushi Hospital, Chikushino, Fukuoka, Japan;

² Department of Internal Medicine, Nagasaki Prefecture Iki Hospital, Iki, Nagasaki, Japan;

³ Department of Internal Medicine, Shinagawa Surgical Hospital, Iki, Nagasaki, Japan;

⁴ Department of Pharmacotherapeutics, Faculty of Pharmaceutical Sciences, Fukuoka University, Fukuoka, Japan;

⁵ Department of Preventive Medicine, Kyushu University Faculty of Medical Sciences, Fukuoka, Japan.

Summary

Sodium glucose transporter 2 inhibitors (SGLT2is), new antidiabetic agents, were reported to improve not only glycemic parameters but also metabolic and circulatory parameters. Whereas, several adverse events caused by SGLT2is were also reported. We aimed to investigate the changes of glycemic, metabolic, and circulatory parameters as well as safety with low-dose administration of two SGLT2is, canagliflozin and ipragliflozin, and also the difference between the two agents. 25 individuals with type-2 diabetes mellitus (T2DM) were recruited and administered with low-dose SGLT2is, canagliflozin ($n = 10$, 50 mg/day) and ipragliflozin ($n = 15$, 25 mg/day). We examined glycemic, metabolic, and circulatory parameters at baseline and 24 weeks after administration. All patients completed the study without complications. Compared with baseline, levels of glycosylated hemoglobin, fasting plasma glucose, and homeostasis model assessment of β -cell function improved significantly at 24 weeks after administration ($p < 0.05$). Levels of body weight, low-density lipoprotein-cholesterol, aspartate transaminase, γ -glutamyl transferase, and urinary excretion of albumin also improved significantly ($p < 0.05$). Moreover, systolic/diastolic blood pressure and levels of brain natriuretic peptide improved significantly ($p < 0.05$). The comparison of improvement ratio (values of improvement/values of basement) of each agent revealed that there was a significant difference between low-dose canagliflozin and low-dose ipragliflozin for brain natriuretic peptide (0.4404 vs. 0.0970, $p = 0.0275$). Hence, low-dose SGLT2is could be useful for patients of T2DM not only for hyperglycemia but also for metabolic and circulatory disorders without eliciting adverse events. In addition, with regard to the efficacy upon cardiovascular function, canagliflozin could be more suitable than ipragliflozin.

Keywords: Sodium glucose transporter 2 inhibitors, type-2 diabetes mellitus, canagliflozin, ipragliflozin

[§]These authors contributed equally to this work.

*Address correspondence to:

Dr. Ichiro Abe, Department of Endocrinology and Diabetes Mellitus, Fukuoka University Chikushi Hospital, 1-1-1, Zokumyoin, Chikushino, Fukuoka, 818-8502 Japan.
E-mail: abe1ro@fukuoka-u.ac.jp

1. Introduction

Sodium glucose transporter-2 inhibitors (SGLT2is) are new antidiabetic agents for patients with type-2 diabetes mellitus (T2DM). Sodium glucose transporter-2 (SGLT2) is a member of the sodium glucose transporter (SGLT)

family of solute transporters and expressed highly in the proximal tubules of kidneys. SGLT2 has an important role in glucose reabsorption, and inhibition of SGLT2 prevents hyperglycemia caused by reduced reabsorption of glucose (1-3). SGLT2is were proposed as an insulin-independent approach for treatment of hyperglycemia (4), and have the effects of reducing body weight and fat mass (5,6). SGLT2is were also reported to improve several metabolic parameters other than glycemic parameters (7-10). Moreover, some studies revealed that the SGLT2is reduce the prevalence of death from cardiovascular causes and hospitalization for heart failure (11-13).

On the other hand, it was reported SGLT2is often caused adverse events. In detail, infection of the urinary and genital tracts, dehydration, diabetic ketosis/ketoacidosis have been reported as adverse events of SGLT2is (14,15). A way to prevent these adverse effects of SGLT2is have yet to be established.

Interestingly, it was reported that the inhibition of sodium glucose transporter-1 (SGLT1) led to same diuretic effect as that of SGLT2 (16,17). It was also reported that SGLT2is could inhibit SGLT1 as well as SGLT2, implying differences in potencies of inhibition of SGLT1 among available SGLT2is (18,19).

Hence, we investigated the efficacy of low-dose SGLT2is, 50 mg/day of canagliflozin (a half of commonly used dose: 100 mg/day) or 25 mg/day of ipragliflozin (a half of commonly used dose: 50 mg/day), upon glycemic parameters, metabolic parameters,

and circulatory parameters, and also checked the safety of low-dose administration of these two SGLT2is to seek whether it can circumvent the adverse effects of SGLT2is that have been reported to be problematic recently. Besides, we also investigated the difference of effects upon available parameters between the two SGLT2is, canagliflozin and ipragliflozin.

2. Subjects and Methods

2.1. Ethical approval of the study protocol

The study protocol was approved by the Ethics Review Committee of Nagasaki Prefecture Iki Hospital (Nagasaki, Japan). All participants provided written informed consent to participate in the study.

2.2. Subjects

We recruited 25 individuals with T2DM at Nagasaki Prefecture Iki Hospital and Shinagawa Surgical Hospital from April 2015 to March 2018. Participant characteristics are shown in Table. 1 and Table. 2. None of the drugs of patients were changed during the study.

2.3. Study design

To examine the efficacy and safety of low-dose SGLT2is (canagliflozin 50 mg/day, ipragliflozin 25 mg/day), we administered them and continued treatment for 24 weeks.

Table 1. Clinical characteristics of patient cohort

	All (n = 25)	Canagliflozin (n = 10)	Ipragliflozin (n = 15)
Age (years)	62.4 ± 11.0	60.9 ± 9.4	63.5 ± 12.2
Male/female	12/13	5/5	7/8
Body weight (kg)	69.0 ± 14.2	69.3 ± 13.3	68.8 ± 14.1
Fasting plasma glucose (mg/dL)	147.7 ± 30.9	144.3 ± 30.3	149.9 ± 32.1
Glycated hemoglobin (%)	7.68 ± 0.61	7.78 ± 0.55	7.59 ± 0.65
HOMA-β	31.8 ± 21.6	31.0 ± 26.5	32.3 ± 18.6
HOMA-IR	2.69 ± 2.05	2.51 ± 2.10	2.81 ± 2.08
Low-density lipoprotein-cholesterol (mg/dL)	106.6 ± 19.8	106.4 ± 19.8	106.7 ± 20.4
High-density lipoprotein-cholesterol (mg/dL)	56.5 ± 15.2	59.6 ± 17.6	54.5 ± 13.6
Triglyceride (mg/dL)	117.8 ± 62.8	134.0 ± 89/7	107.0 ± 35.7
Aspartate transaminase (U/L)	22.4 ± 10.8	22.0 ± 6.2	22.7 ± 13.3
Alanine aminotransferase (U/L)	24.1 ± 17.9	19.4 ± 7.0	27.3 ± 22.2
γ-glutamyl transferase (U/L)	26.6 ± 14.5	31.3 ± 15.4	23.4 ± 13.5
Urinary albumin (mg/gCr)	164.1 ± 393.3	183.1 ± 406.0	151.5 ± 398.4
Estimated glomerular filtration rate (mL/min/1.73 m ²)	75.3 ± 21.2	81.8 ± 21.3	71.0 ± 20.3
Brain natriuretic peptide (pg/mL)	26.8 ± 21.0	25.7 ± 10.2	27.6 ± 26.2
Systolic blood pressure (mmHg)	137.0 ± 17.3	135.1 ± 14.9	138.2 ± 19.2
Diastolic blood pressure (mmHg)	74.7 ± 10.2	77.1 ± 7.8	73.1 ± 11.6
Detail of medication for diabetes mellitus			
Only dipeptidyl peptidase-4 inhibitor	3	2	1
Only biguanide	4	2	2
Dipeptidyl peptidase-4 inhibitor and biguanide	11	3	8
Sulfonylurea and dipeptidyl peptidase-4 inhibitor	5	2	3
Sulfonylurea and biguanide	1	0	1
Sulfonylurea, dipeptidyl peptidase-4 inhibitor, and biguanide	1	1	0

Data are shown as means ± standard deviation (SD). HOMA-β: homeostasis model assessment of β-cell function, HOMA-IR: homeostasis model assessment of insulin resistance.

Table 2. Glycemic parameters, the metabolic parameters, and circulatory parameters at baseline and 24 weeks after administration of low-dose SGLT2is

	baseline	24 weeks after	<i>p</i>
Body weight (kg)	69.0 ± 14.2	66.0 ± 13.4	< 0.0001*
Fasting plasma glucose (mg/dL)	147.7 ± 30.9	134.3 ± 21.4	0.0023*
Glycated hemoglobin (%)	7.68 ± 0.61	7.12 ± 0.62	0.0002*
HOMA-β	31.8 ± 21.6	39.0 ± 31.0	0.0201*
HOMA-IR	2.69 ± 2.05	2.46 ± 1.99	0.1582
Low-density lipoprotein-cholesterol (mg/dL)	106.6 ± 19.8	97.6 ± 20.4	0.0034*
High-density lipoprotein-cholesterol (mg/dL)	56.5 ± 15.2	57.6 ± 13.4	0.2959
Triglyceride (mg/dL)	117.8 ± 62.8	102.1 ± 49.6	0.2149
Aspartate transaminase (U/L)	22.4 ± 10.8	18.4 ± 3.9	0.0203*
Alanine aminotransferase (U/L)	24.1 ± 17.9	20.0 ± 12.2	0.0644
γ-glutamyl transferase (U/L)	26.6 ± 14.5	23.7 ± 14.0	0.0128*
Urinary albumin (mg/gCr)	164.1 ± 393.3	69.8 ± 153.6	0.0492*
Estimated glomerular filtration rate (mL/min/1.73 m ²)	75.3 ± 21.2	75.2 ± 21.2	0.4558
Brain natriuretic peptide (pg/mL)	26.8 ± 21.0	17.3 ± 16.3	0.0013*
Systolic blood pressure (mmHg)	137.0 ± 17.3	124.6 ± 16.5	0.0003*
Diastolic blood pressure (mmHg)	74.7 ± 10.2	69.6 ± 13.0	0.0152*

Data are shown as means ± standard deviation (SD). The significance of differences between means was estimated by paired *t*-test. *p* < 0.05 were considered to indicate statistical significance (*). HOMA-β: homeostasis model assessment of β-cell function, HOMA-IR: homeostasis model assessment of insulin resistance.

The following variables were measured at baseline and 24 weeks after administration of parameters of glycemic control (glycated hemoglobin (HbA_{1c}), fasting plasma glucose (FPG), homeostasis model assessment of insulin resistance (HOMA-IR), homeostasis model assessment of β-cell function (HOMA-β); markers of lipid metabolism (low-density lipoprotein-cholesterol (LDL-C), high-density lipoprotein cholesterol (HDL-C), and triglycerides (TG)); liver enzymes (aspartate transaminase (AST), alanine transaminase (ALT), γ-glutamyl transferase (γ-GTP)), estimated glomerular filtration rate (eGFR), urinary albumin (U-Alb), brain natriuretic peptide (BNP), systolic and diastolic blood pressure (SBP and DBP), and body weight (BW). Blood samples were obtained after an overnight fast, and HOMA-IR was calculated using the following formula: HOMA-IR = FPG × fasting insulin/405. HOMA-β was calculated using the following formula: HOMA-β = 360 × fasting insulin/(FPG - 63). Adverse events (including side effects) were examined based on patient data and interviews with patients. In addition, to evaluate the difference between two agents, canagliflozin and ipragliflozin, glycemic, metabolic, and circulatory parameters at baseline and 24 weeks after administration were investigated and the comparison of improvement ratio (values of improvement/values of basement) in each parameter of the two different agents was performed.

2.4. Statistical analyses

Data are the mean ± standard deviation (SD). Statistical analyses were performed using STATA[®] SE version 13.1 (Stata Corporation, College Station, TX, USA). Significance of differences between mean values was estimated by paired *t*-test (for investigations except comparison of improve ratio) and unpaired *t*-test (for

comparison of improve ratio). *p* < 0.05 was considered significant.

3. Results

All patients completed the present study without adverse events such as infection of urinary or genital tracts, dehydration, diabetic ketosis/ketoacidosis. Changes in glycemic parameters (HbA_{1c}, FPG, HOMA-IR, HOMA-β), metabolic parameters (BW, LDL-C, HDL-C, TG, AST, ALT, γ-GTP, eGFR, U-Alb), circulatory parameters (BNP, SBP, DBP) at baseline and 24 weeks after administration of low-dose SGLT2is for all patients are shown in Table 2. In terms of glycemic parameters, levels of HbA_{1c}, FPG, and HOMA-β improved significantly after 24 weeks of SGLT2is administration compared to baseline (HbA_{1c}: 7.68 ± 0.61 vs. 7.12 ± 0.62 %, *p* = 0.0002; FPG: 147.7 ± 30.9 vs. 134.3 ± 21.4 mg/dL, *p* = 0.0023; HOMA-β: 31.8 ± 21.6 vs. 39.0 ± 31.0, *p* = 0.0201). HOMA-IR also improved but not significant (2.69 ± 2.05 vs. 2.46 ± 1.99 mg/dL, *p* = 0.1582). BW decreased significantly (69.0 ± 14.2 vs. 66.0 ± 13.4 kg, *p* < 0.0001). Concerning lipid metabolism, levels of LDL-C improved significantly (106.6 ± 19.8 vs. 97.6 ± 20.4 mg/dL, *p* = 0.0034), while levels of HDL-C and TG also improved but were not significant (HDL-C: 56.5 ± 15.2 vs. 57.6 ± 13.4 mg/dL, *p* = 0.2959; TG: 117.8 ± 62.8 vs. 102.1 ± 49.6 mg/dL, *p* = 0.2149, respectively). As for liver enzymes, levels of AST and γ-GTP were reduced significantly (AST: 22.4 ± 10.8 vs. 18.4 ± 3.9 U/L, *p* = 0.0203; γ-GTP: 26.6 ± 14.5 vs. 23.7 ± 14.0 U/L, *p* = 0.0128, respectively), though the reduction of ALT was not significant (24.1 ± 17.9 vs. 20.0 ± 12.2 U/L, *p* = 0.0644). U-Alb levels were improved significantly (164.1 ± 393.3 vs. 69.8 ± 153.6 mg/gCr, *p* = 0.0492), while there was not significant change of eGFR level

(75.3 ± 21.1 vs. 75.2 ± 21.2 mL/min/1.73 m², $p = 0.4558$). Concerning circulatory parameters, all parameters improved significantly (BNP: 26.8 ± 21.0 vs. 17.3 ± 16.3 pg/mL, $p = 0.0013$; SBP: 137.0 ± 17.3 vs. 124.6 ± 16.5 mmHg, $p = 0.0003$; DBP: 74.7 ± 10.2 vs. 69.6 ± 13.0 mmHg, $p = 0.0152$, respectively).

The differences between baseline and 24 weeks after administration for patients with low-dose canagliflozin and those of low-dose ipragliflozin are shown in Table 3. The change of parametric values were similar, except for those of HOMA-IR, AST, ALT, and DBP, that were significantly decreased for low-dose canagliflozin ($p = 0.0221$, $p = 0.0243$, $p < 0.0001$, $p = 0.0140$, respectively) but not for low-dose ipragliflozin ($p = 0.3219$, $p = 0.0979$, $p = 0.1613$, $p = 0.1982$, respectively). There was a significant increase for HOMA- β and decrease for γ -GTP with low-dose ipragliflozin ($p = 0.0334$ and $p = 0.0010$) but not for low-dose canagliflozin ($p = 0.1672$ and $p = 0.2849$). Improvement ratio (values of improvement/values of basement) in glycemic parameters, metabolic parameters, and circulatory parameters of both low-

dose canagliflozin and low-dose ipragliflozin is shown in Table 4. Among the parameters, low-dose canagliflozin significantly improved BNP compared to low-dose ipragliflozin (0.4404 vs. 0.0970, $p = 0.0275$).

4. Discussion

T2DM is known for its hyperglycemia symptoms due to impaired glucose homeostasis, which is a result of an imbalance of concerted secretion of pancreatic hormones such as insulin and glucagon, and which is accompanied with insulin resistance in peripheral tissues (20). Appropriate blood glucose control in T2DM patients can be achieved through diet and exercise therapy but is discontinued in most patients. Most of them come to rely on antidiabetic agents (21,22).

SGLT2is are a distinct category of anti-diabetic agents that lower blood glucose level by increasing urine glucose excretion (4). This is a result of decreased reabsorption of glucose by inhibiting SGLT2 (1-3). Unexpectedly, SGLT2is improve various pathological

Table 3. Respective data of each parameter at baseline and 24 weeks after administration of low-dose of canagliflozin and ipragliflozin

	baseline	24 weeks after	<i>p</i>
Canagliflozin (<i>n</i> = 10)			
Body weight (kg)	69.3 ± 15.1	65.5 ± 13.2	0.0056*
Fasting plasma glucose (mg/dL)	144.3 ± 30.3	130.3 ± 19.2	0.0359*
Glycated hemoglobin (%)	7.78 ± 0.55	7.03 ± 0.62	0.0115*
HOMA- β	31.0 ± 26.5	33.3 ± 29.6	0.1672
HOMA-IR	2.51 ± 2.11	1.75 ± 1.36	0.0221*
Low-density lipoprotein-cholesterol (mg/dL)	106.4 ± 19.8	100.4 ± 21.5	0.0424*
High-density lipoprotein-cholesterol (mg/dL)	59.6 ± 17.6	61.4 ± 12.6	0.3402
Triglyceride (mg/dL)	134.0 ± 89.7	101.3 ± 59.1	0.1169
Aspartate transaminase (U/L)	22.0 ± 6.2	17.9 ± 4.3	0.0243*
Alanine aminotransferase (U/L)	19.4 ± 7.0	15.9 ± 5.9	< 0.0001*
γ -glutamyl transferase (U/L)	31.3 ± 15.4	30.2 ± 17.8	0.2849
Urinary albumin (mg/gCr)	183.1 ± 406.0	116.9 ± 238.0	0.1240
Estimated glomerular filtration rate (mL/min/1.73 m ²)	81.8 ± 22.2	81.4 ± 21.3	0.4128
Brain natriuretic peptide (pg/mL)	25.7 ± 10.2	13.3 ± 7.4	0.0024*
Systolic blood pressure (mmHg)	135.1 ± 14.9	124.5 ± 19.8	0.0243*
Diastolic blood pressure (mmHg)	77.1 ± 7.8	67.9 ± 12.0	0.0140*
Ipragliflozin (<i>n</i> = 15)			
Body weight (kg)	68.8 ± 14.1	66.3 ± 14.0	< 0.0001*
Fasting plasma glucose (mg/dL)	149.9 ± 32.1	137.0 ± 23.0	0.0194*
Glycated hemoglobin (%)	7.59 ± 0.65	7.17 ± 0.63	0.0022*
HOMA- β	32.3 ± 18.6	42.9 ± 32.4	0.0334*
HOMA-IR	2.81 ± 2.08	2.94 ± 2.23	0.3219
Low-density lipoprotein-cholesterol (mg/dL)	106.7 ± 20.4	95.7 ± 20.2	0.0163*
High-density lipoprotein-cholesterol (mg/dL)	54.5 ± 13.6	55.1 ± 13.7	0.3779
Triglyceride (mg/dL)	107.0 ± 35.7	102.6 ± 44.4	0.3476
Aspartate transaminase (U/L)	22.7 ± 13.3	18.7 ± 3.7	0.0979
Alanine aminotransferase (U/L)	27.3 ± 22.2	22.8 ± 14.6	0.1613
γ -glutamyl transferase (U/L)	23.4 ± 13.5	19.4 ± 9.0	0.0010*
Urinary albumin (mg/gCr)	151.5 ± 398.4	38.4 ± 37.6	0.1370
Estimated glomerular filtration rate (mL/min/1.73 m ²)	71.0 ± 20.3	71.0 ± 20.8	0.4879
Brain natriuretic peptide (pg/mL)	27.6 ± 26.2	20.0 ± 20.0	0.0446*
Systolic blood pressure (mmHg)	138.2 ± 19.2	124.6 ± 14.7	0.0028*
Diastolic blood pressure (mmHg)	73.1 ± 11.6	70.7 ± 13.9	0.1982

Data are shown as means ± standard deviation (SD). The significance of differences between means was estimated by paired *t*-test. $p < 0.05$ were considered to indicate statistical significance (*). HOMA- β : homeostasis model assessment of β -cell function, HOMA-IR: homeostasis model assessment of insulin resistance.

Table 4. Comparison of improvement ratio (values of improvement/values of basement) between canagliflozin and ipragliflozin, upon each parameter

	Canagliflozin (n = 10)	Ipragliflozin (n = 15)	p
Body weight	0.0512	0.0376	0.3161
Fasting plasma glucose	0.0770	0.0713	0.9186
Glycated hemoglobin	0.0925	0.0534	0.2205
HOMA- β	0.0956	0.3133	0.1170
HOMA-IR	0.1032	- 0.0985	0.3554
Low-density lipoprotein-cholesterol	0.0563	0.0920	0.5541
High-density lipoprotein-cholesterol	0.0735	0.0176	0.4800
Triglyceride	0.1147	0.0022	0.4741
Aspartate transaminase	0.1539	0.0750	0.3750
Alanine transaminase	0.1775	0.0378	0.1823
γ -glutamyl transferase	0.0476	0.1236	0.1825
Urinary albumin	0.0115	0.0330	0.9443
Estimated glomerular filtration rate	0.0016	0.0036	0.9567
Brain natriuretic peptide	0.4404	0.0970	0.0275*
Systolic blood pressure	0.0775	0.0906	0.7703
Diastolic blood pressure	0.1179	0.0264	0.1547

Data are shown as means \pm standard deviation (SD). The significance of differences between means was estimated by unpaired *t*-test. $p < 0.05$ were considered to indicate statistical significance (*). HOMA- β : homeostasis model assessment of β -cell function, HOMA-IR: homeostasis model assessment of insulin resistance.

conditions in addition to high blood glucose levels. It was reported that SGLT2is decrease body weight and fat mass, and improve concomitant insulin resistance (5,6). Meanwhile, it was reported that SGLT2is could improve insulin secretion of beta cells in the pancreas (23,24). They were also reported to improve metabolic disorders, such as hyperlipidemia, fatty liver, albuminuria (7-9). Furthermore, several previous studies demonstrated that the SGLT2is lowers the prevalence of death from cardiovascular causes and hospitalization for heart failure (11-13). Thus, SGLT2is have various advantages besides their occasional side effects. These adverse events: infection of urinary or genital tracts; dehydration; and diabetic ketosis/ketoacidosis may sometimes lead to unwelcomed results (14,15). We hypothesized low-dose administration of SGLT2is might be useful for prevention of such serious adverse effects. Indeed, we previously investigated several patients with low-dose ipragliflozin and showed that adverse events did not occur (25). In the present study, all patients completed the study without complications such as infection of urinary or genital tracts, diabetic ketosis/ketoacidosis. Moreover, there were no changes in eGFR between baseline and 24 weeks after administration of SGLT2is. In previous studies, it was reported that the recommended dose of SGLT2is cause decrease of eGFR at 24-48 weeks after administration (11-13). Considering eGFR did not change, low-dose of SGLT2is could carry a low risk of severe dehydration. Hence, patients with low-dose SGLT2is could avoid the adverse effects of SGLT2is that have been reported to be problematic.

In terms of efficacy of SGLT2is, our investigations demonstrated that the levels of HbA_{1c}, FPG, and HOMA- β improved significantly. Considering that levels of BW was reduced significantly, we think that levels of HOMA-IR would improve if we continued to use low-dose of SGLT2is over a long

period. With regard to metabolic parameters, levels of LDL-C, AST, γ -GTP, and U-Alb as well as those of BW, decreased significantly. In addition, levels of circulatory parameters, such as BNP, SBP, and DBP, improved significantly. These data suggest that low-dose SGLT2is could have adequate efficacy despite of less adverse events.

On the other hand, we also investigated the differences between two SGLT2is, canagliflozin and ipragliflozin. Our study indicated canagliflozin significantly improved BNP, more than that of ipragliflozin. Decreased BNP could indicate the improvement in cardiovascular function (26). Actually, SGLT2is were reported to have the efficacy for heart failure mainly by diuretic effects of the inhibition of SGLT2. Whereas, SGLT2is could inhibit SGLT1 as well as SGLT2 (18,19). Recently, several reports demonstrated the inhibition of SGLT1 could have diuretic effects (16,17). Actually, canagliflozin was reported to be more effective for SGLT1 among the available SGLT2is (24). The difference between two different SGLT2is, canagliflozin and ipragliflozin, in the present study, can be found in previous reports. Our results indicate that canagliflozin, which has more potency for SGLT1 inhibition than ipragliflozin, might be suitable for patients with disorders of cardiovascular function, such as heart failure.

In summary, our study revealed that low-dose SGLT2is were useful for hyperglycemia in T2DM patients but also their metabolic and circulatory disorders without eliciting adverse events. Furthermore, in regard of the efficacy for cardiovascular function, canagliflozin could be more promising than ipragliflozin. However, our study has limitations. The present study is a nonrandomized study with a small number of cases and short duration. Thus, randomized control studies with larger cohorts and longer terms are required to confirm our results in the future.

Acknowledgements

None of the authors received funding from any organization to undertake this study. We thank Ms. Yumi Iriguchi for providing assistance in our study.

References

- Kanai Y, Lee WS, You G, Brown D, Hediger MA. The human kidney low affinity Na⁺/glucose cotransporter SGLT2: delineation of the major renal reabsorptive mechanism for D-glucose. *J Clin Invest.* 1994; 93:397-404.
- Neumiller JJ, White Jr JR, Campbell RK. Sodium-glucose co-transport inhibitors: progress and therapeutic potential in type 2 diabetes mellitus. *Drugs.* 2010; 70:377-385.
- Mather A, Pollock C. Renal glucose transporters: novel targets for hyperglycemia management. *Nat Rev Nephrol.* 2010; 6:307-311.
- Nair S, Wilding JP. Sodium glucose cotransporter 2 inhibitors as a new treatment for diabetes mellitus. *J Clin Endocrinol Metab.* 2010; 95:34-42.
- Bolinder J, Ljunggren Ö, Kullberg J, Johansson L, Wilding J, Langkilde AM, Sugg J, Parikh S. Effects of dapagliflozin on body weight, total fat mass, and regional adipose tissue distribution in patients with type 2 diabetes mellitus with inadequate glycemic control on metformin. *J Clin Endocrinol Metab.* 2012; 97:1020-1031.
- Seufert J. SGLT2 inhibitors – an insulin-independent therapeutic approach for treatment of type 2 diabetes: focus on canagliflozin. *Diabetes Metab Syndr Obes.* 2015; 8:543-554.
- Tahara A, Kurosaki E, Yokono M, Yamajuku D, Kihara R, Hayashizaki Y, Takasu T, Imamura M, Li Q, Tomiyama H, Kobayashi Y, Noda A, Sasamata M, Shibasaki M. Effects of SGLT2 selective inhibitor ipragliflozin on hyperglycemia, hyperlipidemia, hepatic steatosis, oxidative stress, inflammation, and obesity in type 2 diabetic mice. *Eur J Pharmacol.* 2013; 715:246-255.
- Inagaki N, Goda M, Yokota S, Maruyama N, Iijima H. Effects of baseline blood pressure and low-density lipoprotein cholesterol on safety and efficacy of canagliflozin in Japanese patients with type 2 diabetes mellitus. *Adv Ther.* 2015; 32:1085-1103.
- Scheen AJ. Beneficial effects of SGLT2 inhibitors on fatty liver in type 2 diabetes: A common comorbidity associated with severe complications. *Diabetes Metab.* 2019; 45:213-223.
- De Nicola L, Gabbai FB, Liberti ME, Saggiocca A, Conte G, Minutolo R. Sodium/glucose cotransporter 2 inhibitors and prevention of diabetic nephropathy: targeting the renal tubule in diabetes. *Am J Kidney Dis.* 2014; 64:16-24.
- Zinman B, Wanner C, Lachin JM, Fitchett D, Bluhmki E, Hantel S, Matthews M, Devins T, Johansen OE, Woerle HJ, Broedl UC, Inzucchi SE; EMPA-REG OUTCOME Investigators. Empagliflozin, cardiovascular outcomes, and mortality in type 2 diabetes. *N Engl J Med.* 2015; 373:2117-2128.
- Neal B, Perkovic V, Mahaffey KW, de Zeeuw D, Fulcher G, Erond N, Shaw W, Law G, Desai M, Matthews DR; CANVAS Program Collaborative Group. Canagliflozin and cardiovascular and renal events in type 2 diabetes. *N Engl J Med.* 2017; 377:644-657.
- Wiviott SD, Raz I, Bonaca MP, *et al.* Dapagliflozin and cardiovascular outcomes in type 2 diabetes. *N Engl J Med.* 2019; 380:347-357.
- Taylor SI, Blau JE, Rother KI. SGLT2 inhibitors may predispose to ketoacidosis. *J Clin Endocrinol Metab.* 2015; 100:2849-2852.
- Nauck MA. Update on developments with SGLT2 inhibitors in the management of type 2 diabetes. *Drug Des Devel Ther.* 2014; 8:1335-1380.
- Song P, Huang W, Onishi A, Patel R, Kim YC, van Ginkel C, Fu Y, Freeman B, Koepsell H, Thomson S, Liu R, Vallon V. Knockout of Na⁺-glucose cotransporter SGLT1 mitigates diabetes-induced upregulation of nitric oxide synthase NOS1 in the macula densa and glomerular hyperfiltration. *Am J Physiol Renal Physiol.* 2019; 317:F207-F217.
- Loo DD, Zeuthen T, Chandy G, Wright EM. Cotransport of water by the Na⁺/glucose cotransporter. *Proc Natl Acad Sci U S A.* 1996; 93:13367-13370.
- Han S, Hagan DL, Taylor JR, Xin L, Meng W, Biller SA, Wetterau JR, Washburn WN, Whaley JM. Dapagliflozin, a selective SGLT2 inhibitor, improves glucose homeostasis in normal and diabetic rats. *Diabetes.* 2008; 57:1723-1729.
- Suzuki M, Honda K, Fukazawa M, Ozawa K, Hagita H, Kawai T, Takeda M, Yata T, Kawai M, Fukuzawa T, Kobayashi T, Sato T, Kawabe Y, Ikeda S. Tofogliflozin, a potent and highly specific sodium/glucose cotransporter 2 inhibitor, improves glycemic control in diabetic rats and mice. *J Pharmacol Exp Ther.* 2012; 341:692-701.
- Virally M, Blicklé JF, Girard J, Halimi S, Simon D, Guillausseau PJ. Type 2 diabetes mellitus: epidemiology, pathophysiology, unmet needs and therapeutical perspectives. *Diabetes Metab.* 2007; 33:231-244.
- Edelman SV. Importance of glucose control. *Med Clin North Am.* 1998; 82:665-687.
- Kudo T, Abe I, Minezaki M, *et al.* Investigation of metabolic and circulatory parameters that predict effects of dapagliflozin, a sodium-glucose cotransporter 2 inhibitor, on blood glucose and body weight in a retrospective, multicenter study. *J Diabetes Metab.* 2018; 9:810.
- Polidori D, Mari A, Ferrannini E. Canagliflozin, a sodium glucose co-transporter 2 inhibitor, improves model-based indices of beta cell function in patients with type 2 diabetes. *Diabetologia.* 2014; 57:891-901.
- Takahara M, Shiraiwa T, Matsuoka TA, Katakami N, Shimomura I. Ameliorated pancreatic β -cell dysfunction in type 2 diabetic patients treated with a sodium-glucose cotransporter 2 inhibitor ipragliflozin. *Endocr J.* 2015; 62:77-86.
- Abe I, Ohnishi Y, Koga M, Sugimoto K, Kudo T, Kunihisa K, Mukoubara S. Efficacy and safety of low-dose ipragliflozin, a selective sodium glucose transporter 2 inhibitor, in patients with type 2 diabetes mellitus. *Int J Allied Med Sci Clin Res.* 2016; 4:376-382.
- Ibrahim N, Januzzi JL. The potential role of natriuretic peptides and other biomarkers in heart failure diagnosis, prognosis and management. *Expert Rev Cardiovasc Ther.* 2015; 13:1017-1030.

(Received November 8, 2019; Revised December 18, 2019; Accepted December 22, 2019)

Safflower seed extract synergizes the therapeutic effect of cisplatin and reduces cisplatin-induced nephrotoxicity in human colorectal carcinoma RKO cells and RKO-transplanted mice

Chan Hum Park¹, Min Jo Kim¹, Chang Yeol Yang¹, Takako Yokozawa^{2,*}, Yu Su Shin^{1,*}

¹ Department of Medicinal Crop Research, National Institute of Horticultural and Herbal Science, Rural Development Administration, Eumseong, Republic of Korea;

² Graduate School of Science and Engineering for Research, University of Toyama, Toyama, Japan.

Summary

Safflower seed is effective against oxidative stress, mediating the activation of the apoptotic signaling pathway in the renal tissues of cisplatin-treated mice. The anticancer activity of safflower in various cancer cell lines has also been reported. The present study was conducted to evaluate the potential synergistic anticancer effects of the co-treatment of safflower seed extracts and cisplatin in RKO cells and in BALB/c mice bearing RKO cell-derived human colorectal tumors. In the cellular system, RKO cells were treated with safflower seed extract in the presence or absence of cisplatin for 48 h and the cytotoxicity was evaluated by using microscopy. In the *in vivo* system, mice were injected with RKO cells and subsequently orally administered 100 or 200 mg/kg body weight safflower seed extract plus cisplatin-treated or untreated mice for 3 days to examine the inhibitory effect on the tumor. Treatment with safflower seed extract or cisplatin to RKO cells resulted in a greater cell death than in with untreated cells. In the RKO cells co-treated with both safflower seed extract and cisplatin, greater cell damage was observed. In addition, mice co-administered safflower seed extract and cisplatin had lower concentrations of serum creatinine, which were indicative of less damage to the kidney, and had a lower solid tumor mass and higher expression of the caspase-3 protein. The results showed that safflower seed extract was highly toxic to RKO cells and inhibited tumor growth in cisplatin-treated mice through renoprotective effects.

Keywords: Safflower seed, cisplatin, nephrotoxicity, anticancer activity

1. Introduction

Colorectal cancer has become one of the most common cancers in Asian countries and is now considered a serious health problem (1). Several factors have been suggested to increase the risk of colon cancer (2). Although many anticancer drugs have been developed,

resistance to these drugs is ubiquitous. Moreover, most anticancer drugs are not selective toward cancer cells and attack rapidly dividing normal cells, which is a known harmful side effect of topoisomerase inhibitors [e.g. irinotecan (neutropenia and diarrhea), doxorubicin (cardiotoxicity), and alkylating agents, such as oxaliplatin, melphalan, carboplatin, cyclophosphamide, and cisplatin (gastrointestinal toxicity, cardiovascular toxicity, pulmonary, hematologic toxicity, and nephrotoxicity)]. Thus, the development of an adjuvant anticancer agent that protects against anticancer drug-induced toxicity, but does not impair the efficacy of chemotherapy, is an important clinical aim (3).

In the Asia-Pacific region, many plants have traditional uses as foods and medicines. Many candidate compounds have been identified for use in the prevention of human cancers (4). Among various oriental herbs, the

*Address correspondence to:

Dr. Takako Yokozawa, Graduate School of Science and Engineering for Research, University of Toyama, 3190 Gofuku, Toyama 930-8555, Japan.

E-mail: yokozawa@inm.u-toyama.ac.jp

Dr. Yu Su Shin, Department of Medicinal Crop Research, National Institute of Horticultural and Herbal Science, Rural Development Administration, Eumseong 369-873, Republic of Korea.

E-mail: totoro69@korea.kr

flowers and leaves of safflower (*Carthamus tinctorius* L.), a member of the chrysanthemum family, have a long history of use in traditional Chinese medicine in treatments for stroke, gynecological diseases, coronary heart disease, angina pectoris, and hypertension (5-8). Furthermore, safflower has been used for centuries to treat urological diseases in China (9), and the consumption of safflower seed oil is popular worldwide. Safflower seed is used as an herbal medicine in Korea to promote bone formation and to treat osteoporosis and rheumatism. Moreover, our previous study suggested that safflower seed was effective against oxidative stress, mediated the activation of the mitogen-activated protein kinase (MAPK)-related apoptotic signaling pathway in renal tissue, and exerted renoprotective effects in cisplatin-treated mice (10). Anticancer activity, through the induction of cyclin D1 proteasomal degradation, has also been reported in various human colorectal cancer cell lines (11). Thus, safflower seed may be a promising candidate adjuvant anticancer agent.

Therefore, the present study examined whether safflower seed extract acted synergistically as an anticancer agent with cisplatin chemotherapy, and evaluated its protective effect against cisplatin-induced nephrotoxicity, in RKO cells and mice bearing RKO cell-derived tumors.

2. Materials and Methods

2.1. Materials

Human colorectal carcinoma cell line, RKO, was obtained from American Type Culture Collection (Manassas, Virginia, USA). Minimum essential medium (MEM) was purchased from Gibco Laboratories (Paisley, UK). Fetal bovine serum (FBS) and [3-(4,5-dimethylthiazol-2-yl)-2,5-diphenyltetrazolium bromide] (MTT) were purchased from Sigma-Aldrich Chemical Company (Dorset, UK). Six-well flat-bottom tissue culture plates were purchased from Nunc Inc. (Hereford, UK). Phenylmethylsulfonyl fluoride (PMSF) was purchased from Sigma-Aldrich Co., Ltd. (St. Louis, MO, USA) and protease inhibitor mixture solution was obtained from Wako Pure Chemical Industries, Ltd. (Osaka, Japan). Enhanced chemiluminescence (ECL) western blotting detection reagents and pure nitrocellulose membranes were purchased from GE Healthcare (Buckinghamshire, UK). Primary antibodies for the detection of caspase 3 and β -actin and goat anti-rabbit and goat anti-mouse IgG horseradish peroxidase (HRP)-conjugated secondary antibodies were purchased from Santa Cruz Biotechnology, Inc. (Santa Cruz, CA, USA). All chemicals and reagents were of analytical grade and purchased from Sigma-Aldrich Co., Ltd. unless otherwise specified.

2.2. Preparation of safflower seed extract

Safflower seeds were purchased from Geunyang Oriental Medicine Co. (Chungju, Korea). A voucher for the herbarium specimen, identified by a plant systematist from the Herbal Crop Research Division, was deposited at the Department of Medicinal Crop Research, National Institute of Horticultural and Herbal Science, Rural Development Administration (voucher specimen No. MC20150528). The dried safflower seeds were pulverized and ultrasonically extracted twice in 70% ethanol (60 Hz, room temperature, 3 h). Subsequently, the solvent was evaporated *in vacuo* to obtain an extract with a yield of 4.65% by weight of the original safflower seed.

2.3. Analysis of safflower seed extract

An aliquot of 10 mg of the 70% ethanol extract of safflower seed was dissolved in 10 mL of 50% methanol by repeated vortexing, and passed through a Dismic-25 JP membrane filter (Advantec Toyo, Tokyo, Japan; pore diameter: 5 μ m). Next, 5 μ L of the sample was injected into a reverse-phase HPLC system with an INNO C18 column (4.6 \times 250 mm, 5 μ m pore size, YoungJin Biochrom, Korea) at 35°C. The mobile phase comprised (A) a 0.1% aqueous solution of formic acid and (B) acetonitrile, and the following gradient conditions were used: 0 min, 0% B; 5 min, 6% B; 10 min, 22% B; 50 min, 28% B; 66 min, 50% B; and 70 min, 100% B. The flow rate was 0.8 mL/min. The UV absorbance at 254 nm was monitored by using an Agilent 1200 series diode array detector (Agilent Technologies, Waldbronn, Germany). All peaks were assigned through co-injection tests with authentic samples and comparison of the UV spectral data; through this process, compounds including serotonin and its derivatives were detected from safflower seed extract. All measurements were repeated in triplicate. Representative HPLC results are illustrated in Figure 1. The quantification of serotonin, *N*-(*p*-coumaroyl)serotonin, *N*-feruloyl serotonin, luteolin, and luteolin-7-*O*-glucoside was achieved by peak area measurement. The quantity of each identified compound is shown in Table 1.

2.4. Cell culture

The human colon cancer cell line RKO was maintained and cultured in MEM supplemented with 10% FBS, 100 U/mL penicillin, and 100 μ g/mL streptomycin at 37°C in a humidified atmosphere containing 5% CO₂. For all experiments, cells in the exponential growth phase were used.

2.5. Cell cytotoxicity

RKO cells were seeded at a density of 4 \times 10⁴ cells/well in 6-well plates. After incubation for 24 h, the cells were treated with safflower seed extract (100 μ g/mL),

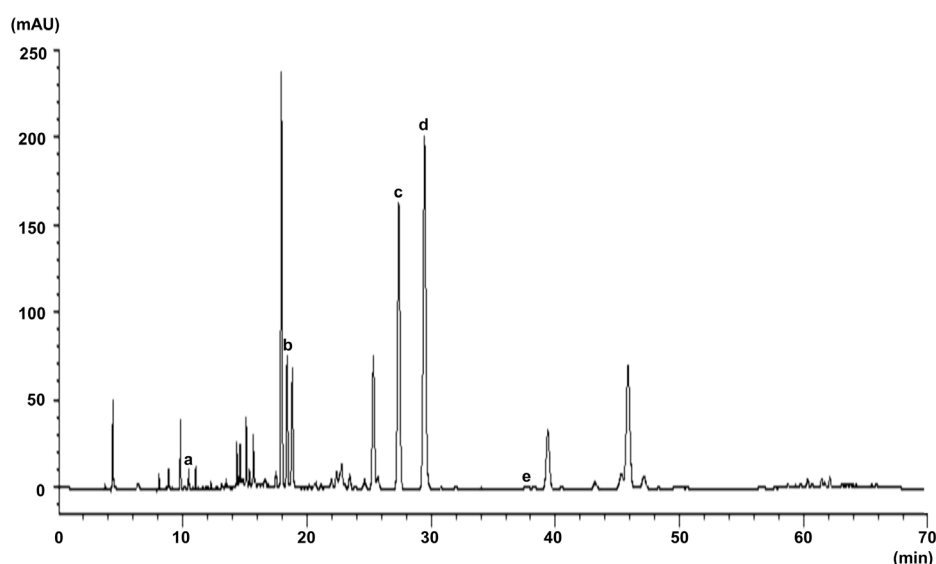


Figure 1. HPLC profile of safflower seed. a, serotonin; b, luteolin-7-*O*-glucoside; c, *N*-(*p*-coumaroyl)serotonin; d, *N*-feruloyl serotonin; e, luteolin.

Table 1. Contents of compound

Compound	Content (mg/g)	RSD (%)
Serotonin	1.47 ± 0.06	4.19
<i>N</i> -(<i>p</i> -Coumaroyl)serotonin	28.70 ± 1.82	6.35
<i>N</i> -Feruloyl serotonin	37.06 ± 2.25	6.07
Luteolin	0.89 ± 0.04	4.07
Luteolin-7- <i>O</i> -glucoside	12.85 ± 0.77	5.98

Values are the mean ± SEM.

cisplatin (1.5 µg/mL), or safflower seed extract (100 µg/mL) and cisplatin (1.5 µg/mL) for 48 h. Treatment doses were determined based on a previous study (11). The images of the cell cytotoxicity were obtained by using a Leica CTR 5000 microscope (×200) and a DM 5000B microscope (Leica Microsystems GmbH, Wetzlar, Germany).

2.6. Xenograft mouse model experiments

All experimental procedures were permitted using the guidelines established by the Pusan National University Institutional Animal Care and Use Committee. BALB/c nude mice (female, 5 weeks old; Joong-ang Animal Experiment Company, Republic of Korea) were used to construct the xenograft animal model. Mice were housed individually under a 12-h light/dark cycle at a controlled temperature (25 ± 2°C) and humidity (approximately 60%), and given free access to food and water. After adaptation (approximately 1 week), the animals were randomly divided into seven equal groups containing five mice: (1) mice were orally administered drinking water; (2) RKO cell-transplanted mice were orally administered drinking water; (3) RKO cell-transplanted mice were orally administered safflower seed extract (100 mg/kg body weight/day); (4) RKO cell-transplanted mice were

orally administered safflower seed extract (200 mg/kg body weight/day); (5) RKO cell-transplanted mice were administered an intraperitoneal injection of cisplatin (5 mg/kg body weight); (6) RKO cell-transplanted mice were orally administered safflower seed extract (100 mg/kg body weight/day) followed by an intraperitoneal injection of cisplatin (5 mg/kg body weight); (7) RKO cell-transplanted mice were orally administered safflower seed extract (200 mg/kg body weight/day) followed by an intraperitoneal injection of cisplatin (5 mg/kg body weight). To produce tumors, each mouse was implanted with RKO cells (5 × 10⁶ cells per mouse) in the back next to the right hind leg. After 2 weeks, the safflower seed extract (100 or 200 mg/kg body weight in water) was administered *via* oral gavage. The treatment dose of safflower seed extract was determined from our previous report (10). Subsequently, cisplatin (5 mg/kg body weight) was injected intraperitoneally. The treatment compounds were administered a total of three times, with each administration 3 days apart. Sixteen hours after the test compound administration, the mice were euthanized by CO₂ gas (70%) and the tumor was removed and weighed. The blood samples were collected by cardiac puncture from anesthetized mice and the serum was immediately separated by centrifugation.

2.7. Protein extraction and immunoblotting analyses

Protein was extracted according to the method of Komatsu (12). Briefly, the solid tumor was homogenized with ice-cold lysis buffer, pH 7.5 [137 mM NaCl, 20 mM Tris-HCl, 1% Tween 20, 10% glycerol, 1 mM PMSF, and protease inhibitor mixture] and the homogenates were centrifuged at 3,000 × g for 10 min at 4°C. The protein concentration of each sample was determined by using a Pierce BCA protein assay kit

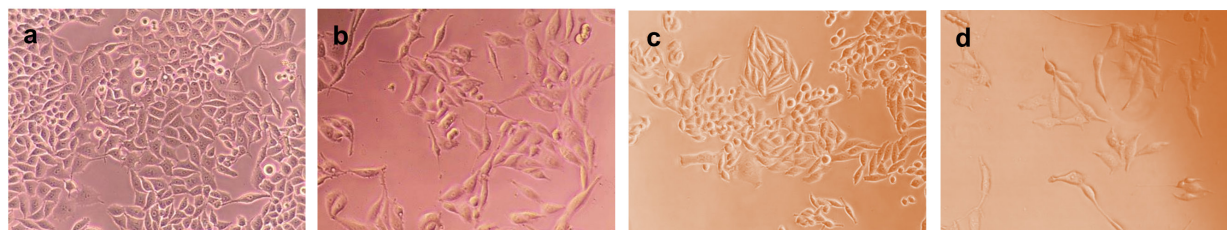


Figure 2. Cell cytotoxicity in human colorectal carcinoma RKO cells. a, untreated RKO cells; **b,** safflower seed extract-treated RKO cells; **c,** cisplatin-treated RKO cells; **d,** co-treated RKO cells.

(Thermo Scientific, Rockford, IL, USA) and equal amounts of protein were subjected to immunoblotting analyses. To determine caspase 3 and β -actin, each sample (10 μ g of protein) was electrophoresed on an 8-15% sodium dodecylsulfate polyacrylamide gel. The separated proteins were electrophoretically transferred to a nitrocellulose membrane, which was blocked by incubation in 5% (w/v) skim milk solution for 1 h, and then incubated with the appropriate primary antibody overnight at 4°C. The blots were washed and then incubated with goat anti-rabbit and/or goat anti-mouse IgG HRP-conjugated secondary antibodies for 90 min at room temperature. Each antigen-antibody complex was visualized by the application of ECL western blotting detection reagents and chemiluminescence was detected by using a Sensi-Q2000 Chemidoc (Lugen Sci Co., Ltd., Seoul, Korea). The band densities were measured by using ATTO Densitograph Software (ATTO Corporation, Tokyo, Japan) and quantified as a ratio to β -actin. Protein abundance was expressed relative to non-transplanted normal mice, which were considered to have an expression of 1.

2.8. Measurement of renal functional parameter

Serum creatinine level was measured using a commercial kit (CREA-Lq; Asan Pharm Co., Seoul, Republic of Korea).

2.9. Statistical analysis

The data are expressed as the mean \pm SEM. Significance was assessed by one-way analysis of variance (ANOVA) followed by Dunnett's multiple comparison test (SPSS 11.5.1 for Windows, 2002, SPSS Inc., USA), with values of $p < 0.05$ considered to indicate statistical significance.

3. Results

3.1. Cytotoxicity

The effect of safflower seed extract and cisplatin on the viability of human colorectal carcinoma RKO cells is shown in Figure 2. The cells were treated with the extract of safflower seed (100 μ g/mL), cisplatin (1.5 μ g/mL), or a combination of safflower seed extract (100 μ g/

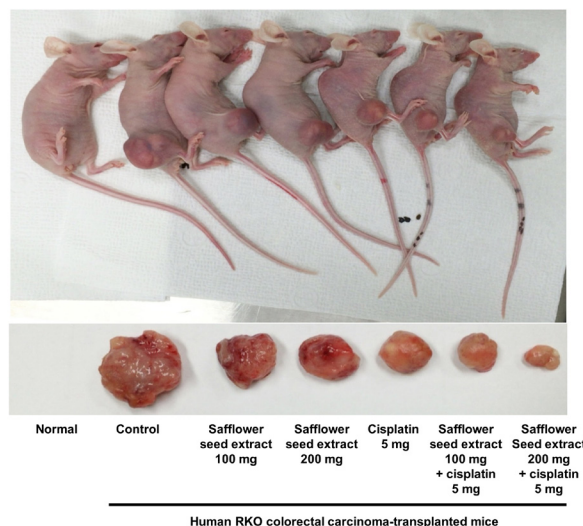


Figure 3. Xenograft mouse bearing RKO cell-derived human colorectal cancer.

mL) and cisplatin (1.5 μ g/mL). Treatment with safflower seed extract (100 μ g/mL) led to lower cell viability than that of untreated cells (Figure 2b). The changes in cell morphology induced by cisplatin are illustrated in Figure 2c. The combination treatment of safflower seed extract and cisplatin resulted in greater cell damage than the treatment of safflower seed extract or cisplatin alone (Figure 2d).

3.2. In vivo evaluation

Representative images of mice bearing RKO cell-derived human colorectal cancer xenografts are shown in Figure 3. In untreated mice bearing the xenografts (the control), the tumors weighed 1.57 ± 0.22 g, whereas the tumors in mice orally administered 100 and 200 mg/kg safflower seed weighed significantly less than the control tumors (0.94 ± 0.09 g and 0.91 ± 0.02 g, respectively). The tumor weight in cisplatin-treated mice was 51% lower than that in untreated and human RKO colorectal carcinoma-transplanted mice (0.70 ± 0.09 g), with greater reductions observed in mice co-administered safflower seed extract (0.52 ± 0.02 g and 0.43 ± 0.12 g, respectively), as shown in Figure 4. In addition, a significant increase in caspase 3 protein expression was observed in safflower seed-, cisplatin-,

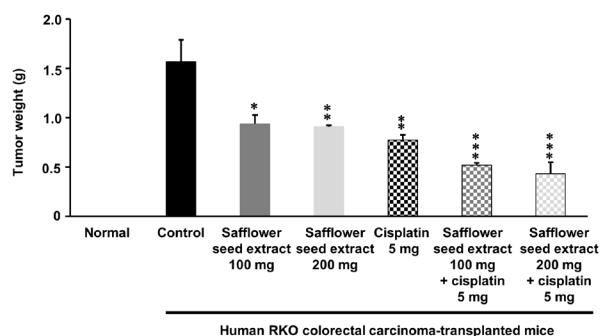


Figure 4. RKO cell-derived tumor weight. Data are the mean \pm SEM. Significance: * $p < 0.05$, ** $p < 0.01$, *** $p < 0.001$ vs. human RKO colorectal carcinoma-transplanted control mouse values.

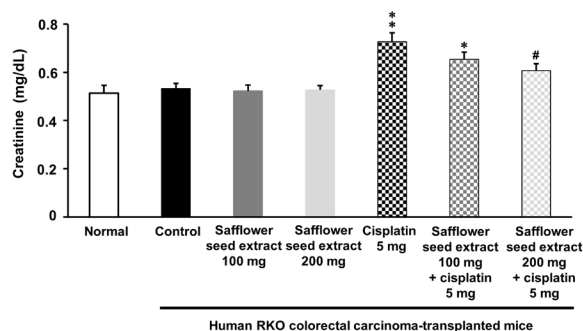


Figure 6. Serum creatinine level. Data are the mean \pm SEM. Significance: * $p < 0.05$, ** $p < 0.01$ vs. human RKO colorectal carcinoma-transplanted control mouse values; # $p < 0.05$ vs. human RKO colorectal carcinoma transplantation and cisplatin-treated mouse values.

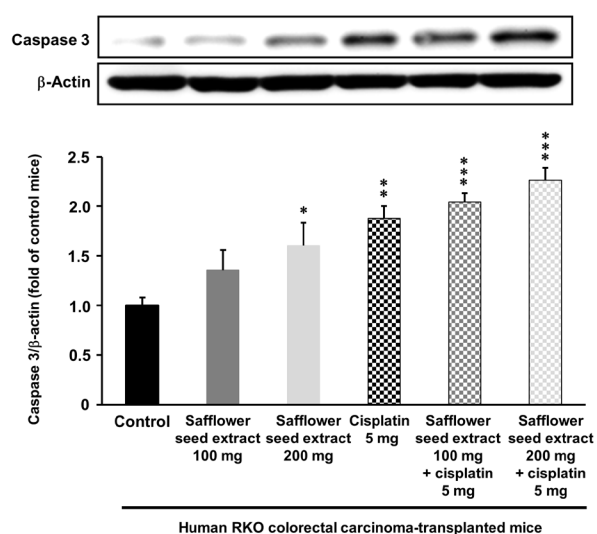


Figure 5. Caspase 3 protein expression in solid tumor. Data are the mean \pm SEM. Significance: * $p < 0.05$, ** $p < 0.01$, *** $p < 0.001$ vs. human RKO colorectal carcinoma-transplanted control mouse values.

and safflower seed plus cisplatin-treated mice compared with normal mice (Figure 5). Mice co-administered 200 mg/kg body weight safflower seed and cisplatin exhibited a more significant increase in caspase 3 protein expression. With regard to renal function, the mean serum creatinine concentration in cisplatin-treated mice (0.73 mg/dL) was markedly higher than the mean concentration in untreated mice (normal, human RKO colorectal carcinoma-transplanted control, or human RKO colorectal carcinoma-transplanted safflower seed-treated mice). However, the serum creatinine concentration of cisplatin-treated mice administered safflower seed extract decreased in a dose-dependent manner, as shown in Figure 6.

4. Discussion

Many therapeutic drugs have been developed and explored in clinical trials (13,14). Cisplatin is a potent

anticancer agent, with clinical activity against a wide spectrum of solid neoplasms and has been in use for many years (15). However, the therapeutic efficacy of cisplatin is limited by its toxicity to normal tissues, notably the kidneys, where it induces cell injury and death in renal tubular cells and leads to acute renal failure (16). Hayes *et al.* (17) reported that high concentrations of cisplatin, between 3 and 5 mg/kg, induced renal toxicity; in particular, dose of 5 mg/kg resulted in dose-limiting toxicities to the kidney, bone marrow, and the ear, and led to death. Hence, we selected 5 mg/kg cisplatin for the induction of renal toxicity in the present study.

Traditional herbs have an important role in the prevention or the reduction of the symptoms of side effects from drugs. Therefore, we explored the potential renoprotective pharmacological properties of oriental herbs. We investigated the efficacy of safflower seed extract in a previous study by using the swine kidney-derived cultured epithelial cell line, LLC-PK₁, which retains proximal tubule characteristics. The oral administration of safflower seed extract to cisplatin-treated mice exerted a pleiotropic effect on several oxidative stress- and apoptosis-related parameters and was also renoprotective (10). Safflower has been used in drugs with pharmacological activities for decades worldwide (18). Recent studies have reported that the safflower seeds exert potential anti-inflammatory, anti-oxidant, and anti-cancer activities (19-21). Bae *et al.* (21) showed that the methanolic extract of safflower seeds exhibited inhibitory effects on three cancer cell lines (HepG2, MCF-7, and Hela cells), indicating that safflower seed may be moderately cytotoxic to cancer cells. Therefore, it was suggested that safflower seed might have the potential to reduce nephrotoxicity and enhance the anticancer activity of cisplatin. This study was designed to evaluate the anticancer activity of safflower seed in addition to its effects on the therapeutic efficacy of cisplatin and cisplatin-induced nephrotoxicity in RKO cells and RKO-transplanted mice.

Safflower seed was reported to reduce the proliferation of four human colorectal cell lines (HCT116, SW480, LoVo, and HT-29) (11). In addition, the treatment of safflower seed was shown to result in a high survival cell rate of human colon carcinoma SW 620 cell line, which indicated the protective effect of safflower seed treatment on intestinal cancer (22). As described in the Methods section, the cells were cultured in the presence of safflower seed extract, cisplatin, or co-cultured with safflower seed extract and cisplatin. Culture in the presence of safflower seed resulted in a decrease of RKO cell viability. We also observed the anticancer effect of safflower seed extract in a mouse with tumor xenografts. As He *et al.* (23) had shown that the tumor volume increased after 2 weeks in a RKO cell xenograft mouse model, the present study evaluated whether safflower seed exerted a beneficial effect on the growth of RKO-transplanted mice at this time, and found that the administration of the extract significantly inhibited the growth of RKO cell-derived tumors. In addition, mice orally administered safflower seed extract prior to intraperitoneal cisplatin administration showed greater reductions in tumor weight.

Serum creatinine concentration is commonly used for the measurement of renal function (24). Although cisplatin is used widely for the treatment of cancer, the toxicity to the kidney cannot be ignored. In the present study, the mean serum creatinine concentration in cisplatin-treated mice was significantly higher than the mean concentration in untreated control mice, and was significantly decreased by the administration of 200 mg/kg safflower seed extract. Safflower seed extract therefore represents a promising herbal medicine for the prevention or inhibition of cisplatin-induced renal damage.

Although multiple signaling pathways are activated by cisplatin in renal tubular cells (25), the mechanism of renal cell death during cisplatin nephrotoxicity is unclear. Effective renoprotective intervention during cisplatin chemotherapy is currently lacking. Programmed cell death (apoptosis) is an essential physiological process that plays a critical role in cell development and tissue homeostasis. The progress of apoptosis is regulated by a series of signal cascades (26). Caspases are crucial mediators of apoptosis; in particular, caspase 3 is required for some typical hallmarks of apoptosis (26,27). The activation and function of caspases are regulated by various types of molecules, such as the inhibitor of apoptosis protein and the Bcl-2 family of proteins. Asselin *et al.* (28) indicated that cisplatin treatment in human ovarian epithelial cancer cells induced cleavage of caspase 3. Moreover, we have previously shown the ameliorative effect of safflower seed on cisplatin-induced renal damage in a mouse model *via* caspase 3 protein expression, which may be used as a basis for the present study (10). Therefore, we examined the expression of caspase 3 protein by using western blotting

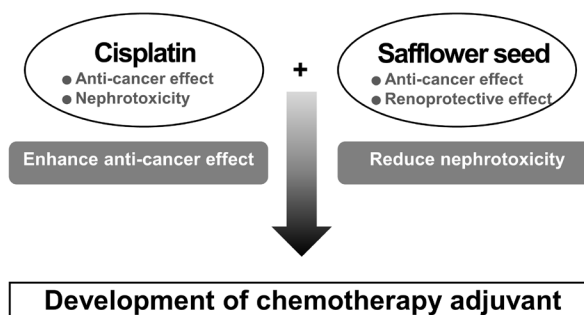


Figure 7. The potential of safflower seed as an adjuvant anticancer agent.

to clarify the responsible apoptotic-related proteins. We observed an increase in the expression of caspase 3 in the mouse xenograft model treated with safflower seed extract. These results contrasted with the inhibition of human colorectal tumor growth observed in mice bearing xenograft tumors.

As mentioned in the Introduction, traditional herbal medicines have emerged as one of the most important alternative therapies for cancer. We therefore believe that safflower seed extract may represent an effective nutritional supplement for cancer therapy. In this study, safflower seed extract was demonstrated as a potential adjuvant anticancer agent conferring protection against anticancer drug-induced toxicity without impairing the efficacy of chemotherapy (Figure 7).

5. Conclusion

Our results suggested that the reduction in tumor growth induced by safflower seed extract in RKO cells and mice bearing RKO xenografts was most likely associated with the chemical components, particularly the indolic phenols, *N*-(*p*-coumaroyl)serotonin and *N*-feruloyl serotonin, and the flavonoid luteolin-7-glucoside. Therefore, we will perform further characterization of the anticancer effects of the active compounds present in this extract and conduct a detailed investigation of the responsible molecular mechanisms.

Acknowledgements

This work was supported by grants from Rural Development Administration (Cooperative Research Program for Agriculture Science and Technology Development, Project no. PJ01312303), Republic of Korea.

References

1. John A, Al Kaabi S, Dweik N, *et al.* Emerging role for colorectal cancer screening in Asian countries. *Trop Gastroenterol.* 2014; 35:21-24.
2. Reddy BS, Kawamori T, Lubet R, Steele V, Kelloff G,

- Rao CV. Chemopreventive effect of *S*-methylmethane thiosulfonate and sulindac administered together during the promotion/progression stages of colon carcinogenesis. *Carcinogenesis*. 1999; 20:1645-1648.
3. Ijaz S, Akhtar N, Khan MS, Hameed A, Irfan M, Arshad MA, Ali S, Asrar M. Plant derived anticancer agents: a green approach towards skin cancers. *Biomed Pharmacother*. 2018; 103:1643-1651.
 4. Nishino H, Tokuda H, Satomi Y, Masuda M, Onozuka M, Yamaguchi S, Takayasu J, Tsuruta J, Takemura M, Ii T, Ichiishi E, Kuchide S, Okuda M, Murakoshi M. Cancer chemoprevention by phytochemicals and their related compounds. *Asian Pacific J Cancer Prev*. 2000; 1:49-55.
 5. Han SY, Li HX, Ma X, Zhang K, Z. Z. Ma ZZ, Tu PF. Protective effects of purified safflower extract on myocardial ischemia *in vivo* and *in vitro*. *Phytomedicine*. 2009; 16:694-702.
 6. Li HX, Han SY, Wang XW, Ma X, Zhang K, Wang L, Ma ZZ, Tu PF. Effect of the carthamins yellow from *Carthamus tinctorius* L. on hemorheological disorders of blood stasis in rats. *Food Chem Toxicol*. 2009; 47:1797-1802.
 7. Lin WC, Lai MT, Chen HY, Ho CY, Man KM, Shen JL, Lee YJ, Tsai FJ, Chen YH, Chen WC. Protective effect of *Flos carthami* extract against ethylene glycol-induced urolithiasis in rats. *Urol Res*. 2012; 40:655-661.
 8. Mandade R, Sreenivas SA, Wanare R. Antiulcer screening of *Carthamus tinctorius* on volume and acidity of stimulated gastric secretion in rats. *J Pharmacol Pharmacother*. 2012; 3:185-188.
 9. Miyaoka R, Monga M. Use of traditional Chinese medicine in the management of urinary stone disease. *Int Braz J Urol*. 2009; 35:396-405.
 10. Park CH, Lee AY, Kim JH, Seong SH, Jang GY, Cho EJ, Choi JS, Kwon J, Kim YO, Lee SW, Yokozawa T, Shin YS. Protective effect of safflower seed on cisplatin-induced renal damage in mice *via* oxidative stress and apoptosis-mediated pathways. *Am J Chin Med*. 2018; 46:157-174.
 11. Park GH, Hong SC, Jeong JB. Anticancer activity of the safflower seeds (*Carthamus tinctorius* L.) through inducing cyclin D1 proteasomal degradation in human colorectal cancer cells. *Korean J Plant Res*. 2016; 29:297-304.
 12. Komatsu S. Extraction of nuclear proteins. *Methods Mol Biol*. 2007; 355:73-77.
 13. Lipson EJ, Forde PM, Hammers HJ, Emens LA, Taube JM, Topalian SL. Antagonists of PD-1 and PD-L1 in cancer treatment. *Semin Oncol*. 2015; 42:587-600.
 14. Salazar R, Ciardiello F. Optimizing anti-EGFR therapy in colorectal cancer. *Clin Cancer Res*. 2015; 21:5415-5416.
 15. Boulikas T, Vougiouka M. Cisplatin and platinum drugs at the molecular level. *Oncol Rep*. 2003; 10:1663-1682.
 16. Arany I, Safirstein RL. Cisplatin nephrotoxicity. *Semin Nephrol*. 2003; 23:460-464.
 17. Hayes DM, Cvitkovic E, Golbey RB, Scheiner E, Helson L, Krakoff IH. High dose cis-platinum diammine dichloride. Amelioration of renal toxicity by mannitol diuresis. *Cancer*. 1977; 39:1372-1381.
 18. Asgarpanah J, Kazemivash N. Phytochemistry, pharmacology and medicinal properties of *Carthamus tinctorius* L. *Chin J Integr Med*. 2013; 19:153-159.
 19. Bae SJ, Shim SM, Park YJ, Lee JY, Chang EJ, Choi SW. Cytotoxicity of phenolic compounds isolated from seeds of safflower (*Carthamus tinctorius* L.) on cancer cell lines. *Food Sci Biotechnol*. 2002; 11:140-146.
 20. Koyama N, Kuribayashi K, Seki T, Kobayashi K, Furuhashi Y, Suzuki K, Arisaka H, Nakano T, Amino Y, Ishii K. Serotonin derivatives, major safflower (*Carthamus tinctorius* L.) seed antioxidants, inhibit low-density lipoprotein (LDL) oxidation and atherosclerosis in apolipoprotein E-deficient mice. *J Agric Food Chem*. 2006; 54:4970-4976.
 21. Kim DH, Moon YS, Park TS, Son JH. Serotonins of safflower seeds play a key role in anti-inflammatory effect in lipopolysaccharide-stimulated RAW 264.7 macrophages. *J Plant Biotechnol*. 2015; 42:364-369.
 22. Arpornsuwan T, Petvises S, Thim-uam A, Boondech A, Roytrakul S. Effects of *Carthamus tinctorius* L. solvent extracts on anti-proliferation of human colon cancer (SW 620 cell line) *via* apoptosis and the growth promotion of lymphocytes. *Songklanakarin J Sci Technol*. 2012; 34:45-51.
 23. He XW, Feng T, Yin QL, Jian YW, Liu T. NOB1 is essential for the survival of RKO colorectal cancer cells. *World J Gastroenterol*. 2015; 21:868-877.
 24. Perrone RD, Madias NE, Levey AS. Serum creatinine as an index of renal function: new insights into old concepts. *Clin Chem*. 1992; 38:1933-1953.
 25. Zhuang S, Schnellmann RG. A death-promoting role for extracellular signal-regulated kinase. *J Pharmacol Exp Ther*. 2006; 319:991-997.
 26. Fan TJ, Han LH, Cong RS, Liang J. Caspase family proteases and apoptosis. *Acta Biochim Biophys Sin*. 2005; 37:719-727.
 27. Porter AG, Jänicke RU. Emerging roles of caspase-3 in apoptosis. *Cell Death Differ*. 1999; 6:99-104.
 28. Asselin E, Mills GB, Tsang BK. XIAP regulates Akt activity and caspase-3-dependent cleavage during cisplatin-induced apoptosis in human ovarian epithelial cancer cells. *Cancer Res*. 2001; 61:1862-1868.

(Received November 11, 2019; Revised December 20, 2019; Accepted December 22, 2019)

Methanol extract of *Lonicera caerulea* var. *emphylocalyx* fruit has anti-motility and anti-biofilm activity against enteropathogenic *Escherichia coli*

Masaaki Minami^{1,*}, Hiroshi Takase², Mineo Nakamura³, Toshiaki Makino⁴

¹ Department of Bacteriology, Graduate School of Medical Sciences, Nagoya City University, Nagoya, Japan;

² Core Laboratory, Graduate School of Medical Sciences, Nagoya City University, Nagoya, Japan;

³ Nakamura Pharmacy, Sapporo, Japan;

⁴ Department of Pharmacognosy, Graduate School of Pharmaceutical Sciences, Nagoya City University, Nagoya, Japan.

Summary

Foodborne diseases have become a worldwide problem that threatens public health and welfare. Enteropathogenic *Escherichia coli* (EPEC) is one of major pathogens of moderate to severe diarrhea. The increased prevalence of EPEC strains that produce extended spectrum β -lactamase (ESBL) has deepened the problem. The fruit of *Lonicera caerulea* var. *emphylocalyx* (LCE) has been used as a traditional food preservative and medicine in northern temperate zones such as Hokkaido Island, Japan. In this study, we investigated the antibacterial effect of LCE fruit extract (LCEE) against EPEC. The antibacterial activities of LCEE were examined by bacterial growth, time-kill curve, soft-agar motility, electron microscopy, and 96 well-microplate biofilm assays. We also investigated the bacterial mRNA expression of biofilm-associated genes (*fliC*, *csgA*, and *fimA*) by quantitative real-time PCR assays. LCEE was found to suppress the growth, time-kill curve, and spread of EPEC. It also reduced the biofilm formation in a dose-dependent manner. Morphological analysis using transmission and scanning electron microscopy revealed that LCEE diminished the function of flagella resulting in reduced motility and biofilm formation. The mRNA expression of all three biofilm associated genes was downregulated under LCEE treatment. Extracts of the fruit of LCE inhibit the motility and biofilm formation of EPEC as a result of the inhibition of flagella development and function. We propose LCEE as a therapeutic candidate for the effective therapy of EPEC-associated infectious diseases.

Keywords: *Lonicera caerulea* var. *emphylocalyx*, EPEC, biofilm, flagellar, electron microscopy

1. Introduction

WHO defines foodborne diseases as the infection or poisoning of human bodies, usually due to pathogens that enter the body through ingestion (1). These diseases have become a worldwide problem that threatens public health and well-being, and are therefore attracting an increasing level of attention. Along with these health issues, they also seriously impact the economic

interests of society. Children are especially vulnerable to foodborne diseases; according to a WHO report, approximately 1.5 billion children aged less than 5 years contract diarrhea globally each year, resulting in more than 2.5 million deaths (1). Of these, 70% are caused by the biological contamination of foods. The morbidity of foodborne diseases in the under-5 years is higher than that of the other age groups (1). *Escherichia coli* represents a particular problem as a common contaminant of food, even in developed countries (2).

Enteropathogenic *E. coli* (EPEC) is a leading cause of moderate to severe diarrhea in young children, especially in developing countries (3). EPEC has only a human reservoir of infection (4). The increased prevalence of EPEC strains that produce extended

*Address correspondence to:

Dr. Masaaki Minami, Department of Bacteriology, Graduate School of Medical Sciences, Nagoya City University, 1 Kawsumi, Mizuho-ku, Nagoya, 467-8601, Japan.

E-mail: minami@med.nagoya-cu.ac.jp

spectrum β -lactamase has led to a growing interest in the development of non-antibiotic treatment options (5,6).

Lonicera caerulea var. *emphylocalyx* (LCE) belongs to the honeysuckle family, and its fruits are known as edible berries. LCE grows in northern temperate zones such as Hokkaido (northern Japan), northern China, Korea, and Russia. It is currently commercially produced in Japan and Russia, although the fruits have been as a traditional food preservative and medicinal agent (7). Fresh fruit juice is often used as a general strengthening agent, and therefore has potential in the treatment of stomach diseases and tonsillitis due to its antiseptic properties (8). However, the mode of action and efficacy of the juice remains unclear. In recent years, numerous studies have investigated the therapeutic effects of berries in the prevention of a range of diseases (7). In addition, herbal medicine products have invoked an increasing interest. Berries contain several important health-supporting phytochemicals that are an important part of the human diet (9). They also contain carbohydrates, lipids, proteins, organic acids, ascorbic acid, vitamin B, magnesium, phosphorus, calcium and potassium, as well as other minor compounds (10). Moreover, berries have antitumorigenic, antimicrobial, anti-inflammatory and antimutagenic properties (11). Although the antibacterial effect of LCE fruit toward *E. coli* has been demonstrated, the mode of action of LCE has yet to be elucidated completely (12). We therefore hypothesized that LCE exhibits antibacterial activity toward *E. coli*. The aim of this study was to evaluate a methanol extract of LCE fruits (LCEE) as a novel candidate for anti-EPEC therapy.

2. Materials and Methods

2.1. Preparation of LCEE

LCE fruits were cultivated in marshy grassland of Atsuma-Town, Hokkaido, Northern Japan in 2017. Voucher specimens were preserved in the Department of Pharmacognosy, Graduate School of Pharmaceutical Sciences, Nagoya City University. The LCEE was used in our previous study which included a fingerprint pattern and content of marker compounds (13). LCEEs were dissolved in water to a concentration of 200 mg/mL, and stored at -20°C .

2.2. Preparation of bacteria

EPEC strain E2348/69, which was kindly provided by Dr. James Kaper, was used in this study. A fresh colony was inoculated onto LB agar (Sigma-Aldrich, St. Louis, MO, USA) and cultured for 16 h at 37°C . The bacteria were harvested, centrifuged and resuspended in sterile phosphate-buffered saline (0.15 M, pH 7.2,

PBS). Bacterial density was determined by measuring absorbance at 600 nm (A600). The bacterial suspension was then diluted to 10^9 cells/mL in PBS using a standard growth curve to relate absorbance to bacterial concentration.

2.3. Growth of EPEC

Prior to broth culture analysis, the bacteria were pre-incubated in LB agar for 24 h. To assess growth-inhibitory activity, the bacteria (10^6 cells/mL) were incubated in 5 mL polypropylene tubes (As-One, Osaka, Japan) containing 2 mL LB medium with the LCEE (0.5, 1, and 2 mg/mL). After 24 h, bacterial growth was determined by CFU counts. Aliquot of bacterial culture were plated onto LB agar for 24 h and CFU counts were evaluated. We also performed ^3H -thymidine uptake assay as measurement of bacterial growth. After 24 h of pre-incubation, ^3H -thymidine (2.0 Ci/mmol; PerkinElmer, MA, US) was added to LB medium in the polypropylene tubes. After culturing for 24 h, the cells were adsorbed onto 0.45 μm membrane filters (Advantech Japan, Tokyo, Japan), washed with distilled water, and then dried. The filters were transferred to vials containing liquid scintillator cocktail, and the radioactivity was measured with a liquid scintillation counter (LSC-6100, Hitachi Aloka Medical, Tokyo, Japan). All procedures were performed in triplicate.

2.4. Time-kill analysis

A time-kill analysis was performed as described previously (14). LB medium containing LCEE (0.5, 1, 2 mg/mL) or ampicillin sodium (ABPC) (50 μg /mL) (Fujifilm-Wako Pure Chemical, Osaka, Japan), was inoculated with bacterial suspension at a final concentration of 1×10^8 CFU/mL in triplicate. Aliquots of undiluted and 10-fold serially diluted samples were then plated onto LB agar at both 0 and 60 min after inoculation and the plates were incubated at 37°C for 24 h. The resulting colonies (number of CFUs) were then counted.

2.5. Motility analysis of EPEC

Motility was evaluated by inoculating stationary-phase *E. coli* (10^6 cells) onto the center of a 24-well polystyrene motility plate. LB containing 0.2% (w/v) agar and LCEE (0.5, 1, or 2 mg/mL) was then added. Plates were incubated at 37°C for 24 h, after which the diameters of the colonies were measured (an indication of bacterial migration). Motility assays were performed at least three times on separate days (15).

2.6. Electron microscopic analysis

Bacterial morphology was investigated using a

transmission electron microscope (TEM) and scanning electron microscope (SEM). Bacteria (10^6 cells) pre-treated with LCEE (0.5, 1, 2 mg/mL) were cultured in LB broth for 24 h. Then, approximately one drop of the culture was applied to a Formvar/carbon-coated 300-mesh copper grid (Nisshin EM, Tokyo, Japan). Excess solution was removed and 2% phosphotungstic acid (PTA) (Fujifilm-Wako Pure Chemical) was added for negative staining. The samples were then observed under a TEM (JEM1011J; JEOL, Tokyo, Japan) and digital images were taken with a MegaView Slow-scan camera (JEOL). The square of bacterial shape was measured using NIH Image J, and areas were measured at five arbitrary points in bacterial cells treated with LCEE. Preparation of samples for SEM analysis was performed at first. Briefly, bacterial cells (10^6 cells) pre-treated with LCEE (0.5, 1, or 2 mg/mL) were cultured in LB broth for 24 h. The samples were then immediately fixed in 0.1 M phosphate buffer (pH 7.4) containing 2.5% glutaraldehyde (Nisshin EM, Tokyo, Japan) for 24h at 4°C. The samples were rinsed twice with 0.1 M phosphate buffer, further fixed using 2% osmium tetroxide (Nisshin EM) for 2h at room temperature, and finally rinsed with distilled water. Next, the specimens were dehydrated using serial concentrations of ethyl alcohol (30, 50, 70, 90, 95 and 100%) for 30 min each, followed by immersion in absolute alcohol for a further 30 min. The specimens were dried using a critical point dryer CPD300 (Leica, Wetzlar, Germany). Carbon conductive paint was used for mounting for the specimens which were coated with osmium (NL-OPC-AJ, Filgen, Nagoya, Japan). Finally, several areas of each sample were systematically scanned using a SEM (S-4800; Hitachi High-Technologies. Co, Tokyo, Japan).

2.7. Biofilm analysis

Overnight cultures of *E. coli* were inoculated into each of a 96-well polystyrene plate (Thermo Fisher Scientific, MA, US) to achieve a bacterial concentration of 10^6 cells. The wells contained LB broth with or without LCEE (0.5, 1, or 2 mg/mL). Incubation was allowed at 37°C for 48 h. After removal of the media, the plates were washed three times with PBS, and adherent bacteria stained with 0.2% crystal violet at room temperature for 10 min, before being gently washed a further three times with PBS. The biofilms were quantitated by measuring absorbance at 570 nm (A570). Wells incubated without bacteria were used as controls. The absorbance values from the control wells were subtracted from the test values.

2.8. Total RNA extraction, cDNA synthesis, and quantitative real-time PCR (qPCR) analysis

The bacteria (10^6 cells/mL) were incubated in LB medium with the LCEE (2 mg/mL) for 8 h. Bacterial

cells were washed three times with PBS and RNA samples were prepared with RNeasy Protect Bacteria Mini Kit (Qiagen, Hilden, Germany) according to the enclosed protocol. RNA samples were quantitated with the NanoDrop ND-1000 (Thermo Fisher Scientific, Inc., Waltham, MA). cDNA was synthesized with ReverTra Ace qPCR RT Master Mix (Toyobo Co., Ltd., Osaka, Japan) according instruction. qPCR for the quantification of cDNA was executed with the Thunderbird qPCR Mix (Toyobo) and Applied Biosystems 7900HT Fast Real Time PCR System (Thermo Fisher Scientific) according to the procedure recommended by the manufacturer. The primers designed for qPCR are described elsewhere (16). The following PCR conditions were used: 50°C for 2 min, 95°C for 10 min; 40 cycles of 95°C for 30 s and 60°C for 1 min; followed by 95°C for 15 s, 55°C for 15 s, and 95°C for 15 s. The glyceraldehyde-3-phosphate dehydrogenase (*gapA*) gene was used as an internal control for normalization. The fold changes in the flagellin (*fliC*), major curli subunit (*csgA*), and major type 1 subunit fimbria (*fimA*) expression levels were calculated by the comparative cycle threshold (CT) method.

2.9. Statistical analysis

Experimental data was expressed as mean \pm standard deviation (S.D.). Statistical analysis was conducted using Student's *t*-test between two groups and Tukey's multiple comparison tests for the differences among multiple groups. A probability value less than 0.05 was considered to represent a statistical significance.

3. Results

3.1. Growth of EPEC

Initially, we examined the effect of LCEE on the growth of *E. coli*. Figure 1 showed the absorbance readings of 24 h culture solutions treated with different concentrations of LCEE. The data clearly showed that the decrease in absorbance is proportional to an increase in LCEE concentration. The effect of LCEE on the proliferative ability of EPEC was examined by a thymidine uptake test. Figure 2 showed the tritium value of thymidine concentration for a 24 h culture containing LCEE and thymidine. The tritium value clearly decreases in parallel with an increase in LCEE concentration. These results also confirmed that the growth of *E. coli* was suppressed in the presence of LCEE in a dose-dependent manner.

3.2. Time-kill analysis

We also examined the time-kill effects of LCEE on EPEC. A significant bacterial reduction was observed after 60 min of treatment with LCEE in dose-dependent

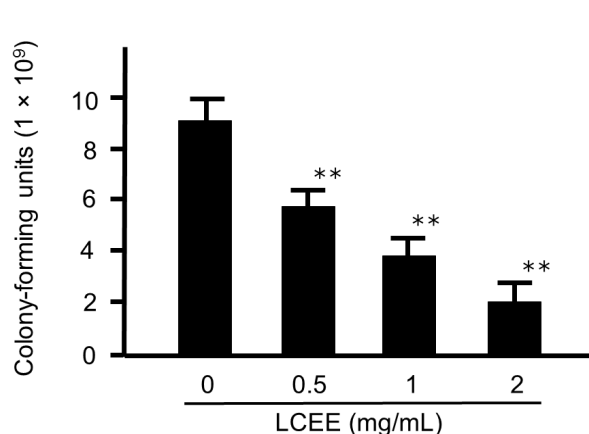


Figure 1. Growth-inhibitory effects of LCEE against *E. coli*. *E. coli* was treated with LCEE (0, 0.5, 1, or 2 mg/mL) for 24 h. Bacterial growth was determined by CFU counts. The data represents the mean \pm S.D. ($n = 6$). ** $p < 0.01$ vs. the untreated group, according to Tukey's multiple comparison test.

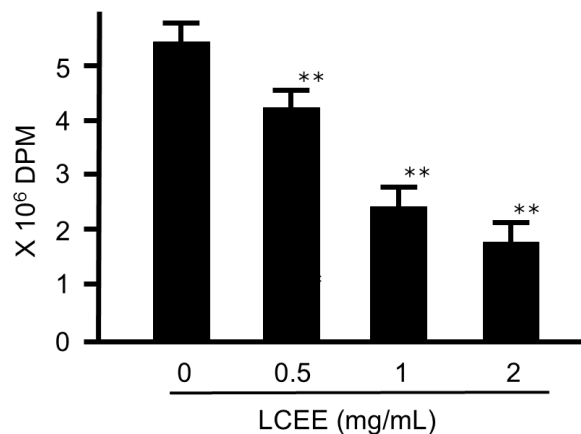


Figure 2. Bacterial growth by ³H-thymidine-uptake assay. *E. coli* was treated with LCEE (0, 0.5, 1, or 2 mg/mL) for 24 h. ³H-thymidine uptake was measured using a liquid scintillation counter. The data represents the mean \pm S.D. ($n = 6$). ** $p < 0.01$ vs. the untreated group, according to Tukey's multiple comparison tests.

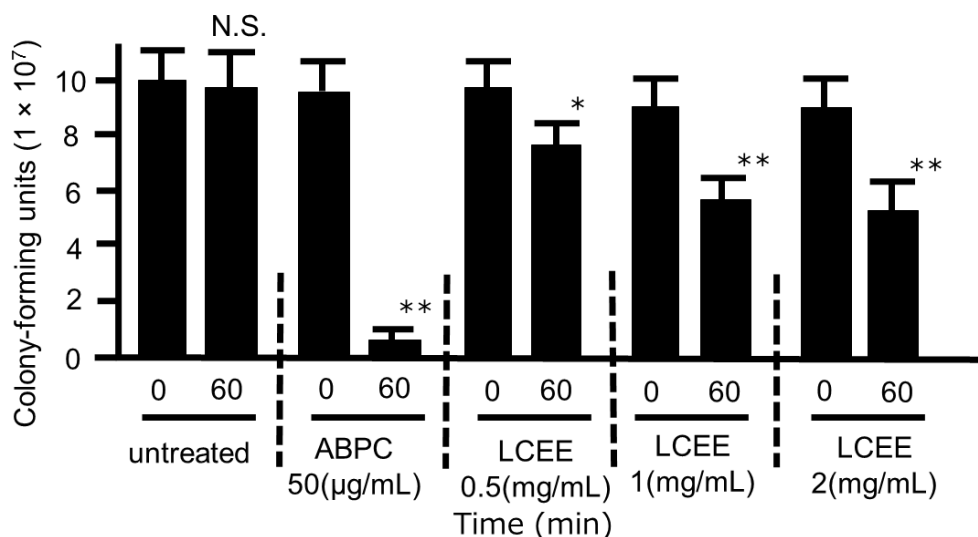


Figure 3. Time-kill analysis of LCEE against *E. coli*. *E. coli* (1×10^8 colony-forming units) was treated with ampicillin sodium (ABPC; 50 μ g/mL), LCEE (0.5, 1, 2 mg / mL) for 60 min, and the number of colony-forming units was then counted. Data represent the numbers of viable cells in a culture medium. Data represent means \pm SD ($n = 6$). * $p < 0.05$, ** $p < 0.01$ vs. each 0 min group (Student's *t*-test).

manner. However, this antibacterial effect of LCEE could not reduce the number of bacteria to less than one-tenth, such as ABPC, even if the concentration of LCEE was increased (Figure 3).

3.3. Motility analysis of EPEC

We then examined the effect of LCEE on motility, a fundamental factor that enhances the pathogenicity of bacteria. The spread of *E. coli* after 24 h of incubation was found to be inhibited when grown in media that contained LCEE (Figure 4A). A decrease in the diameter of the spread zone was found to parallel an increase in LCEE concentration to a significant degree (Figure 4B).

3.4. Bacterial morphology analysis of EPEC

To elucidate the mechanism of motility inhibition, we examined the effect of LCEE on *E. coli* morphology using electron microscopy. Negative staining revealed that the number of flagella decreased with an increase in LCEE concentration; no flagella were observed at a LCEE concentration of 1 mg/mL (Figure 5A). In addition, the morphology of *E. coli* also increased at a LCEE concentration of 1 mg/mL and over. The cell area of *E. coli* also increased significantly under LCEE treatment (Figure 5B). This observation was also corroborated by SEM, which confirmed that an LCEE concentration of 1 mg/mL led to an increase in morphology. Similarly, SEM analysis revealed

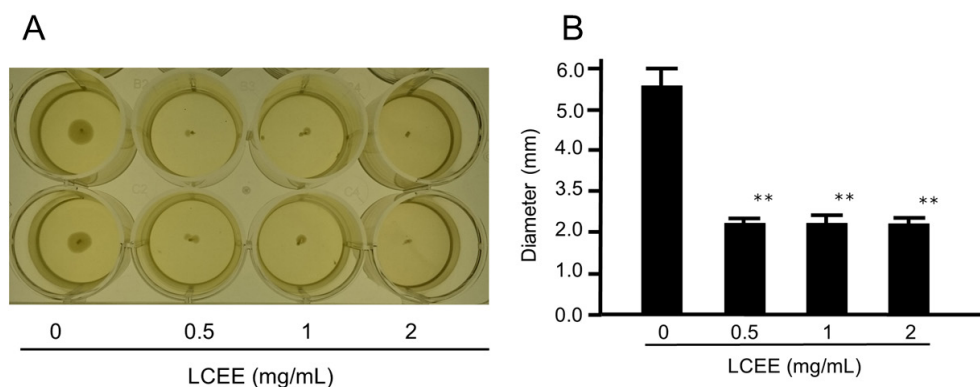


Figure 4. (A) Representative image of *E. coli* motility. (B) Bacterial spread through motility. *E. coli* was treated with LCEE (0, 0.5, 1, or 2 mg/mL) for 24 h. The data represents the mean \pm S.D. ($n = 6$). ** $p < 0.01$ vs. the untreated group, according to Tukey's multiple comparison test.

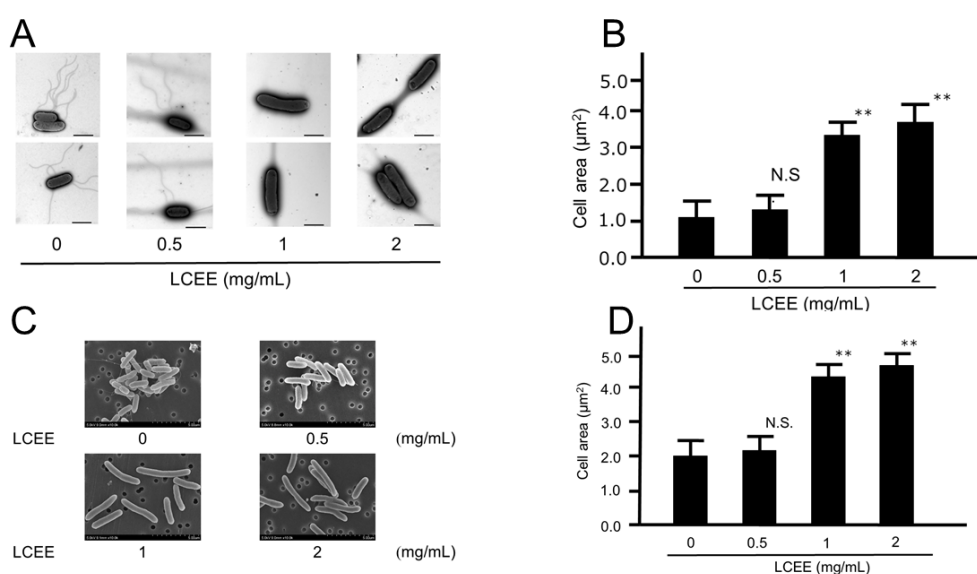


Figure 5. Morphological changes in *E. coli* following treatment with LCEE. Representative TEM (A) and SEM (C) images of *E. coli* following treatment with LCEE. (A) The bars represent 1 μm . The diameter of *E. coli* cells treated with LCEE for 24 h was determined from images obtained using TEM (B) and SEM (D). *E. coli* was treated with LCEE (0, 0.5, 1, or 2 mg/mL) for 24 h. Data represent means \pm S.D. ($n = 6$). ** $p < 0.01$ vs. the control group, according to Tukey's multiple comparison tests. NS: not significant.

an increase in the cell area of *E. coli* due to LCEE treatment (Figures 5C and 5D).

3.5. Biofilm analysis of EPEC

As flagellum was one of important factors of biofilm, the effect of LCEE on biofilm formation as another bacterial virulence was also examined. Crystal violet staining assay showed that biofilm formation decreased in parallel with an increase in LCEE levels (Figure 6A), with a corresponding reduction in the absorbance of the biofilm staining solution (Figure 6B).

3.6. qPCR analysis

Finally, we performed qPCR assay whether the flagella associated genes of EPEC were affected by LCEE.

Our results demonstrated that all of the target genes (*fliC*, *csaA*, and *fimA* genes) were downregulated in expression when bacteria were treated with LCEE significantly. Decreased these genes expression with less than 2-fold lower was observed in the presence of LCEE ($p < 0.01$) (Figure 7).

4. Discussion

This study was designed to investigate the effect of fruit of the LCE on EPEC. Our result revealed that LCEE prepared from the fruits showed significant anti-motility and anti-biofilm actions even if the antibacterial effect of LCEE was limited compared to antibiotics. Furthermore, in morphological analysis, LCEE treated bacteria were swelling and lack of flagella, these morphological changes may contribute

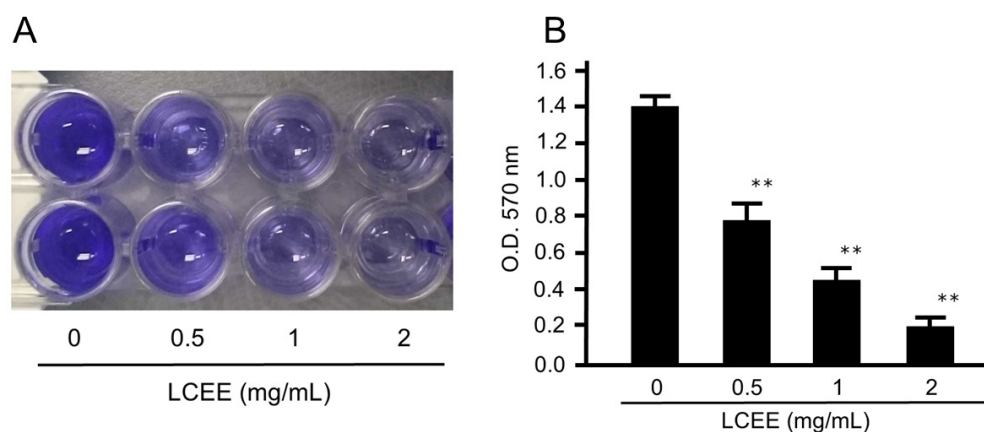


Figure 6. LCEE inhibition of *E. coli* biofilm formation. (A) Representative image of the microplate. (B) *E. coli* was treated with LCEE (0, 0.5, 1, or 2 mg/mL), and the anti-biofilm activity was quantified by crystal violet adsorption at an optical density (O.D.) of 570 nm. The data represents the mean \pm S.D. ($n = 6$). $**p < 0.01$ vs. the control group, according to Tukey's multiple comparison tests.

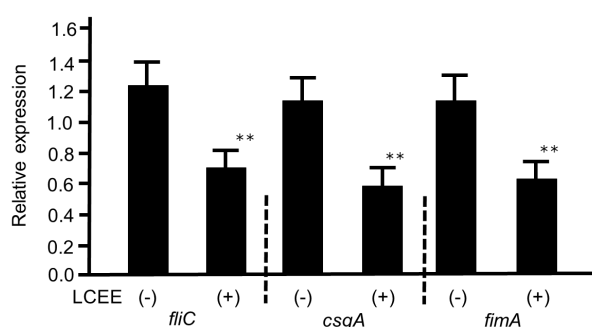


Figure 7. Expression of genes responsible for biofilm formation in EPEC after 8 h under LCEE treatment. Relative mRNA quantities were normalized to that of a housekeeping gene, *gapA*. The data represents the mean \pm S.D. ($n = 6$). $**p < 0.01$ vs. the control group, according to Student's *t*-test.

to the inhibition of bacterial motility. The LCEE fruit will be very useful agent that can be expected for future medical applications against EPEC infectious disease.

Several researchers have described the anti-biofilm effect of extracts from *Lonicera* species. The freeze-dried fruit of *Lonicera caerulea* and its phenolic fraction reduced the biofilm formation and adhesion to the artificial surface of *Candida parapsilosis*, *Staphylococcus epidermidis*, *Enterococcus faecalis*, *Streptococcus mutans* and *E. coli* (12). The fruit of *Lonicera caerulea* also had anti-bacterial and anti-biofilm effects on *Streptococcus pyogenes* *in vitro* (13). As extracts from *Lonicera alpigena* exhibited the biofilm inhibition, limited bacteriostatic activity was also evident (17). However, this study did not reveal the mechanism of anti-biofilm action by molecular biological analysis and morphological evaluation (12). Our analysis results focus on these points.

A biofilm is a highly structured immobile complex entrenched with bacterial communities in an extracellular matrix of exopolysaccharide, along with

proteins and DNA. It is also used to describe matrix-enclosed bacterial population's adherent to each other and to surface (18). Bacterial strains that adhere onto medical devices or damaged tissue can cause persistent infections through biofilm formation. Antibiotics may not be effective when the bacteria form a biofilm even if showing a high level of activity against the planktonic bacterial cells. The formation of a bacterial biofilm often inhibits the activity of an antimicrobial agent (19). Thus, novel drugs which have the ability to target these bacteria are urgently desired.

Flagella as a bacterial virulence factor have three mechanisms of involvement in biofilm formation. Firstly, flagella are required for physical attachment to abiotic surfaces, thus promoting the initiation of biofilm formation. Secondly, motility may enable a bacterium to reach the surface or developing biofilm. Thirdly, motility is thought to allow the bacteria to move within a developing biofilm, thereby enhancing growth and spread of the biofilm (20). Moreover, the process of chemotaxis allows bacteria to swim toward nutrients that are present on a surface. Motility promotes initial cell-to-surface contact and may also contribute to the spread of a growing biofilm along an abiotic surface (18). Flagellated bacteria can adapt their locomotion machinery to achieve a specialized form of flagellum-driven motility when grown on solid surfaces. This motility is characterized by a multicellular movement of bacteria that migrate over solid substrates in groups of tightly bound cells (14). This kind of movement is dependent on the ability of surface-adhering bacteria to undergo a differentiation process characterized by the production of more flagellated than planktonic cells. Thus, this behavioral response to the surface provides flagellated bacteria with the ability to act as a multicellular community that can rapidly colonize nutrient-rich solid substrates (15). Most of the motility-negative mutants tested

were found to be severely defective in their ability to form a biofilm. This mechanism is mainly related to *fli* gene cluster including *fliC*. Thus, we tried to check the mRNA expression of biofilm-associated genes under LCEE treatment. Our study showed that genes involved in adhesion (*csgA* and *fimA*), and motility (*fliC*) were expressed significantly lower in EPEC in the presence of LCEE. Expression of *csgA* in bacterial cells that adhered to cell cultures was similar to that observed for bacteria on abiotic surfaces. This structure might play an important role in increasing bacterial attachment. Other reports have shown that curli fimbriae are also required for biofilm formation and bacterial autoaggregation (21,22). Furthermore, this curli fimbriae associated gene, the *fimA* gene, was possible involved in initial attachment. Previous studies have also demonstrated that *fimA* induction in planktonic cells during the process of *E. coli* biofilm formation (23,24). Our results demonstrated that the mRNA expression of these three biofilm associated genes in EPEC were decreasing under LCEE treatment. The decrease in those gene expression may induce the disappearance of flagella and the like, thereby reducing bacterial motility and biofilm formation. Our results highlight the crucial role of motility in biofilm formation; the non-motile strains were unable to form biofilms. LCEE-treated EPEC cells that lack flagella have a reduced ability to form a biofilm.

Several previous reports have also described the antibacterial effect of extracts of *Lonicera* species on *E. coli*. The monoterpenoids isolated from the dried flower buds of *L. japonica* exhibited antibacterial activities against *E. coli* (25). Xiong demonstrated that these compounds were identified as 3, 5-bis-O-caffeoyl quinic acid, 4, 5-bis-O-caffeoylquinic acid, luteoloside, 3-O-caffeoylquinic acid and secoxyloganin (26). Yang demonstrated an enhanced antimicrobial activity of silver nanoparticles- *L. japonica* combo against *E. coli* (27). Myricetin and quercitrin, derived from cranberries, can significantly decrease uropathogenic *E. coli* biofilm formation, while dihydroferulic acid glucuronide, procyanidin A dimer, quercetin glucoside, myricetin, and prodelfinidin B are known to decrease surface hydrophobicity (28). Although the growth or the production of bacterial effector proteins of the type III secretion system of EPEC was unaffected by proanthocyanidins, inhibition of EPEC pedestal formation was observed (29). Previous study demonstrated the antibacterial effect of cranberry against uropathogenic *E. coli*. It showed that the expression of the *fliC* gene in this bacterial species is inhibited by proanthocyanidins. It explained that bacterial motilities were hindered in the presence of proanthocyanidins (30). LCEE also suppresses the motility and biofilm formation of *E. coli*, however, a full mechanism of activity toward the bacteria cannot be confirmed at present. Proanthocyanidins from LCE

may be as deeply involved in this mechanism of action as cranberry. Further clarification of the mechanism of action of these compounds would facilitate their development as novel antimicrobial agents.

In conclusion, the extracts of the fruit of LCE inhibit the motility and biofilm formation of EPEC as a result of the inhibition of flagella development and function. We propose LCEE as a therapeutic candidate for the effective therapy of EPEC-associated infectious diseases.

Acknowledgements

This study was partly supported by JSPS KAKENHI Grant Number JP16K09251. The authors thank Mr. Masashi Ishihara and Ms. Miwako Fujimura for their excellent support through this investigation.

References

1. Guo S, Lin D, Wang LL, Hu HL. Monitoring the results of foodborne diseases in Sentinel hospitals in Wenzhou city, China from 2014 to 2015. Iran J Public Health. 2018; 47:674-681.
2. Yang SC, Lin CH, Aljuffali IA, Fang JY. Current pathogenic *Escherichia coli* foodborne outbreak cases and therapy development. Arch Microbiol. 2017; 199:811-825.
3. Ochoa TJ, Contreras CA. Enteropathogenic *Escherichia coli* infection in children. Curr Opin Infect Dis. 2011; 24:478-483.
4. Hartland EL, Leong JM. Enteropathogenic and enterohemorrhagic *E. coli*: ecology, pathogenesis, and evolution. Front Cell Infect Microbiol. 2013; 3:15.
5. Islam MA, Amin MB, Roy S, et al. Fecal colonization with multidrug-resistant *E. coli* among healthy infants in rural bangladesh. Front Microbiol. 2019; 10:640.
6. Cointe A, Birgy A, Mariani-Kurkdjian P, Liguori S, Courroux C, Blanco J, Delannoy S, Fach P, Loukiadis E, Bidet P, Bonacorsi S. Emerging multi drug-resistant hybrid pathotype shiga toxin-producing *Escherichia coli* O80 and related strains of clonal complex 165, Europe. Emerg Infect Dis. 2018; 24:2262-2269.
7. Svarcova I, Heinrich J, Valentova K. Berry fruits as a source of biologically active compounds: the case of *Lonicera caerulea*. Biomed Pap Med Fac Univ Palacky Olomouc Czech Repub. 2017; 151:163-174.
8. Jurikova T, Rop O, Mlcek J, Sochor J, Balla S, Szekeres L, Hegedusova A, Hubalek J, Adam V, Kizek R. Phenolic profile of edible honeysuckle berries (genus *Lonicera*) and their biological effects. Molecules. 2011; 17:61-79.
9. Fukumoto LR, Mazza G. Assessing antioxidant and prooxidant activities of phenolic compounds. J Agric Food Chem. 2000; 48:3597-3604.
10. Chaovanalikit A, Thompson MM, Wrolstad RE. Characterization and quantification of anthocyanins and polyphenolics in blue honeysuckle (*Lonicera caerulea* L.). J Agric Food Chem. 2004; 52:848-852.
11. Puupponen-Pimiä R, Nohynek L, Meier C, Kähkönen M, Heinonen M, Hopia A, Oksman-Caldentey KM. Antimicrobial properties of phenolic compounds from berries. J Appl Microbiol. 2001; 90:494-507.

12. Palíková I, Heinrich J, Bednár P, Marhol P, Kren V, Cvak L, Valentová K, Růžicka F, Holá V, Kolár M, Simánek V, Ulrichová J. Constituents and antimicrobial properties of blue honeysuckle: a novel source for phenolic antioxidants. *J Agric Food Chem*. 2008; 56:11883-11889.
13. Minami M, Nakamura M, Makino T. Effect of *Lonicera caerulea* var. *emphyllocalyx* extracts on murine *Streptococcus pyogenes* infection by modulating immune system. *Biomed Res Int* 2019; 2019:1797930.
14. Harshey RM. Bacterial motility on a surface: many ways to a common goal. *Annu Rev Microbiol*. 2003; 57:249-273.
15. Calvio C, Celandroni F, Ghelardi E, Amati G, Salvetti S, Cecilian F, Galizzi A, Senesi S. Swarming differentiation and swimming motility in *Bacillus subtilis* are controlled by *swrA*, a newly identified dicistronic operon. *J Bacteriol*. 2005; 187:5356-5366.
16. Silva VO, Soares LO, Silva Júnior A, Mantovani HC, Chang YF, Moreira MA. Biofilm formation on biotic and abiotic surfaces in the presence of antimicrobials by *Escherichia coli* isolates from cases of bovine mastitis. *Appl Environ Microbiol*. 2014; 80:6136-6145.
17. Quave CL, Plano LR, Pantuso T, Bennett BC. Effects of extracts from Italian medicinal plants on planktonic growth, biofilm formation and adherence of methicillin-resistant *Staphylococcus aureus*. *J Ethnopharmacol*. 2008; 118:418-428.
18. Pratt LA, Kolter R. Genetic analysis of *Escherichia coli* biofilm formation: roles of flagella, motility, chemotaxis and type I pili. *Mol Microbiol*. 1998; 30:285-293.
19. Martinez-Medina M, Naves P, Blanco J, Aldeguer X, Blanco JE, Blanco M, Ponte C, Soriano F, Darfeuille-Michaud A, Garcia-Gil LJ. Biofilm formation as a novel phenotypic feature of adherent-invasive *Escherichia coli* (AIEC). *BMC Microbiol*. 2009; 9:202.
20. Hentzer M, Givskov M. Pharmacological inhibition of quorum sensing for the treatment of chronic bacterial infections. *J Clin Invest*. 2003; 112:1300-1307.
21. Prigent-Combaret C, Prensier G, Le Thi TT, Vidal O, Lejeune P, Dorel C. Developmental pathway for biofilm formation in curli-producing *Escherichia coli* strains: role of flagella, curli and colanic acid. *Environ Microbiol*. 2000; 2:450-464.
22. Vidal O, Longin R, Prigent-Combaret C, Dorel C, Hooreman M, Lejeune P. Isolation of an *Escherichia coli* K-12 mutant strain able to form biofilms on inert surfaces: involvement of a new *ompR* allele that increases curli expression. *J Bacteriol*. 1998; 180:2442-2449
23. Domka J, Lee J, Bansal T, Wood TK. Temporal gene-expression in *Escherichia coli* K-12 biofilms. *Environ Microbiol*. 2007; 9:332-346.
24. Schembri MA, Kjaergaard K, Klemm P. Global gene expression in *Escherichia coli* biofilms. *Mol Microbiol*. 2003; 48:253-267.
25. Yang J, Li YC, Zhou XR, Xu XJ, Fu QY, Liu CZ. Two thymol derivatives from the flower buds of *Lonicera japonica* and their antibacterial activity. *Nat Prod Res*. 2018; 32:2238-2243.
26. Xiong J, Li S, Wang W, Hong Y, Tang K, Luo Q. Screening and identification of the antibacterial bioactive compounds from *Lonicera japonica* Thunb. leaves. *Food Chem*. 2013; 138:327-333.
27. Yang L, Aguilar ZP, Qu F, Xu H, Xu H, Wei H. Enhanced antimicrobial activity of silver nanoparticles-*Lonicera Japonica* Thunb combo. *IET Nanobiotechnol*. 2016; 10:28-32.
28. Rodríguez-Pérez C, Quirantes-Piné R, Uberos J, Jiménez-Sánchez C, Peña A, Segura-Carretero A. Antibacterial activity of isolated phenolic compounds from cranberry (*Vaccinium macrocarpon*) against *Escherichia coli*. *Food Funct*. 2016; 7:1564-1573.
29. Harmidy K, Tufenkji N, Gruenheid S. Perturbation of host cell cytoskeleton by cranberry proanthocyanidins and their effect on enteric infections. *PLoS One*. 2011; 6:e27267.
30. Hidalgo G, Chan M, Tufenkji N. Inhibition of *Escherichia coli* CFT073 *fliC* expression and motility by cranberry materials. *Appl Environ Microbiol*. 2011; 77:6852-6857.

(Received November 13, 2019; Revised December 19, 2019; Accepted December 23, 2019)

Janus microspheres for enhanced enteral drug delivery: Preparation and orientated attachment to a Caco-2 monolayer

Akihiro Matsumoto¹, Chie Watanabe^{1,2}, Masahiro Murakami^{1,*}

¹Laboratory of Pharmaceutics, Faculty of Pharmacy, Osaka Ohtani University, Tondabayashi, Osaka, Japan;

²Laboratory of Clinical Pathology, Faculty of Pharmacy, Josai University, Sakadoshi, Saitama, Japan.

Summary

Conventional oral preparations generally release incorporated drugs omnidirectionally, including into the lumen, leading to a low bioavailability of drugs that are unstable in the gastrointestinal tract. Here, we designed Janus microspheres for efficient mucosal drug delivery as single-sided-release microspheres with the oriented attachment to mucus and evaluated their attachment to and orientation on a Caco-2 (human Caucasian colon adenocarcinoma cell line) monolayer. The microspheres comprised a mucus-oriented hemisphere of an ammonioalkyl methacrylate copolymer and a protective hemisphere of a hard fat. Fluorescein isothiocyanate-dextran with an average molecular weight of 3,000-5,000 Da (FD4) was used as a model hydrophilic drug. A water-in-oil emulsion-type solvent evaporation method was employed for fabrication of the Janus microspheres. The yield of Janus microspheres was found to be dependent on the polymer-to-hard fat ratio, with a maximum yield of over 90% being obtained at a ratio of 1:2, whereas lower and higher ratios resulted in monolithic or star-shaped microspheres. FD4 was specifically localized in the polymeric hemisphere. A cell culture study revealed that the Janus microspheres attached to a Caco-2 monolayer *via* their polymeric hemispheres with the hard fat hemisphere providing a protective sealing. This may lead to the development of an effective enteral drug delivery system for biomedicines, such as polypeptides and nucleic acids.

Keywords: Single-sided-release microspheres, hard-fat, ammonioalkyl methacrylate copolymer, solvent evaporation method

1. Introduction

Although oral drug preparations are the most patient-friendly dosage forms because of their convenience, for drugs that are unstable in the gastrointestinal tract and/or show low permeability in the epithelium, the preparation of oral dosage forms remains difficult. Most biomedicines, including polypeptides, such as hormones, cytokines, and antibodies (*e.g.*, insulin and interferon), or nucleic acids, such as antisense RNA, small interfering RNA (siRNA), and microRNA, have these features. Thus, many researchers in the pharmaceutical field have focused on improving the intestinal absorption of biomedicines.

The use of additives, such as enzyme inhibitors (1-4), membrane permeability enhancers (5,6), and tight junction modulators (7-9), is one of the major strategies used to improve intestinal drug absorption. Alternatively, microparticles have been reported to improve the intestinal absorption of insulin (7,10,11) and siRNAs (12,13). Although micro- and nanoparticles can protect biomedicines against chemical and enzymatic degradation, conventional particulate systems generally show omnidirectional release of a loaded drug. Drugs released into the luminal bulk fluid or content have a higher risk of enzymatic degradation than drugs released directly at the absorptive epithelial surface. In addition, the fluid or contents in the lumen can dilute drugs, causing loss of driving force across the mucosal membrane. Thus, effective drug delivery systems for biomedicines should release the loaded drug only in the vicinity of and toward the epithelial surface.

Some studies have shown that degradation of

*Address correspondence to:

Dr. Masahiro Murakami, Laboratory of Pharmaceutics, Faculty of Pharmacy, Osaka Ohtani University, 3-11-1 Nishikori-kita, Tondabayashi, Osaka 584-0854, Japan.

E-mail: murakam@osaka-ohtani.ac.jp

peptides in the intestine can be suppressed by preventing their dilution. Sinko *et al.* demonstrated that restriction of the dilution of calcitonin and an organic acid additive by localization in a limited portion of the intestine *via* a delivery system improved the intestinal absorption of this peptide drug (14). Maintaining a lower pH at the site of absorption can inhibit the activity of enzymes. Moreover, Takada and coworkers developed a novel hemispherical patch system (GI-MAPS) for peptide drugs. This system releases a drug only from the flat bottom face but not from the spherical body surface, which is coated with ethyl cellulose, an insoluble polymer, thereby limiting the direction of release (15,16). In addition, to maintain a high drug concentration near the site of absorption, the flat face of a hemisphere is adhesive to the mucosal membrane and plays a role in attaching the system to the mucosal surface. In contrast, the coated surface of the spherical body or drug reservoir can prevent drug release toward the lumen and protect a drug from attack by luminal enzymes. It has been demonstrated that the intestinal absorption of peptide drugs, such as granulocyte-colony stimulating factor (G-CSF) (17) and interferon (18), is markedly improved by using GI-MAPS. Thus, GI-MAPS appears to be a unique and attractive intestinal delivery system for biomedicines. However, the fabrication of micro- or nano-sized GI-MAPS or hemispherical preparations remains technically challenging. Hemispheres are produced using several fabrication processes that may require manufacturing systems that are entirely different from those currently used for conventional preparations, and would therefore not be cost-effective to produce.

Janus microspheres are heterogeneous particles composed of two distinct hemispheres and have been proposed for use in various applications, including those for catalysts (19,20), imaging agents/nanosensors (19,21), and cosmetics (19). Several methods, including templating methods (22), colloidal assembly (23), particle lithography techniques (24), glancing-angle deposition (25), and capillary fluid flow (26), have recently been proposed for the fabrication of Janus microspheres.

Janus microspheres have also attracted the attention of researchers in the field of drug delivery systems. Pulmonary delivery of hydrophilic and hydrophobic anticancer drugs has been reported using Janus microspheres (27). Janus microspheres show unique properties that are lacking in conventional homogeneous particles, which inspired us to apply these particles in an attempt to improve drug absorption in the intestine. Namely, Janus microspheres can be designed such that a drug is localized in a particular hemisphere and released from a single side.

In the present study, we investigated the feasibility of fabricating Janus microspheres as an enteral delivery system for biomedicines, which are designed to be

oriented on mucus and release the encapsulated drug only to mucus, and confirmed the designed properties on a Caco-2 (human Caucasian colon adenocarcinoma cell line) monolayer. The results obtained, *i.e.*, the high efficiency of Janus particle production, the localization of a drug in a specific hemisphere, and the fixed directional attachment to the epithelium, should guarantee the feasibility of focusing drug release on the site of absorption, potentially leading to an increased bioavailability of medications that are poorly absorbed and unstable in the intestine. These results will indicate the utility of Janus microspheres in developing an enteral delivery system for biomedicines.

2. Materials and Methods

2.1. Study design and approach

This study was designed with the aim of developing novel Janus microspheres for enteral drug delivery. To achieve this purpose, we selected a biocompatible cationic polymer (ammonioalkyl methacrylate copolymer: Eudragit® RS100) and a hard fat (Suppocire® AM) containing a mixture of glycerides (mainly triglycerides) as materials for Janus particle fabrication. The cationic polymeric hemisphere was expected to be oriented to the intestinal mucosa and release a loaded hydrophilic drug only toward the mucosal side, whereas the glyceride hemisphere would function as a hydrophobic backing to protect against both the leakage of the drug to the luminal side and enzymatic attack from the luminal side (Figure 1). For the fabrication, we adopted a solvent evaporation method using similar conditions to those previously reported to have produced stable Janus microspheres comprising poly

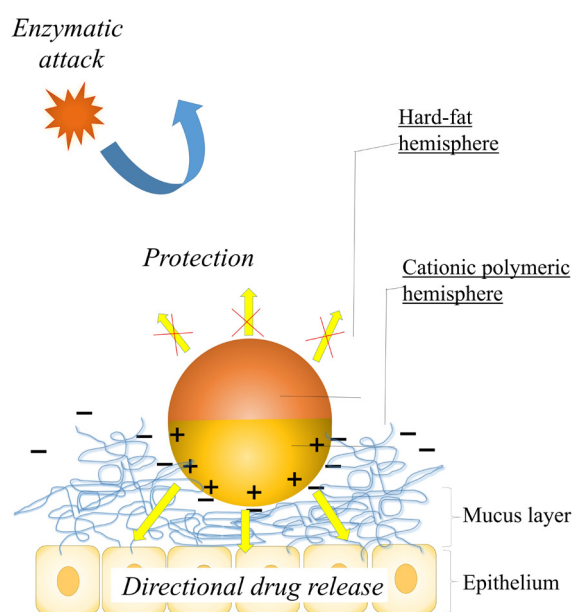


Figure 1. Strategy for promoting drug absorption using single-side releasing microspheres.

(DL-lactide-co-glycolide) and a hard fat (Suppocire AM) (28). We use fluorescein isothiocyanate-dextran with an average molecular weight of 3,000-5,000 Da (FD4) as a model drug because biomedicines such as polypeptides and nucleic acids are generally hydrophilic linear macromolecules.

2.2. Materials

Ammonioalkyl methacrylate copolymer (Eudragit[®] RS100) was purchased from Evonik Industries AG (Essen, Germany). The hard fat (Suppocire[®] AM pellets) was a kind gift from Gattefossé (Lyon, France). Fluorescein isothiocyanate-dextran with an average molecular weight of 3,000-5,000 Da (FD4) was purchased from Sigma-Aldrich Co., Ltd. (St. Louis, MO, USA). Polyvinyl alcohol (PVA; POVAL 220C) was obtained from KURARAY Co., Ltd., (Tokyo, Japan). Ethoxylated hydrogenated castor oil 60 (HCO60) and caprylic/capric triglyceride (Triester F-810) were supplied by Nikko Chemicals Co., Ltd. (Tokyo, Japan). Tripalmitate glyceride was purchased from Alfa Aesar (Lancashire, UK). Caco-2 cells (RCB0988) were provided by Riken BioResource Research Center (Tukuba, Japan) through the National Bio-Resource Project of the MEX. CellTracker[™] Violet BMQC (2,3,6,7-tetrahydro-9bromomethyl-1H,5H-quinolizino [9,1-g] coumarin) Dye was purchased from Thermo Fisher Scientific Inc. (Waltham, MA, USA). Dulbecco's Modified Eagle's medium (D-MEM) and Dulbecco's phosphate buffered saline (D-PBS) were purchased from Wako Pure Chemical Industry, Ltd. (Osaka, Japan). Fetal bovine serum was purchased from Biowest SAS (Nuaille, France). All other chemicals used were of reagent grade.

2.3. Phase diagram analysis

Mixtures of Eudragit RS100 and Suppocire AM at various ratios were dissolved in methylene chloride. The solvent was evaporated slowly at 20-23°C until phase separation was observed. The resulting solution at this point of phase evaporation was weighed to calculate the concentrations of polymer and triglyceride.

2.4. Fabrication of Janus microspheres

Janus microspheres were fabricated using a water-in-oil-in-water (w/o/w)-type emulsion solvent evaporation method (Figure 2a). Eudragit RS100 and Suppocire AM (total amount: 180 mg) were dissolved in methylene chloride (1.5 mL) to prepare the oil phase. Oil Red O or Nile Red (1 mg) was then added to the oil phase as needed. When FD4 was loaded in Janus microspheres, 40 mg/mL FD4 solution (50 µL) as an inner water phase was emulsified into the resulting oil

phase for 1 min at 20 kHz, 200 W, and 25% amplitude using a tip-sonicator (Digital Sonifier 250; Branson Ultrasonics Corporation, Danbury, CT, USA) under ice cooling to prepare a water-in-oil (w/o) emulsion. HCO60 (with 1% final concentration in the inner water phase) was added to the inner water phase as needed. The resulting oil phase or the w/o-type emulsion was emulsified into 0.1% PVA-0.1 M phosphate buffer (pH 8.0; 3 mL) at 3,000 rpm using a homogenizer (ULTRA-TURRAX T18, IKA[®]-Werke GmbH & CO. KG, Staufen, Germany) for 5 min at 20-23°C. The entire resulting w/o/w type emulsion was added to 100 mL of 0.1 M phosphate buffer (pH 8.0), and the diluted emulsion was stirred at 20-23°C for 180 min to remove the solvent. This process is hereinafter referred to as the solvent evaporation process. The hardened microspheres thus obtained were sieved through 149-µm sieves to remove aggregates, washed, and lyophilized. The FD4 content of the resulting Janus microspheres was determined to be 0.500 ± 0.080% (mean ± S.D. $n = 3$ batches) using the method described in section 2.7 below.

2.5. Microscopic observations

During the solvent evaporation process, the emulsion and fabricated Janus microspheres were observed using an optical microscope system (Motic PA300; Shimadzu Co., Ltd., Kyoto, Japan). Fifty microspheres were randomly selected and classified into four conformation types: Janus, double-walled, star-shaped, and monolithic types. The microspheres with each conformation were then counted in triplicate.

2.6. Determination of Janus particle size

The sizes of the fabricated Janus microspheres were determined using a laser diffraction particle size analyzer (SALD-2200; Shimadzu Co., Ltd., Kyoto, Japan).

2.7. Determination of FD4 contents in Janus microspheres

Janus microspheres loaded with FD4 (10 mg) were weighed in a test tube. The weighed Janus microspheres were dissolved in methylene chloride (2 mL), to which was added 0.05% Tween 80-JP second fluid for the subsequent dissolution test (pH 6.8; 5 mL), and FD4 was extracted by shaking overnight. After centrifuging for 5 min at 2,000 rpm, the upper aqueous layer was collected, and the concentration of FD4 in the aqueous layer was determined using a hybrid multimode microplate reader (Synergy H4; BioTek Instruments, Winooski, VT, USA) based on a fluorescent method. The test was performed in triplicate.

2.8. Dissolution test

Janus microspheres loaded with FD4 (10 mg) were weighed in a test tube, to which 0.05% polysorbate 80 (Tween80)-JP second fluid (pH 6.8; 5 mL) maintained at 37°C was added as the dissolution medium, and the microspheres were dispersed. The preparations were immediately shaken at 100 rpm at 37°C in an air-conditioned incubator (BioShaker V-BR-36; TITEC, Koshigaya, Japan) and collected at predetermined times. After centrifugation for 1 min at 2,500 rpm, the medium (0.5 mL) was collected as a sample for assay, and fresh medium (0.5 mL) was added into the tubes. The dissolution test was then continued and performed in triplicate. FD4 remaining after the dissolution test was extracted and determined using the method described in section 2.7. The concentration of FD4 in the samples collected for assay was determined using a fluorescence spectrometer.

2.9. Differential scanning calorimetry (DSC) analysis

The microspheres (10 mg) prepared from Eudragit RS100 alone, Suppocire® AM alone, or Eudragit® RS/Suppocire® AM (1:2 blend; unloaded FD4) were analyzed using differential scanning calorimetry (DSC-60; Shimadzu Co., Ltd.).

2.10. Observation of Janus microspheres on Caco-2 cell monolayers

Caco-2 cells were cultured in D-MEM containing 10% fetal bovine serum in six-well plates (Corning Inc., New York, USA), each well of which contained 5 mL of the medium. The cells were grown for several days until a confluent monolayer had developed. Caco-2 monolayers were stained with CellTracker™ Violet BMQC Dye (at a final staining concentration of 25 µM). Janus microspheres encapsulating FD-4 and Nile red were suspended in 0.1 M phosphate buffer (pH 7.9). A 400-µL aliquot of the resulting suspension containing 6.3×10^4 particles was then added to the apical side of each well. When all particles precipitate at the bottom of the well, a concentration of 6.3×10^4 particles is equivalent to 7.0×10^3 particles/cm². After overnight incubation, the apical side of the well was carefully washed twice with the pre-warmed D-PBS. To evaluate the orientation of attachment of the particles, confocal images were taken under an LSM 510 META microscope (Carl Zeiss Microscopy Ltd, Jena, Germany).

Given that it has previously been suggested that long-term agitation and incubation may cause an increase in the formation of large aggregates and the attachment of microtubes onto B-cells (29), incubations in the present study were carried out without agitation to avoid the formation of aggregates or agglomerates,

since it is difficult to evaluate their orientation.

3. Results

3.1. Phase diagram analysis

Phase separation was observed in the ammonioalkyl methacrylate copolymer, triglyceride, and methylene chloride ternary system. The critical concentration of phase separation showed an approximately negative correlation between the ammonioalkyl methacrylate copolymer and triglyceride concentrations (Figure 2b). The solution at the critical concentration showed a higher viscosity at higher ratios of ammonioalkyl methacrylate copolymer to triglycerides. Under the conditions of a copolymer-to-triglyceride ratio of 1:1, phase separation was observed at 10% (w/w) when

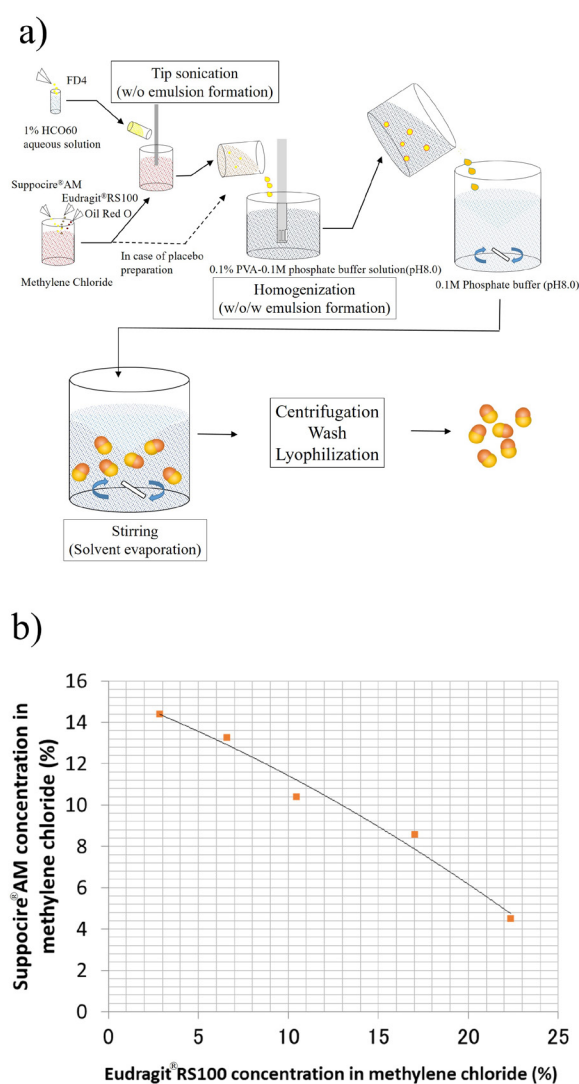


Figure 2. Fabrication of Janus microspheres using a phase separation method. (a) Scheme of the procedure used to fabricate Janus microspheres. **(b)** Phase diagram of the ammonioalkyl methacrylate copolymer (Eudragit® RS100) - triglycerides (Suppocire® AM) - methylene chloride ternary system.

Suppocire AM was used as the triglyceride, whereas it was detected at 23% (w/w) and 14% (w/w) for Triester F-810 and tripalmitate glyceride, respectively.

3.2. Effects of ammonioalkyl methacrylate copolymer/triglyceride ratio on the conformation of microspheres

The optical micrographs of microspheres prepared using different ratios of Eudragit RS100 to Suppocire AM are shown in Figure 3. The nonpolar dye Oil Red O can stain the triglycerides in microspheres.

Microspheres of triglycerides alone showed a double-walled conformation. This conformation changed to that of Janus and star-shaped microspheres as the ammonioalkyl methacrylate copolymer ratio increased. The microspheres fabricated from 90% ammonioalkyl methacrylate copolymer showed a monolithic conformation and had the same conformation as microspheres prepared from ammonioalkyl methacrylate copolymer alone. The frequency of each conformation corresponding the ammonioalkyl methacrylate copolymer/triglyceride ratios is shown

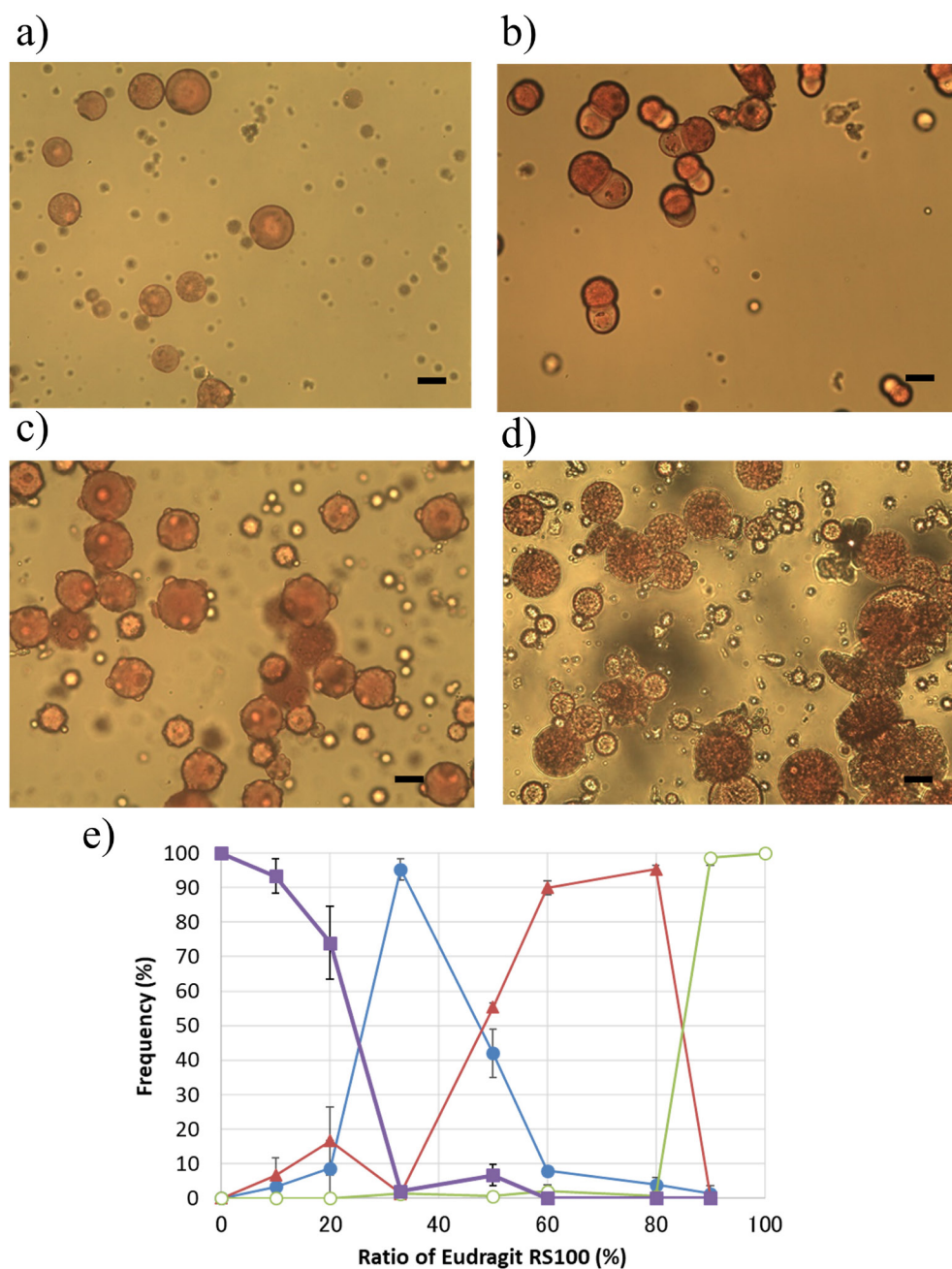


Figure 3. Effect of ammonioalkyl methacrylate copolymer-triglyceride ratio on the conformation of microspheres. Typical images of the optical micrographs of microspheres prepared from (a) triglycerides alone, or with a ammonioalkyl methacrylate copolymer and triglycerides, (b) 1:2, (c) 2:1, and (d) 9:1. Bars represent 20 μm . (e) Frequency of each conformation depending on ammonioalkyl methacrylate copolymer-triglyceride ratio. Janus microspheres: ● blue line, monolithic microspheres: ○ green line, double-walled microspheres: ■ purple line, star-shaped microspheres: ▲ red line. Data represent mean \pm S.D. ($n = 3$).

in Figure 3e. Janus microspheres were obtained at ammonioalkyl methacrylate copolymer /triglyceride ratios of 1:2 to 1:1, with the maximum yield of these particles [mean \pm standard deviation (SD): 90.7% \pm 3.1%] being obtained at a ratio of 1:2.

3.3. DSC analysis of Janus microspheres

The DSC chart presented in Figure 4 shows the melting points and glass transition temperature of Janus microspheres. Compared with microspheres obtained from ammonioalkyl methacrylate copolymer or triglycerides alone, endotherm peaks of Janus microspheres at lower and higher temperatures were identified as the melting of triglycerides and glass transition of the ammonioalkyl methacrylate copolymer, respectively. The endotherm peaks corresponding to the melting of triglycerides in Janus microspheres shifted to a higher temperature than those of triglycerides alone. In contrast, the endotherm peaks corresponding to the glass transition of ammonioalkyl methacrylate copolymer shifted to a lower temperature than those of the ammonioalkyl methacrylate copolymer alone.

3.4. Distribution of FD4 in Janus microspheres

Janus microspheres containing FD4 were fabricated using 1% HCO60 as an inner water phase, which did not substantially affect their conformation. The inner water phase of the w/o emulsion during Janus particle formation was finely dispersed. The prepared Janus microspheres incorporated FD4, and optical and

fluorescence microscopic observations revealed that the FD4 was localized in the hemisphere containing the ammonioalkyl methacrylate copolymer opposite to that stained by Oil Red O (Figures 5a and 5b). The mean particle size was 31.1 \pm 0.5 μ m.

3.5. Dissolution profile of FD4 from Janus microspheres

The *in vitro* release of FD4 from Janus microspheres was slow, reaching approximately 60% after 5 days (Figure 5c). The cumulative amount of FD4 released from the Janus microspheres obtained was proportional to the 0.75 power of time during a period of 0 to 2 days (correlation coefficient: 0.9984).

3.6. Observation of Janus microspheres on Caco-2 cell monolayers

We prepared Janus microspheres loaded with FD4, a hydrophilic fluorescent dye, and Nile red, a hydrophobic fluorescent dye. Nile red and FD4 were observed to be localized in the hard-fat hemisphere and the polymeric hemisphere of the Janus microspheres, respectively. Fluorescence of the middle part of the Janus microspheres became yellow, which is considered to be indicative of interference between the two fluorescent dyes. Therefore, identification of each hemisphere was based on the luminescent color of the tip of each hemisphere, where the tips of ammonioalkyl methacrylate copolymer and hard-fat hemispheres were green due to FD4 and red due to Nile red, respectively.

On addition of Janus microspheres to the apical

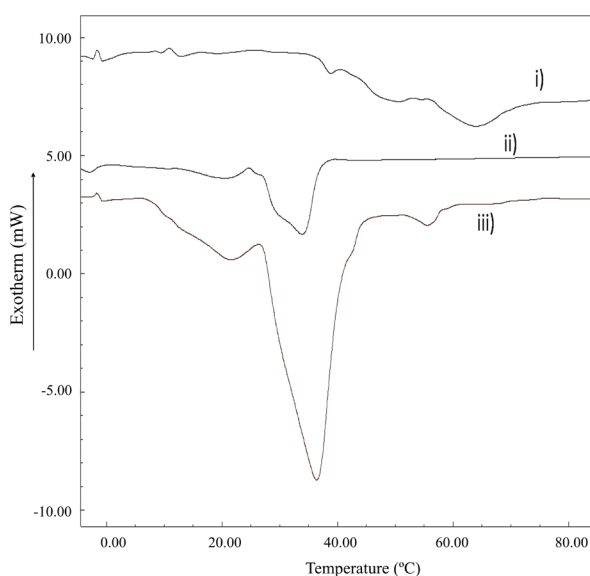


Figure 4. Differential scanning calorimetry chart of Janus microspheres. (i) Ammonioalkyl methacrylate copolymer, **(ii)** Triglycerides, **(iii)** Janus microspheres (ammonioalkyl methacrylate copolymer/triglycerides = 1/2).

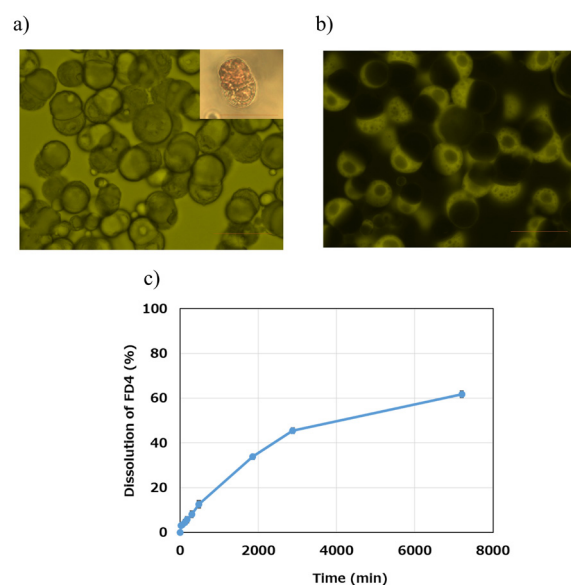


Figure 5. Distribution of fluorescein isothiocyanate-dextran (FD4) in Janus microspheres. (a) Optical micrograph image and **(b)** fluorescence micrograph image. **(c)** FD4 release profiles from Janus microspheres. The dissolution test was performed at 37C using a second fluid (pH 6.8) containing 0.05% Tween 80. Bars represent 50 μ m.

side of a Caco-2 monolayer, we observed that most of the particles settled onto the surface of the monolayer within 5 min, with the polymeric hemisphere oriented downwards and the hard-fat hemisphere facing upwards (Figures 6a and 6b). We detected no Janus microspheres with hard-fat hemisphere attachment. Side-on attachment was rarely observed, whereas in contrast, $22.3 \pm 3.4\%$ of the precipitated particles were found to be side-on at the bottom of wells lacking a monolayer. After overnight incubation, $6.01 \pm 0.79 \times 10^3$ particles/cm² of the Janus microspheres were

observed on the surface of the Caco-2 monolayer. In addition, even after washing with the PBS(-), we observed that 42% of the particles ($2.53 \pm 0.48 \times 10^3$ particles/cm²) remained attached to the monolayer (Figures 6c and 6d).

4. Discussion

The phase separation method is based on a phenomenon in which phase separation occurs between two materials as the solvent is evaporated. We have previously reported

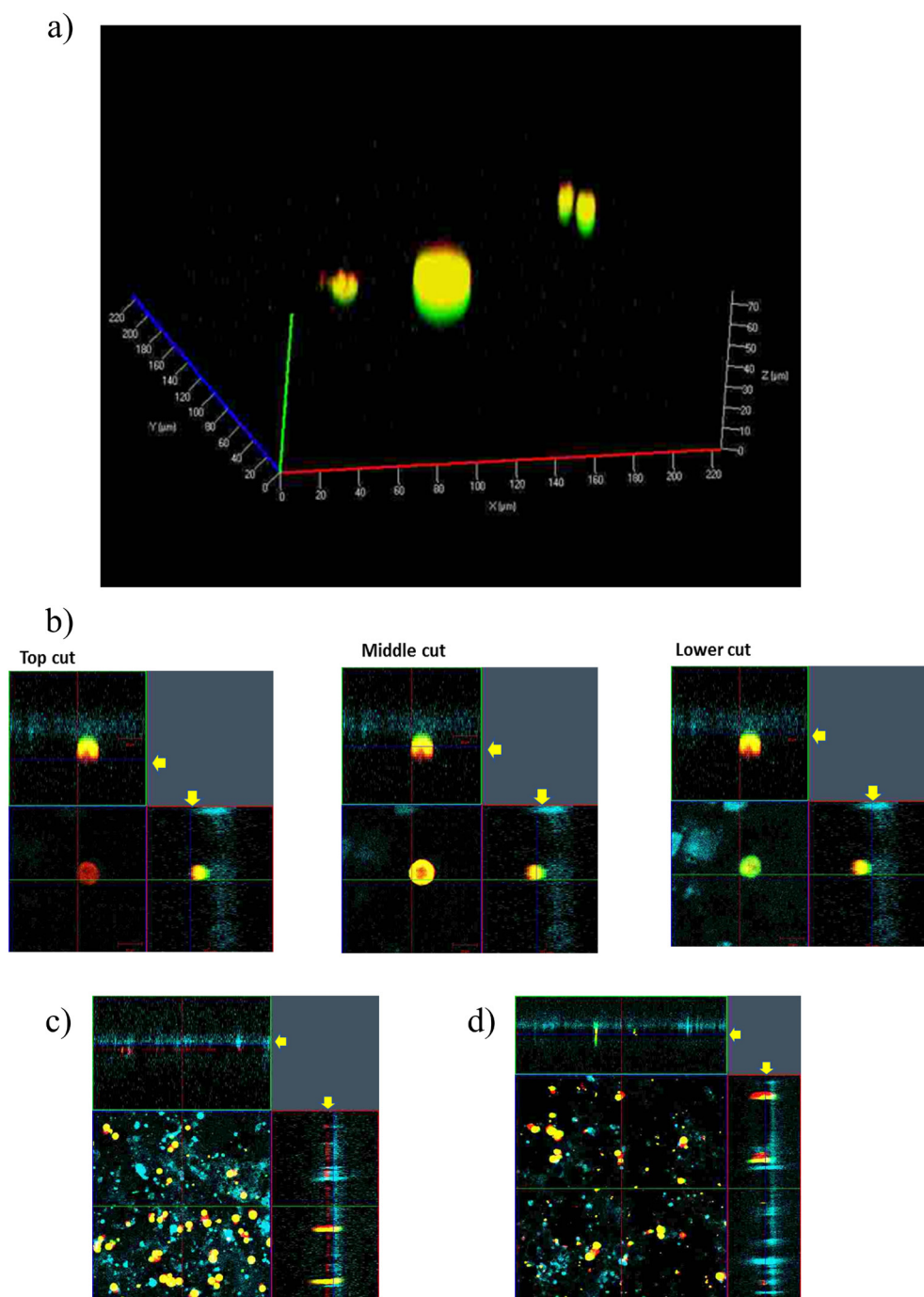


Figure 6. Confocal images of Janus microspheres on a Caco-2 monolayer. Images of Janus microspheres after 30 min incubation, (a) on an unstained Caco-2 monolayer and (b) on a cell tracker violet-stained Caco-2 monolayer. Images of Janus microspheres after overnight incubation, (c) before and (d) after washing.

that solvent evaporation following formation of an o/w-type emulsion can yield Janus microspheres composed of poly (lactide-co-glycolide) and triglycerides (28). Phase separation between poly (lactide-co-glycolide) and triglycerides occurs in a dispersed oil droplet as the solvent is evaporated. In addition, we revealed that the decremental profiles of solvent in an oil phase influences the stability of the conformation as Janus microspheres. In the present study, we applied optimized conditions based on conformation stability, as reported in a previous study, for the fabrication conditions of Janus microspheres composed of ammonioalkyl methacrylate copolymer and triglycerides. Initially, we examined whether phase separation occurred in an ammonioalkyl methacrylate copolymer, triglyceride, and methylene chloride ternary system. Although methylene chloride is a good solvent for both ammonioalkyl methacrylate copolymer and triglycerides, phase separation was observed above a certain concentration, referred to as the critical concentration. The critical concentration between ammonioalkyl methacrylate copolymer and triglycerides was found to be higher than that between poly (lactide-co-glycolide) and triglycerides in methylene chloride, as reported previously (28). In addition, at the critical concentration of the ammonioalkyl methacrylate copolymer/triglyceride/methylene chloride ternary system, the solution showed higher viscosity than that of the poly (lactide-co-glycolide)/triglyceride/methylene chloride ternary system. This is not only due to the higher critical concentration of the ammonioalkyl methacrylate copolymer/triglyceride/methylene chloride ternary system but also because the ammonioalkyl methacrylate copolymer (molecular weight: 32 kDa) used in this study has a higher molecular weight than the poly (lactide-co-glycolide) used in the previous study (molecular weight: 20 kDa) (28). The higher viscosity is a notable point. For mixtures of ammonioalkyl methacrylate copolymer and triglycerides, phase separation in the dispersed oil phase is believed to occur at higher viscosity than that for mixtures of poly (lactide-co-glycolide) and triglycerides in the process of solvent evaporation as reflected in the results of phase diagram analysis. In our previous study, we proposed a mechanism whereby Janus microspheres are formed: the droplets produced by phase separation in the dispersed oil phase of the emulsion aggregate and coalesce before the coalescing droplets migrate to form two layers, resulting in the formation of Janus microspheres (28). It is believed that obtaining a Janus conformation using mixtures of ammonioalkyl methacrylate copolymer and triglycerides is more difficult because high viscosity may prevent coalescence and migration of the separated droplets. Our data revealed that the formation of Janus microspheres is influenced by the ratio of ammonioalkyl methacrylate copolymer to triglycerides. A high ratio of ammonioalkyl methacrylate copolymer (50-80%) yielded star-shaped microspheres, but not Janus microspheres, and resulted

in a higher viscosity at the critical concentration than lower ratios. The development of microspheres with a star-shaped conformation may be attributable to the fact that although the limited droplets separated in the oil phase can migrate to the surface of the oil phase, the droplets will be prevented from coalescing due to the high viscosity in the oil phase. Moreover, we also found that the size of droplets on the surface of a microsphere decreased as the ratio of ammonioalkyl methacrylate copolymer to triglycerides increased (*i.e.*, as the viscosity of the oil phase increased). However, increasing the proportion of ammonioalkyl methacrylate copolymer to more than over 90% yielded monolithic microspheres. This is believed to be attributable to the formation of a solid solution of triglycerides and ammonioalkyl methacrylate copolymer. Decreasing the glass transition temperature, as determined from the DSC chart, indicated that a certain amount of triglyceride had dissolved in the ammonioalkyl methacrylate copolymer.

Notably, a high ratio of triglycerides yielded double-walled microspheres, similar to the microspheres prepared from triglycerides alone. The triglycerides used in this study were mixtures of triglycerides containing various acyl chains, and the double-wall conformation is believed to be a consequence of phase separation between the different triglycerides. When microspheres were prepared with 80% triglycerides, double-walled microspheres were also obtained. However, we were not able to clarify the origin of the droplets in these microspheres, *i.e.*, whether they were derived from triglyceride components or separation of the ammonioalkyl methacrylate copolymer phase.

Janus microspheres were found to be obtained within a narrow range of the ammonioalkyl methacrylate copolymer/triglyceride ratios (between 1:2 and 1:1), at which the viscosity of the dispersed oil phase permitted the separated droplets to migrate to the surface and coalesce to form hemispheres during phase separation. The Janus microspheres thus contained triglyceride droplets within the ammonioalkyl methacrylate copolymer hemisphere, which are believed to be formed from glycerides with short acyl chains. The concentrations at which a phase separation between triglyceride and ammonioalkyl methacrylate copolymer occurred decreased as increasing the length of the acyl chains of triglycerides: Suppocire AM (C12-C18) < tripalmitate glyceride (C16) < Triester F810 (C6 and C8). This indicated that the phase separation of short-chain triglycerides in the dispersed oil phase occurred later in the solvent evaporation process than that of long-chain triglycerides. The separated droplets of long-chain triglycerides can migrate to the surface of the dispersed oil droplets and coalesce, as described above. However, when droplets of short-chain triglycerides were separated, the viscosity of the dispersed oil phase was too high for the droplets to migrate to the surface.

We prepared Janus microspheres loaded with FD4

using the w/o/w-type emulsion solvent evaporation method with an inner water phase of 1% HCO60. The triglyceride hemisphere of the Janus microspheres was stained with Oil Red O, as previously reported (28), and the fluorescence of FD4 was detected in the other (polymeric) hemisphere. When phase separation between the polymer and triglycerides occurred in the oil phase, the inner water phase containing FD4 was distributed in accordance with the partition phenomenon. Because the ammonioalkyl methacrylate copolymer is more hydrophilic than triglycerides, the inner water phase should tend to be in ammonioalkyl methacrylate copolymer hemispheres.

The cumulative dissolution rate of FD4 from the Janus microspheres was proportional to the 0.75 power of time (correlation coefficient: 0.9984) over a period of 0-2 days. Among mathematical models used for dissolution from pharmaceutical formulations, the Higuchi model is known to show release proportional to the square root of time (30). This model can be applied to an erodible formulation with drug homogeneously dispersed in a matrix; however, the model does not consider swelling and interaction between polymer and drug. In the case of Janus microspheres composed of an ammonioalkyl methacrylate copolymer and triglycerides, drug release from the ammonioalkyl methacrylate copolymer hemisphere is also speculated to be controlled by swelling of the polymer and electric interaction between the polymer and FD4. Namely, ammonioalkyl methacrylate copolymer has quaternary ammonium groups, which show cationic charges under acidic and neutral conditions. The exchange of the quaternary ammonium group counterions with the surrounding medium develops a water flux within which drug molecules can diffuse out of the dosage form (31). The attraction of ions in the release medium to the quaternary ammonium groups determines the extent of water flux and hence the drug release rate (32). In addition, the contribution of the interaction between ammonioalkyl methacrylate copolymer and FD4, which are cationic and anionic, respectively, at pH 6.8 in the dissolution test, has to be taken into consideration. Drug release through the interaction *via* electric charge is known to be related to ion exchange, and ion exchange with the chloride ion is considered to influence the permeability and drug release of Eudragit RS30D films (33). Therefore, the swelling and ionic interaction as an additional release mechanism may be one reason why release from the Janus microspheres differs from that predicted by the Higuchi model.

The direction of release of a hydrophilic drug from Janus microspheres will be limited to the side of the polymeric hemisphere because the triglyceride hemisphere functions as an impermeable backing. The polymeric hemisphere has two surfaces, *i.e.*, the spherical and flat surfaces, with the latter lying at the interface with the triglyceride hemisphere. We speculate that

hydrophilic drugs are released predominantly from the spherical surface compared with that from the flat surface. At polymer interfaces, polymers have been shown to be orientated in hydrophilic or hydrophobic groups along an adjacent material depending on the properties of the adjacent material (34). The ammonioalkyl methacrylate copolymer has both hydrophilic and hydrophobic groups, and at the interface of an ammonioalkyl methacrylate copolymer hemisphere with a triglyceride hemisphere, the ammonioalkyl methacrylate copolymer is believed to form a hydrophobic layer composed of its hydrophobic moieties along the adjacent triglycerides (hydrophobic materials). Hence, the interface between the ammonioalkyl methacrylate copolymer hemisphere and the triglyceride hemisphere may be so hydrophobic that it restricts the access of water to the interface, thereby inhibiting the release of a hydrophilic drug. In contrast, the surface of the spherical part of the hemisphere is covered by the hydrophilic group of the ammonioalkyl methacrylate copolymer because the surface comes in contact with water during fabrication. Accordingly, water can gain access to the spherical part of an ammonioalkyl methacrylate copolymer hemisphere, thereby facilitating release of the incorporated hydrophilic drug.

Our investigation using Caco-2 monolayers revealed that the Janus microspheres can attach onto the monolayer in an orientated manner. Only a few agglomerates were observed in the present study. With regards to the particles existing as a primary particle, the attachment to the monolayer can be categorized into four groups, namely, (a) unattached, (b) polymeric hemisphere-oriented attachment (c) hard-fat hemisphere-oriented attachment, and (d) side-oriented or laterally oriented attachment. In this study, most of the Janus microspheres were observed to be attached to the apical surface of the monolayer *via* the ammonioalkyl methacrylate hemisphere. No particles with hard-fat hemisphere-oriented attachment were detected, and only a few particles with side-oriented or laterally oriented attachment were observed, which was characterized by polymeric and hard-fat spheres combined to form a shape resembling a figure eight (data not shown). The orientation of Janus microspheres on the Caco-2 monolayer may be due to difference in the specific gravity of the two hemispheres. This is supported by data showing that 78% of the Janus microspheres were observed in polymeric hemisphere-on settlement on the walls of culture plate wells lacking cells. The specific gravity of the polymeric hemisphere is higher than that of the hard-fat hemisphere, and we found that 42% of the particles remained attached to the monolayer after overnight incubation. We thus believe that the polymeric hemisphere of Janus microspheres may initially attach to Caco-2 monolayers *via* gravity, followed by strong binding to the surface. The major binding force is considered to be electrostatic. Although the surface of the Caco-2 monolayer appears to be

hydrophobic, it is known that charged particles can become strongly attached. In studies using liposomes (35) and oil droplets (36), it has been demonstrated that cationic particles can attach to Caco-2 monolayers to a greater extent than anionic and neutral particles. The polymeric hemisphere-orientated attachment of the Janus microspheres to Caco-2 monolayers observed in the present study appears to be consistent with the findings of these studies, because these microspheres consist of cationic polymer and neutral hard-fat hemispheres. Thus, the oriented attachment of Janus microspheres to the monolayer appears to be attributable mainly to the electrostatic properties of the two hemispheres, although the contribution of gravity remains to be fully clarified.

Mucin is a highly glycosylated protein with oligosaccharide side chains containing terminal sialic acid and sulfate residues (37,38), the negative charges of which can interact with cationic particles. The non-glycosylated regions of the mucin protein backbone and lipids associated with mucin contribute to the hydrophobicity of this protein, which can interact with hydrophobic materials. These properties of mucin may influence the orientation of Janus microspheres *in vivo*. Positively charged oil droplets have been reported to exhibit stronger binding to mucosal surfaces than negatively charged droplets (39) and also to bind to the surface of Caco-2 cells by electrostatic attraction (36). Taking these details into consideration, it appears that the oriented attachment on a mucosal surface is similar to that on Caco-2 cells, which do not secrete mucin.

In order to achieve focused drug release in a specific direction, we have recently demonstrated that the condensation of insulin within a limited surface area or the dimple of a hard-fat suppository, which releases a high concentration of insulin only toward the mucosal side within a limited area, reduces blood glucose levels following rectal administration (40). This supports our concept shown in Figure 1. We are currently performing experiments to obtain proof of concept.

Particle size is an important factor affecting intestinal drug absorption *via* a particulate delivery system, and in the present study we adjusted the size of the particles to approximately 30 μm in order to observe the disposition of a drug contained within Janus microspheres. As particles on the nanometer scale can readily penetrate the mucus layer to access the epithelial surface (41), nanosized Janus particles may function as a patch, adhering directly to the apical membranes of enterocytes. Accordingly, the feasibility of reducing the size of Janus microspheres should be evaluated in further studies.

In conclusion, in the present study, we demonstrated that Janus particles prepared using an ammonioalkyl methacrylate copolymer and a hard fat could be fabricated using the w/o/w emulsion solvent evaporation method to release a model hydrophilic drug from a single hemisphere. These mucoadhesive Janus microspheres may be useful for the non-parenteral, particularly enteral,

mucosal delivery of biomedicines. In future studies, the adhesion to mucous membranes and local retainability of Janus microspheres should be further investigated *in vivo* under conditions relevant to drug delivery.

Acknowledgements

We would like to thank Ms. Kayoko Murakami for her technical assistance. We are also grateful to Editage (www.editage.jp) for English language editing. We gratefully acknowledge the financial support for this study provided by CBC Co., Ltd.

References

1. Nishihata T, Liversidge G, Higuchi T. Effect of aprotinin on the rectal delivery of insulin. *J Pharm Pharmacol.* 1983; 35:616-617.
2. Aungst BJ, Rogers NJ. Site dependence of absorption-promoting actions of lauroth-9, Na salicylate, Na2EDTA, and aprotinin on rectal, nasal, and buccal insulin delivery. *Pharm Res.* 1988; 5:305-308.
3. Yamamoto A, Taniguchi T, Rikyu K, Tsuji T, Fujita T, Murakami M, Muranishi S. Effects of various protease inhibitors on the intestinal absorption and degradation of insulin in rats. *Pharm Res.* 1994; 11:1496-1500.
4. Tozaki H, Emi Y, Horisaka E, Fujita T, Yamamoto A, Muranishi S. Degradation of insulin and calcitonin and their protection by various protease inhibitors in rat caecal contents: implications in peptide delivery to the colon. *J Pharm Pharmacol.* 1997; 49:164-168.
5. Hayakawa E, Yamamoto A, Shoji Y, Lee VH. Effect of sodium glycocholate and polyoxyethylene-9-lauryl ether on the hydrolysis of varying concentrations of insulin in the nasal homogenates of the albino rabbit. *Life Sci.* 1989; 45:167-174.
6. Uchiyama T, Sugiyama T, Quan YS, Kotani A, Okada N, Fujita T, Muranishi S, Yamamoto A. Enhanced permeability of insulin across the rat intestinal membrane by various absorption enhancers: their intestinal mucosal toxicity and absorption-enhancing mechanism of n-lauryl-beta-D-maltopyranoside. *J Pharm Pharmacol.* 1999; 51:1241-1250.
7. Teply BA, Tong R, Jeong SY, Luther G, Sherifi I, Yim CH, Khademhosseini A, Farokhzad OC, Langer RS, Cheng J. The use of charge-coupled polymeric microparticles and micromagnets for modulating the bioavailability of orally delivered macromolecules. *Biomaterials.* 2008; 29:1216-1223.
8. Kondoh M, Masuyama A, Takahashi A, Asano N, Mizuguchi H, Koizumi N, Fujii M, Hayakawa T, Horiguchi Y, Watanabe Y. A novel strategy for the enhancement of drug absorption using a claudin modulator. *Mol Pharmacol.* 2005; 67:749-756.
9. Lemmer HJ, Hamman JH. Paracellular drug absorption enhancement through tight junction modulation. *Expert Opin Drug Deliv.* 2013; 10:103-114.
10. Morishita M, Goto T, Peppas NA, Joseph JI, Torjman MC, Munsick C, Nakamura K, Yamagata T, Takayama K, Lowman AM. Mucosal insulin delivery systems based on complexation polymer hydrogels: effect of particle size on insulin enteral absorption. *J Cont Rel.* 2004; 97:115-124.
11. Rekha MR, Sharma CP. Synthesis and evaluation of lauryl

- succinyl chitosan particles towards oral insulin delivery and absorption. *J Cont Rel.* 2009; 135:144-151.
12. Murakami M, Nishina K, Watanabe C, Yoshida-Tanaka K, Piao W, Kuwahara H, Horikiri Y, Miyata K, Nishiyama N, Kataoka K, Yoshida M, Mizusawa H, Yokota T. Enteral siRNA delivery technique for therapeutic gene silencing in the liver *via* the lymphatic route. *Sci Rep.* 2015; 5:17035-17047.
 13. He C, Yin L, Song Y, Tang C, Yin C. Optimization of multifunctional chitosan-siRNA nanoparticles for oral delivery applications, targeting TNF- α silencing in rats. *Acta Biomater.* 2015; 17:98-106.
 14. Sinko PJ, Lee YH, Makhey V, Leesman GD, Sutyak JP, Yu H, Perry B, Smith CL, Hu P, Wagner EJ, Falzone LM, McWhorter LT, Gilligan JP, Stern W. Biopharmaceutical approaches for developing and accessing oral peptide delivery strategies and systems: *in vitro* permeability and *in vivo* oral absorption of salmon calcitonin (sCT). *Pharm Res.* 1999; 16:527-533.
 15. Eaimtrakarn S, Prasad YV, Puthli SP, Yoshikawa Y, Shibata N, Takada K. Evaluation of gastrointestinal transit characteristics of oral patch preparation using caffeine as a model drug in human volunteers. *Drug Metab Pharmacokinet.* 2002; 17:284-291.
 16. Venkatesan N, Uchino K, Amagase K, Ito Y, Shibata N, Takada K. Gastro-intestinal patch system for the delivery of erythropoietin. *J Cont Rel.* 2006; 111:19-26.
 17. Eiamtrakarn S, Itoh Y, Kishimoto J, Yoshikawa Y, Shibata N, Murakami M, Takada K. Gastrointestinal mucoadhesive patch system (GI-MAPS) for oral administration of G-CSF, a model protein. *Biomaterials.* 2002; 23:145-152.
 18. Ito Y, Tosh B, Togashi Y, Amagase K, Kishida T, Kishida T, Sugioka N, Shibata N, Takada K. Absorption of interferon alpha from patches in rats. *J Drug Target.* 2005; 13:383-390.
 19. Lee KJ, Yoon J, Lahann J. Recent advances with anisotropic particles. *Curr Opin Coll Int Sci.* 2011; 16:195-202.
 20. Cobo S, Heidkamp J, Jacques PA, Fize J, Fourmond V, Guetaz L, Jousset B, Ivanova V, Dau H, Palacin S, Fontecave M, Artero VA. Janus cobalt-based catalytic material for electro-splitting of water. *Nat Mater.* 2012; 11:802-807.
 21. Zhang Q, Zhang L, Li S, Chen X, Zhang M, Wang T, Li L, Wang C. Designed synthesis of Au/Fe₃O₄@C Janus nanoparticles for dual-modal imaging and actively targeted chemo-photothermal synergistic therapy of cancer cells. *Chemistry.* 2017; 23:17242-17248.
 22. Cui J, Kretzschmar I. Surface-anisotropic polystyrene spheres by electroless deposition. *Langmuir.* 2006; 22:8281-8284.
 23. Manoharan VN, Elsesser MT, Pine DJ. Dense packing and symmetry in small clusters of microspheres. *Science.* 2003; 301:483-487.
 24. Snyder CE, Yake AM, Feick JD, Velegol D. Nanoscale functionalization and site specific assembly of colloids by particle lithography. *Langmuir.* 2005; 21:4813-4815.
 25. Perro A, Reculosa S, Ravaine S, Bourgeat-Lami E, Duguet E. Design and synthesis of Janus micro- and nanoparticles. *J Mat Chem.* 2005; 15:3745-3760.
 26. Marquis M, Davy J, Cathala B, Fang A, Renard D. Microfluidics assisted generation of innovative polysaccharide hydrogel microparticles. *Carbohydr Polym.* 2015; 116:189-199.
 27. Garbuzenko OB, Winkler J, Tomassone MS, Minko T. Biodegradable Janus nanoparticles for local pulmonary delivery of hydrophilic and hydrophobic molecules to the lungs. *Langmuir.* 2014; 30:12941-12949.
 28. Matsumoto A, Murao S, Matsumoto M, Watanabe C, Murakami M. Fabrication of Janus particles composed of poly (lactic-co-glycolic) acid and hard fat using a solvent evaporation method. *Drug Discov Ther.* 2016; 10:307-313.
 29. Gibert JB, O'Brien JS, Suresh HS, Cohen RE, Rubner MF. Orientation-specific attachment of polymeric microtubes on cell surfaces. *Adv Mater.* 2013; 25:5948-5952.
 30. Higuchi T. Rate of release of medicaments from ointment bases containing drugs in suspension. *J Pharm Sci.* 1961; 50:874-875.
 31. Wagner KG, Grützmann R. Anion-induced water flux as drug release mechanism through cationic Eudragit RS 30D film coatings. *AAPS J.* 2005; 7:E668-677.
 32. Wulff R, Leopold CS. Coatings of Eudragit[®] RL and L-55 blends: Investigations on the drug release mechanism. *AAPS Pharm Sci Tech.* 2016; 17:493-503.
 33. Wagner K, McGinity J. Influence of chloride ion exchange on the permeability and drug release of Eudragit RS 30 D films. *J Cont Rel.* 2002; 82:385-397.
 34. Hongwei L, Wilhelm TSH. Polymers in nanotechnology. *Curr Opin Solid State Mat Sci.* 2002; 6:3-8.
 35. Kono Y, Jinzai H, Kotera Y, Fujita T. Influence of physicochemical properties and PEG modification of magnetic liposomes on their interaction with intestinal epithelial Caco-2 cells. *Biol Pharm Bull.* 2017; 40:2166-2174.
 36. Gershanik T, Lehr CM, Haltner E, Benita S. Charge-dependent interaction of self-emulsifying oil formulations with Caco-2 cells monolayers: binding, effects on barrier function and cytotoxicity. *Int J Pharm.* 2000; 211:29-36.
 37. Dekker J, Van Beurden-Lamer WM, Oprins A, Strous GJ. Isolation and structural analysis of rat gastric mucus glycoprotein suggests a homogeneous protein backbone. *Biochem J.* 1989; 260:717-723.
 38. Larsson JM, Karlsson H, Sjövall H, Hasson GC. A complex, but uniform O-glycosylation of the human MUC2 mucin from colonic biopsies analyzed by nanoLC/MSn. *Glycobiology.* 2009; 19:1568-1569.
 39. Gershanik T, Benzeno S, Benita S. Interaction of a self-emulsifying lipid drug delivery system with the everted rat intestinal mucosa as a function of droplet size and surface charge. *Pharm Res.* 1998; 15:863-869.
 40. Matsumoto A, Murakami K, Watanabe C, Murakami M. Improved systemic delivery of insulin by condensed drug loading in a dimpled suppository. *Drug Discov Ther.* 2017; 11:293-299.
 41. Lai SK, Wang YY, Hanes J. Mucus-penetrating nanoparticles for drug ad gene delivery to mucosal tissues. *Adv Drug Deliv Rev.* 2009; 61:158-171.

(Received November 30, 2019; Revised December 20, 2019; Accepted December 21, 2019)

FADS2 and ELOVL6 mutation frequencies in Japanese Crohn's disease patients

Yutaro Motoi¹, Zensho Ito², Shizuka Suzuki², Shinichiro Takami², Kaori Matsuo¹, Mio Sato¹, Yuki Ota¹, Mizuki Tsuruta¹, Masahiro Kojima¹, Mitsutaka Noguchi¹, Kan Uchiyama², Takahiro Kubota^{1,*}

¹Department of Biopharmaceutics, Faculty of Pharmaceutical Sciences, Niigata University of Pharmacy and Applied Life Sciences, Niigata, Japan;

²Department of Internal Medicine, Division of Gastroenterology and Hepatology, The Jikei University Kashiwa Hospital, Chiba, Japan.

Summary

Crohn's disease (CD) development is thought to involve genetic factors related to immune response as well as environmental factors, such as intestinal bacteria and diet, though no clear cause has yet been identified. In our previous study, we found that the concentrations of linoleic acid, stearic acid, and metabolites in erythrocytes differed between CD patients and healthy subjects. These factors related to lipid metabolism are controlled by $\Delta 6$ desaturase (fatty acid desaturase 2, FADS2) and elongase 6 (ELOVL6), respectively. In the present study, we analyzed the gene sequences of FADS2 and ELOVL6 in 52 Japanese CD patients, and then compared mutation frequencies with findings in healthy individuals. Nineteen FADS2 mutations and 33 ELOVL6 mutations were found. Furthermore, a new variant in the promoter region was shown in both genes, though no mutation in the coding region was found in either. For the FADS2 intron, the allele frequency of rs227784 (0.3365; 95% CI = 0.0337-0.01460) was higher than that in healthy subjects (0.0190). Furthermore, allele rs227784 had a greater association with CD (odds ratio = 4.4; 95% CI = 2.1-9.3). As compared with healthy Japanese healthy individuals, no mutations were found with a largely deviated allele frequency in the present CD group. However, the number of patients examined was small, thus the reliability of our results is limited. The present findings regarding genetic effects on CD onset and lipid metabolism may be weak.

Keywords: FADS2, ELOVL6, Crohn's disease, Japanese

1. Introduction

Crohn's disease (CD) patients have discontinuous inflammation in the digestive tract extending from the mouth to anus. Currently, there are more than 40,000 such patients in Japan, twice the number of 20 years ago (1). CD occurrence is thought to be caused by genetic factors related to immune response as well as environmental factors, such as intestinal bacteria and diet, though no clear causes have been clarified (2-

5). One such factor is considered to be lipotoxicity due to excessive intake of lipids. Linoleic acid (LA), a vegetable oil-derived n-6 polyunsaturated fatty acid (n-6 PUFA), is metabolized to pro-inflammatory eicosanoids, such as prostaglandin, leukotriene, and thromboxane, via dihomo- γ -linoleic acid (DGLA) and arachidonic acid (AA) (Figure 1). The metabolic rate-limiting enzyme from LA to AA is $\Delta 6$ desaturase (fatty acid desaturase 2, FADS2), which is involved in desaturation of LA, with the FADS2 gene located on chromosome 11 and mainly expressed in the liver, heart, and brain (6). Enzyme activities show individual differences, and it is thought that the onset of CD is caused by an imbalance between LA and its metabolites, as previous studies have reported that the ratio of LA metabolites to LA in erythrocyte

*Address correspondence to:

Dr. Takahiro KUBOTA, Department of Biopharmaceutics, Faculty of Pharmaceutical Sciences, Niigata University of Pharmacy and Applied Life Sciences, F103a, 265-1 Higashijima, Akiha-ku, Niigata city 956-8603, Japan.
E-mail: tkubota-ky@umin.net

membranes and plasma was higher in CD patients as compared to healthy individuals (7,8). Additionally, those studies found that the ratio of palmitic acid (PA) to stearic acid (SA) was different between CD patient and healthy groups. Elongation from PA to SA involves elongase 6 (elongation of the very long chain fatty acids protein 6, ELOVL6). The *ELOVL6* gene is encoded on chromosome 4 and lipid-induced inflammation has been found to be reduced in *ELOVL6* knockout mice (9). Therefore, we speculated that individual differences in *ELOVL6* activity can also have effects on intestinal inflammation in CD patients.

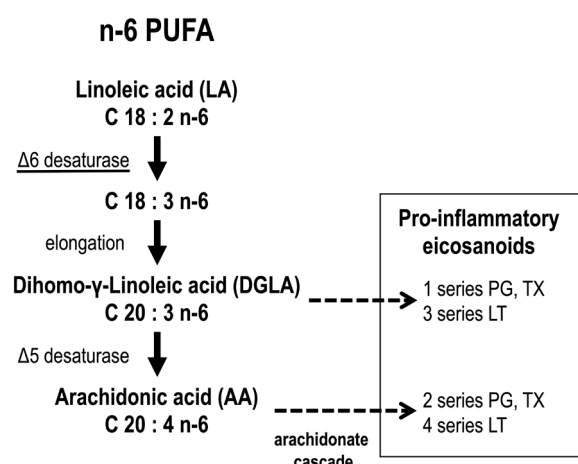


Figure 1. Metabolism of n-6 polyunsaturated fatty acids. LA is metabolized to DGLA and AA by $\Delta 6$ desaturase and elongation. The metabolites are converted to pro-inflammatory eicosanoids, prostaglandin, thromboxane, and leukotriene.

In the present study, we focused on the *FADS2* and *ELOVL6* genes, known to be involved in lipid metabolism, and performed gene sequence analysis with CD patients. The obtained genetic information was compared with that of healthy subjects to detect mutations specific to CD.

2. Materials and Methods

2.1. Subjects and ethical considerations

Fifty-two CD patients receiving treatment at Jikei University Kashiwa Hospital in Japan were enrolled and DNA samples extracted from obtained blood were analyzed. This study was approved by the ethics committee of Jikei University {26-363(7869)}, as well as the ethics committee of Niigata University of Pharmacy and Applied Life Sciences (H27-005). All participants received an explanation regarding the purpose of the study and methods involved prior to enrollment, and each provided individual consent.

2.2. PCR conditions

We designed specific primers for amplification of the promoter, translated, and untranslated regions (5'UTR, 3'UTR) of human *FADS2* and *ELOVL6* (Figure 2, Tables S1 and S2, <http://www.ddtjournal.com/action/getSupplementalData.php?ID=52>). Oligo DNA synthesis was performed by Hokkaido System Science Co., Ltd. (Hokkaido, Japan). The composition of the reaction solution and PCR conditions are shown in

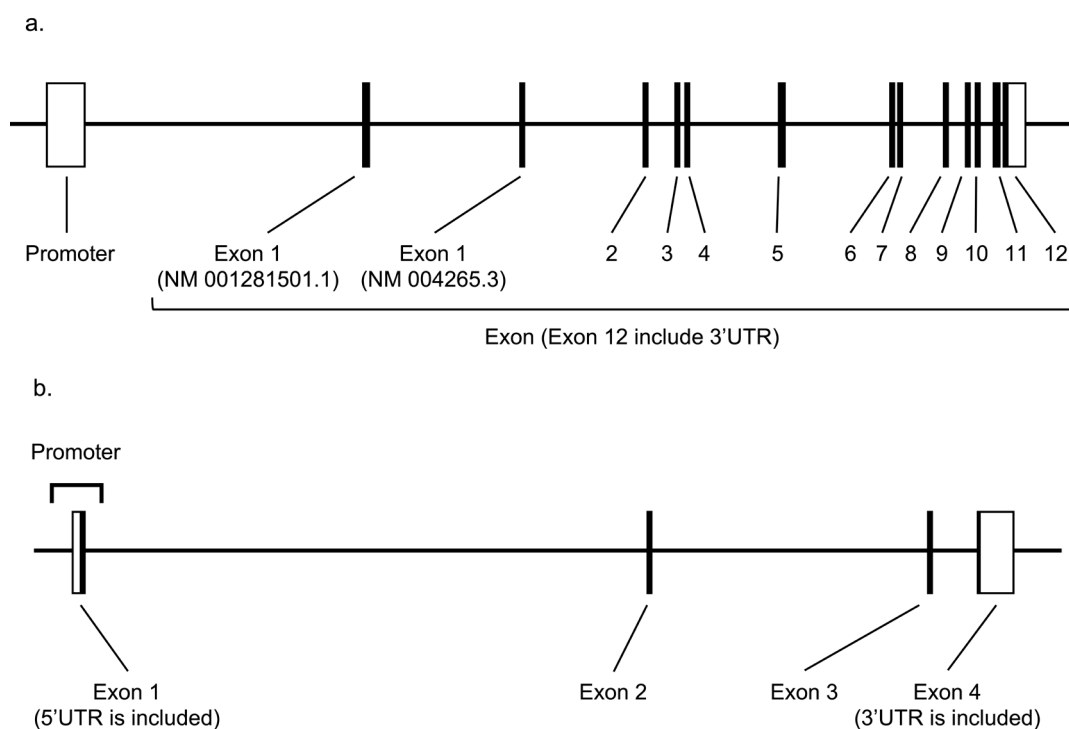


Figure 2. Amplified region of each gene. (a) *FADS2* gene region. (b) *ELOVL6* gene region.

the Tables S3-6 (<http://www.ddtjournal.com/action/getSupplementalData.php?ID=52>). The promoter region and 3'UTR of each gene were arbitrarily divided and amplified. Amplification of PCR products was detected by ultraviolet irradiation after agarose electrophoresis.

2.3. Direct sequencing

For pretreatment prior to direct sequencing, 1 μ L of alkaline phosphatase and 1 μ L of exonuclease I were added to 5 μ L of the PCR product, then heated at 37°C for 15 minutes and 80°C for 15 minutes. DNA sequencing was performed by Eurofins Genomics K.K. (Tokyo, Japan). Direct sequencing was done using the obtained PCR products as templates. The sequences of Homo sapiens chromosome 11, GRCh 37.p5 primary assembly (NC_000011.10) for *FADS2*, and sequences of Homo sapiens chromosome 4 and GRCh 38.p12 primary assembly (NC_000004.12) for *ELOVL6* were used as controls to confirm the gene sequences.

2.4. Statistical analysis

Allele frequencies were calculated based on genotype frequencies. Hardy-Weinberg equilibrium was determined by comparing genotype frequency with the expected value using a χ^2 test. A *p*-value less than 0.05 was considered to indicate statistical significance. The 95% confidence interval (95% CI) of the allele frequencies was calculated on the basis of binomial distribution.

We used data in a genome database of healthy Japanese individuals as a control group to verify the association between mutations and CD. Fisher's exact test was utilized for statistical differences, with the level of rejection of a null hypothesis denoted as $\alpha = 0.05$ for two tails. The odds ratio (OR) and its 95%CI were calculated for strength of relevance. All statistical processing was performed using the BellCurve[®] software package for Excel (Social Survey Research Information Co., Ltd.).

3. Results and Discussion

Sequence analyses of *FADS2* and *ELOVL6* were performed with 52 Japanese CD patients. In *FADS2*, we found 2, 12, and 5 mutations in the promoter, intron, and 3'UTR, respectively, while 14 mutations were detected in the promoter, 1 in the intron, and 18 in 3'UTR of *ELOVL6*. One novel mutation was confirmed in the promoter regions of both genes, whereas no mutation was detected in the coding region of either. The genotype and allele frequencies, and 95% CI of the mutations were calculated (Tables 1 and 2, <http://www.ddtjournal.com/action/getSupplementalData.php?ID=52>). Furthermore, we compared the 95%

CI values with those in database records containing human genome information (Tables 1 and 2, <http://www.ddtjournal.com/action/getSupplementalData.php?ID=52>). The Japanese Multi Omics Reference Panel (jMorp) (10) was used for comparisons with healthy Japanese and The Genome Aggregation Database (gnomAD) (11) for comparisons with other species.

In the comparison of *FADS2*, the allele frequency of rs2277284 (0.0769; 95% CI = 0.0337-0.1460) was higher than that in jMorp (0.0190) and the odds ratio was 4.4 (95% CI = 2.1-9.3). However, the genotype frequency of rs2277284 deviated from Hardy Weinberg's equilibrium and no heterozygotes were detected, in contrast to detection of 4 homozygotes. In addition, the rs2277284 allele frequency for East Asians (EAS) in gnomAD (0.0611) was nearly the same as the present result.

As for *ELOVL6*, the allele frequency of rs150566425 (0.0192; 95% CI = 0.0023-0.0677) deviated from the findings in jMorp (0.0004). On the other hand, the frequencies of allele rs755746 (0.0288; 95% CI = 0.0060-0.0820) and that in jMorp (0.0315) were lower than the frequency of EAS in gnomAD (0.1137).

In the present CD patients, no mutation was detected in the coding region of either *FADS2* or *ELOVL6*. At present, none of the genes that cause amino acid mutations have been reported to have a frequency greater than 1%. Therefore, it can be concluded that there are no contradictions with these analysis results.

For *FADS2*, the allelic frequencies of rs174538 and rs174578 in our results and in jMorp were approximately 20% lower than those of EAS in gnomAD. The frequency of these mutations is considered to be low in Japanese as compared to other East Asians. Allele rs2277284 was more frequent in the present CD patients than in healthy Japanese, suggesting that this mutation might be related to disease onset. However, there was no divergence of the allele frequency between our results and that of EAS in gnomAD, as well as only homozygotes with no heterozygosity, thus it will be necessary to examine for verification for relevance to the disease. The allele mutations rs174589, rs526126, and rs2072114 have been reported to have influence on lipid metabolism (12-16). However, there was no divergence of frequency in this study, and no association with CD onset was found.

Regarding *ELOVL6*, the mutation frequency of allele rs755746 in our results and in jMorp was about 10% lower than that of EAS in gnomAD. Among East Asian races, Japanese are thought to have a low frequency of this mutation. Allele rs150566425 is suggested to be related to onset and mutation, because it was found more frequently in CD patients than healthy individuals. The allele frequencies of rs5860996 and rs200600528 obtained in the present study were slightly lower than

Table 1. Allele frequencies and odds ratio of FADS2.

Items	rsID	Position [†]	Mutation	Genotype (%; N = 52)		Allele frequency (95%CI)	Odds ratio (95%CI)	p value	jMorp (5)	gnomAD (6)				
				A/A	A/a					EAS	AMR	ASJ	NFE	AFR
Promoter	rs174538	61,792,609	g > a	36.5	42.3	0.4231 (0.3267~0.5239)	1.2170 (0.8224~1.8011)	0.3590	0.3770	0.5722	0.5955	0.2690	0.3060	0.0685
	New	61,792,811	a > c	98.1	1.9	0.0096 (0.0002~0.0524)	NA	NA	NA	NA	NA	NA	NA	NA
Intron	rs2072114	61,837,743	a > g	48.1	36.5	0.3365 (0.2468~0.4358)	1.2689 (0.8420~1.9121)	0.2743	0.2872	0.4310	0.3085	0.1379	0.1523	0.1293
	rs174578	61,838,027	t > a	36.5	40.4	0.4327 (0.3358~0.5335)	1.2391 (0.8380~1.8322)	0.3091	0.3803	0.5788	0.6312	0.3414	0.3495	0.3738
	rs174589	61,848,331	c > g	78.9	21.2	0.1058 (0.0539~0.1814)	1.1140 (0.5933~2.0916)	0.7364	0.0990	0.1477	0.3042	0.1621	0.1887	0.0432
	rs144659223	61,848,406	c > a	92.3	7.7	0.0385 (0.0105~0.0956)	2.5193 (0.9110~6.9665)	0.0843	0.0158	0	0.0035	0	0.0005	0
	rs374558244	61,857,127	c > t	98.1	1.9	0.0096 (0.0002~0.0524)	NA	NA	NA	0.0006	0	0	0.0001	0.0005
	rs526126	61,857,413	g > c	1.9	21.2	0.8750 (0.7957~0.9317)	0.6837 (0.3801~1.2297)	0.2222	0.9131	0.8329	0.8491	0.7862	0.8235	0.3297
	rs553613434	61,857,613	g > a	98.1	1.9	0.0096 (0.0002~0.0524)	NA	NA	0.0017	0.0026	0	0	0	0
	rs2277284	61,857,643	g > t	92.3	0.0	0.0769 (0.0337~0.1460)	4.4218 (2.1055~9.2863)	0.0009	0.0190	0.0611	0.0378	0.0103	0.0055	0.2950
	rs141055240	61,863,162	t > c	86.5	13.5	0.0673 (0.0274~0.1338)	2.1457 (0.9849~4.6746)	0.0856	0.0334	0.0783	0.0024	0.0069	0.0004	0.0358
	rs145771202	61,863,592	c > t	98.1	1.9	0.0096 (0.0002~0.0524)	0.9600 (0.1320~6.9817)	1.0000	0.0104	0	0	0	0	0
	rs1162570716	61,863,638	c > a	98.1	1.9	0.0096 (0.0002~0.0524)	NA	NA	NA	NA	NA	NA	NA	NA
	rs520298	61,863,810	c > a	98.1	1.9	0.0096 (0.0002~0.0524)	NA	NA	0.0003	0	0	0	0	0
3'UTR	rs139145063	61,865,702	c > t	86.5	13.5	0.0673 (0.0274~0.1338)	2.1579 (0.9908~4.7001)	0.0849	0.0334	0.0770	0.0012	0.0069	0.0002	0.0053
	rs11539527	61,866,116	a > g	86.5	13.5	0.0673 (0.0274~0.1338)	2.0804 (0.9555~4.5296)	0.0901	0.0336	0.0770	0.0024	0.0069	0.0005	0.0547
	rs142344045	61,866,134	c > t	98.1	1.9	0.0096 (0.0002~0.0524)	NA	NA	0.0086	0	0	0	0	
	rs17156516	61,866,232	g > a	86.5	13.5	0.0673 (0.0274~0.1338)	2.1178 (0.9726~4.6115)	0.0874	0.0335	0.0764	0.0024	0.0069	0.0006	0.0547
	rs1359586116	61,866,402	c > t	98.1	1.9	0.0096 (0.0002~0.0524)	NA	NA	NA	NA	NA	NA	NA	NA

3'UTR, 3' untranslated region; 95%CI, 95% Confidence interval; AFR, African; AMR, American (Latino); ASI, Ashkenazi Jewish; EAS, East Asian; NFE, Non-Finnish European; NA, Not applicable. [†]NC_000011.10.

Table 2. Allele frequencies and odds ratio of *Elovl6*.

Items	rsID	Position [†]	Mutation	Genotype (% <i>N</i> , <i>N</i> = 52)		Allele frequency (95%CI)	Odds ratio (95%CI)	<i>p</i> value	jMorp (δ)	gnomAD (<i>g</i>)						
				A/A	A/a					A/a	a/a	EAS	AMR	ASJ	NFE	AFR
Promoter	rs6824447	110,199,557	<i>g > a</i>	46.2	38.5	15.4	0.3462 (0.2555-0.4458)	0.9354 (0.6228-1.4051)	0.8372	0.3615	0.3404	0.3955	0.5931	0.5032	0.7302	
	rs3813830	110,199,112	<i>g > a</i>	94.2	5.8	0.0	0.0288 (0.0060-0.0820)	0.9501 (0.2980-3.0294)	1.0000	0.0314	0.0508	0.0498	0	0.0025	0.0002	
	rs3813829	110,199,010	<i>a > g</i>	61.5	32.7	5.8	0.2212 (0.1457-0.3131)	0.8716 (0.5467-1.3894)	0.6463	0.2466	0.2487	0.2783	0.4688	0.3431	0.3761	
	rs3813828	110,198,992	<i>a > g</i>	76.9	21.2	1.9	0.1250 (0.0683-0.2043)	1.2040 (0.6699-2.1637)	0.5206	0.1066	0.0721	0.0330	0.0345	0.0496	0.0362	
	rs140223270	110,198,740	<i>g > t</i>	96.2	3.8	0.0	0.0192 (0.0023-0.0677)	NA	NA	NA	0	0	0	0	0.0001	
	rs1054469231	110,198,568	<i>g > a</i>	98.1	1.9	0.0	0.0096 (0.0002-0.0524)	NA	NA	0.0014	NA	NA	NA	NA	NA	NA
	rs755746	110,198,070	<i>a > t</i>	94.2	5.8	0.0	0.0288 (0.0060-0.0820)	0.8608 (0.2708-2.7364)	1.0000	0.0315	0.1137	0.0979	0	0.0046	0.0320	
	rs755747	110,197,906	<i>g > a</i>	76.9	21.2	1.9	0.1250 (0.0683-0.2043)	1.2312 (0.6851-2.2125)	0.5159	0.1064	0.0718	0.0330	0.0345	0.0497	0.0360	
	rs990095271	110,196,887	<i>ggaggag > ggag</i>	98.1	1.9	0.0	0.0096 (0.0002-0.0524)	NA	NA	0.0001	NA	NA	NA	NA	NA	NA
	rs968600	110,196,633	<i>g > a</i>	5.8	23.1	71.2	0.8269 (0.7403-0.8941)	0.9731 (0.5833-1.6236)	0.8953	0.8311	0.8245	0.8534	0.8138	0.8284	0.8595	
	rs575275791	110,196,465	<i>g > a</i>	98.1	1.9	0.0	0.0096 (0.0002-0.0524)	NA	NA	0.0045	0.0006	0	0	0	0	
	New	110,196,388	<i>g > a</i>	98.1	1.9	0.0	0.0096 (0.0002-0.0524)	NA	NA	NA	NA	NA	NA	NA	NA	NA
	rs569200155	110,196,189	<i>g > c</i>	98.1	1.9	0.0	0.0096 (0.0002-0.0524)	NA	NA	0.0023	0.0090	0	0	0	0	
	rs11098070	110,196,091	<i>a > g</i>	13.5	44.2	42.3	0.6442 (0.5440-0.7361)	1.4213 (0.9487-2.1291)	0.0912	0.5602	0.5613	0.5260	0.4552	0.5206	0.3405	
	Intron	rs3733623	110,105,364	<i>t > c</i>	5.8	36.5	57.7	0.7596 (0.6659-0.8380)	NA	0.7242	0.7089	0.3389	0.2743	0.2344	0.4178	
	3'UTR	rs537457824	110,050,844	<i>atata > atatatata</i>	98.1	1.9	0.0	0.0096 (0.0002-0.0524)	NA	0.0160	0.0167	0	0	0	0.0001	0.0001
		rs149752874	110,050,418	<i>c > g</i>	94.2	5.8	0.0	0.0288 (0.0060-0.0820)	1.2414 (0.3897-3.9543)	0.7368	0.0235	NA	NA	NA	NA	NA
		rs4698806	110,050,333	<i>a > g</i>	21.2	51.9	26.9	0.5288 (0.4285-0.6275)	0.7308 (0.4958-1.0772)	0.1294	0.6056	0.5889	0.5849	0.4103	0.3346	0.8035
		rs9995789	110,049,874	<i>g > t</i>	30.8	55.8	13.5	0.4135 (0.3177-0.5142)	0.7887 (0.5323-1.1684)	0.2764	0.4720	0.4478	0.3631	0.2448	0.1740	0.6874
		rs150566425	110,049,550	<i>t > c</i>	96.2	3.8	0.0	0.0192 (0.0023-0.0677)	NA	NA	0.0004	NA	NA	NA	NA	NA
rs371671518		110,049,258	<i>a > g</i>	98.1	1.9	0.0	0.0096 (0.0002-0.0524)	NA	NA	0.0034	0.0006	0	0	0	0	
rs17041272		110,048,926	<i>c > g</i>	73.1	25.0	1.9	0.1442 (0.0822-0.2277)	0.7527 (0.4341-1.3051)	0.3707	0.1834	0.1722	0.0932	0.0655	0.0524	0.1759	
rs5860996		110,048,716	<i>aaaaaaaa > aaaaaaa</i>	19.2	42.3	25.0	0.4615 (0.3633-0.5620)	NA	NA	0.5345	0.5715	0.5095	0.4097	0.3779	0.8208	
rs200600528		110,048,706	<i>tgtttgtttta > t</i>	80.8	17.3	1.9	0.1058 (0.0540-0.1814)	0.7028 (0.4770-1.0355)	0.0855	0.6068	0.5938	0.4941	0.4034	0.3407	0.8006	
rs6837303		110,048,429	<i>c > t</i>	23.1	50.0	26.9	0.5192 (0.4189-0.6186)	0.6370 (0.3552-1.1426)	0.1582	0.1834	0.1727	0.0934	0.0655	0.0525	0.1767	
rs6836309		110,048,416	<i>c > t</i>	76.9	21.2	1.9	0.1250 (0.0683-0.2043)	0.8485 (0.4524-1.5915)	0.7624	0.1223	0.1211	0.0165	0.0207	0.0306	0.0202	
rs78610984		110,047,988	<i>a > c</i>	80.8	17.3	1.9	0.1058 (0.0540-0.1814)	0.8586 (0.4577-1.6107)	0.7619	0.1220	0.1210	0.0154	0.0207	0.0306	0.0078	
rs77807740		110,047,676	<i>g > a</i>	73.1	23.1	3.8	0.1538 (0.0906-0.2378)	0.9018 (0.5273-1.5423)	0.7920	0.1722	0.1497	0.0165	0.0207	0.0305	0.0078	
rs3733624		110,047,354	<i>c > g</i>	42.3	53.8	3.8	0.3077 (0.2209-0.4058)	1.0726 (0.7050-1.6317)	0.7453	0.3397	0.3077	0.2043	0.0182	0.0339	0.0155	
rs3813826		110,046,632	<i>t > g</i>	73.1	25.0	1.9	0.1442 (0.0822-0.2277)	0.7475 (0.4311-1.2961)	0.3710	0.1852	0.1735	0.0884	0.0655	0.0520	0.1116	
rs3813825		110,046,513	<i>t > a</i>	28.8	55.8	15.4	0.4327 (0.3359-0.5335)	0.8557 (0.5789-1.2647)	0.4888	0.4718	0.4402	0.3113	0.1793	0.1982	0.0883	
rs9030		110,046,154	<i>a > g</i>	28.8	55.8	15.4	0.4327 (0.3359-0.5335)	0.8542 (0.5779-1.2625)	0.4888	0.4721	0.4406	0.4005	0.3379	0.2881	0.6462	

3'UTR, 3' untranslated region; 95%CI, 95% Confidence interval; AFR, African; AMR, American (Latino); ASI, Ashkenazi Jewish; EAS, East Asian; NFE, Non-Finnish European; NA, Not applicable. [†]NC_000004.12.

those in jMorp and EAS in gnomAD. These deletion mutations are very close to each other and overlap in registered defective bases, thus it is unclear whether they can be correctly distinguished in the existing databases. Although there is no report regarding *ELOVL6* in CD, an association with diabetes has been shown. *ELOVL6* activity was reported to have effects on development of diabetes and inflammation associated with onset of that disease (9). Also, Morcillo *et al.* reported that the risk of insulin resistance was decreased when the rs6824447 mutation was present, while the risk increased in individuals with the rs17041272 mutation (17). On the other hand, Liu *et al.* reported that there were no significant differences regarding those mutations between healthy and type 2 diabetic patients (18). We consider that the association with CD onset is low, because no divergence was found in the frequency of any of the mutations examined in this study.

In the present study, gene sequence analyses of *FADS2* and *ELOVL6* in CD patients were performed. In general, no mutations were found that largely deviated in allele frequency as compared with healthy Japanese individuals. However, the number of patients examined was few, which limits the reliability of our results. The present findings suggest that genetic effects may be weak between CD onset and lipid metabolism. Nevertheless, it is possible that some healthy individuals may carry mutations associated with CD development. In the future, we intend to analyze lipid distribution in plasma and erythrocyte membrane specimens, and investigate the causal relationship with genetic information for CD patients obtained in this study.

References

1. Japan intractable diseases information center. <http://www.nanbyou.or.jp/entry/5354> (accessed October 21, 2019).
2. Abraham C, Cho JH. Inflammatory bowel disease. *N Engl J Med.* 2009; 361:2066-78.
3. Harris ML, Bayless TM. Dietary antigens as aggravating factors in Crohn's disease. *Dig Dis Sci.* 1989; 34:1613-1614.
4. Sartor RB. Pathogenesis and immune mechanisms of chronic inflammatory bowel diseases. *Am J Gastroenterol.* 1997; 92:5S-11S.
5. Powell JJ, Harvey RS, Ashwood P, Wolstencroft R, Gershwin ME, Thompson RP. Immune potentiation of ultrafine dietary particles in normal subjects and patients with inflammatory bowel disease. *J Autoimmun.* 2000; 14:99-105.
6. Cho HP, Nakamura MT, Clarke SD. Cloning, expression, and nutritional regulation of the mammalian Δ -6 desaturase. *J Biol Chem.* 1999; 274:471-477.
7. Uchiyama K, Odahara S, Nakamura M, Koido S, Katahira K, Shiraishi H, Ohkusa T, Fujise K, Tajiri H. The fatty acid profile of the erythrocyte membrane in initial-onset inflammatory bowel disease patients. *Dig Dis Sci.* 2013; 58:1235-1243.
8. Ito Z, Uchiyama K, Odahara S, Takami S, Saito K, Kobayashi H, Koido S, Kubota T, Ohkusa T, Saruta M. Fatty acids as useful serological markers for Crohn's disease. *Dig Dis.* 2018; 36:209-217.
9. Zhao H, Matsuzaka T, Nakano Y, *et al.* *Elovl6* deficiency improves glycemic control in diabetic db/db mice by expanding β -cell mass and increasing insulin secretory capacity. *Diabetes.* 2017; 66:1833-1846.
10. Tadaka S, Katsuoka F, Ueki M, *et al.* 3.5KJPNv2, an allele frequency panel of 3,552 Japanese Individuals. *bioRxiv.* 2019. DOI: <http://dx.doi.org/10.1101/529529>
11. Karczewski KJ, Francioli LC, Tiao G, *et al.* Variation across 141,456 human exomes and genomes reveals the spectrum of loss-of-function intolerance across human protein-coding genes. *bioRxiv.* 2019. DOI: <https://doi.org/10.1101/531210>
12. Schaeffer L, Gohlke H, Müller M, Heid IM, Palmer LJ, Kompauer I, Demmelmair H, Illig T, Koletzko B, Heinrich J. Common genetic variants of the *FADS1* *FADS2* gene cluster and their reconstructed haplotypes are associated with the fatty acid composition in phospholipids. *Hum Mol Genet.* 2006; 15:1745-1756.
13. Martinelli N, Girelli D, Malerba G, Guarini P, Illig T, Trabetti E, Sandri M, Friso S, Pizzolo F, Schaeffer L, Heinrich J, Pignatti PF, Corrocher R, Olivieri O. *FADS* genotypes and desaturase activity estimated by the ratio of arachidonic acid to linoleic acid are associated with inflammation and coronary artery disease. *Am J Clin Nutr.* 2008; 88:941-949.
14. Malerba G, Schaeffer L, Xumerle L, *et al.* SNPs of the *FADS* gene cluster are associated with polyunsaturated fatty acids in a cohort of patients with cardiovascular disease. *Lipids.* 2008; 43:289-299.
15. Bokor S, Dumont J, Spinneker A, Gonzalez-Gross M, Nova E, Widhalm K, Moschonis G, Stehle P, Amouyel P, De Henauw S, Molnár D, Moreno LA, Meirhaeghe A, Dallongeville J. Single nucleotide polymorphisms in the *FADS* gene cluster are associated with delta-5 and delta-6 desaturase activities estimated by serum fatty acid ratios. *J Lipid Res.* 2010; 51:2325-2333.
16. Merino DM, Johnston H, Clarke S, Roke K, Nielsen D, Badawi A, El-Sohehy A, Ma DWL, Mutch DM. Polymorphisms in *FADS1* and *FADS2* alter desaturase activity in young Caucasian and Asian adults. *Mol Genet Metab.* 2011; 103:171-178.
17. Morcillo S, Martín-Núñez GM, Rojo-Martínez G, Almaraz MC, García-Escobar E, Mansego ML, de Marco G, Chaves FJ, Soriguer F. *ELOVL6* genetic variation is related to insulin sensitivity: A new candidate gene in energy metabolism. *PLoS One.* 2011; 6:e21198.
18. Liu Y, Wang F, Yu XL, Miao ZM, Wang ZC, Chen Y, Wang YG. Genetic analysis of the *ELOVL6* gene polymorphism associated with type 2 diabetes mellitus. *Braz J Med Biol Res.* 2013; 46:623-628.

(Received October 23, 2019; Revised December 21, 2019; Accepted December 22, 2019)

Feasibility of microbial sample collection on the skin from people in Yaoundé, Cameroon

Nana C. Benderli^{1,2,§}, Kazuhiro Ogai^{3,§}, Yukie M. Lloyd⁴, John Paul Arios⁴, Boonyanudh Jiyarom⁴, A. Honore Awanakam¹, Livo Forgu Esemu¹, Aki Hori⁵, Rosette Megnekou^{1,2}, Rose G.F. Leke¹, Takayuki Kuraishi^{5,*}, Shigefumi Okamoto^{3,*}, Gabriel Loni Ekali^{1,6}

¹The Biotechnology Center, University of Yaoundé I, Yaoundé, Cameroon;

²Department of Animals Biology and Physiology, University of Yaoundé I, Yaoundé, Cameroon;

³Faculty of Health Sciences, Institute of Medical, Pharmaceutical and Health Sciences, Kanazawa University, Ishikawa, Japan;

⁴Department of Tropical Medicine, Medical Microbiology and Pharmacology, John A. Burns School of Medicine, University of Hawaii at Manoa, Honolulu, Hawaii, U.S.A.;

⁵Department of Faculty of Pharmacy, Institute of Medical, Pharmaceutical and Health Sciences, Kanazawa University, Ishikawa, Japan;

⁶National AIDS Control Committee, Yaoundé, Cameroon.

Summary

Characterization of microbial communities in the skin in healthy individuals and diseased patients holds valuable information for understanding pathogenesis of skin diseases and as a source for developing novel therapies. Notably, resources regarding skin microbiome are limited in developing countries where skin disorders from infectious diseases are extremely common. A simple method for sample collection and processing for skin microbiome studies in such countries is crucial. The aim of this study is to confirm the feasibility of collecting skin microbiota from individuals in Yaoundé, a capital city of Cameroon, and subsequent extraction of bacterial DNA in a resource limited setting. Skin swabs from several individuals in Yaoundé were successfully obtained, and sufficient amount of bacterial 16S ribosomal RNA-coding DNA was collected, which was confirmed by quantitative PCR. The median copy number of 16S ribosomal RNA gene varied across participants and collection sites, with significantly more copies in samples collected from the forehead compared to the left and right forearm, or back. This study demonstrated that collecting surface skin microbes using our swabbing method is feasible in a developing country. We further showed that even with limited resources, we could collect sufficient amount of skin microbiota from the inhabitants in Yaoundé where no studies of skin microbiome were reported, which can be passed to further metagenomic analysis such as next generation sequencing.

Keywords: Skin swabs, surface skin microbiome, developing countries, Cameroon

[§]These authors contributed equally to this work.

*Address correspondence to:

Dr. Takayuki Kuraishi, Faculty of Pharmacy, Institute of Medical, Pharmaceutical and Health Sciences, Kanazawa University, Kakuma-machi, Kanazawa, Ishikawa 920-1192, Japan.

E-mail: tkuraishi@staff.kanazawa-u.ac.jp

Dr. Shigefumi Okamoto, Faculty of Health Sciences, Institute of Medical, Pharmaceutical and Health Sciences, Kanazawa University, 5-11-80 Kodatsuni, Kanazawa, Ishikawa 9200942, Japan.

E-mail: sokamoto@mhs.mp.kanazawa-u.ac.jp

1. Introduction

The skin is one of the largest organ of human beings. In addition to its role in physical protection and temperature regulation, it serves as a unique and dynamic ecosystem that is inhabited by over 10^{10} microorganisms (*i.e.*, skin microbiota) (1). In a homeostatic environment, the skin microbiota are harmless and play a protective and/or regulatory role by controlling the innate and adaptive immune systems found in our skin (2). However, when the

environment on the skin is altered, the composition of skin microbiota can also be disrupted: a phenomenon known as dysbiosis. Studying the type of dysbiosis, for example, whether the alteration occurs at the species or strain level, provides important information for understanding skin pathology, developing a diagnostic tool and an appropriate treatment (3).

A number of studies on the association between dysbiosis and skin disorders such as atopic dermatitis (4), psoriasis (5), seborrheic dermatitis (6) and acne vulgaris (7) have been published. However, how dysbiosis of the skin microbiome relates to tropical diseases that affect skin integrity is understudied. For example, there are only a few studies to date that report dysbiosis in the skin of patients with leprosy (8,9) or leishmaniasis (10). Whether other skin-affecting tropical diseases or neglected infectious diseases (*e.g.*, tuberculosis, filariasis, schistosomiasis), as well as the infection of human immunodeficiency virus (HIV) and acquired immunodeficiency syndrome (AIDS) that may alter the skin immune system, could interact with the dysbiosis of the skin microbiota remains unclear.

The major limitation for studying the skin microbiome is the complexity of sample collection, such as consistency in collection methods and contamination risks (11), handling and storage of samples. Processing of microbial DNA is also a challenge (12,13), due to the relatively low abundance of skin microbiome compared to the gut. Along with these complexities, many developing countries in Africa also face issues with limited resources and inadequate research facilities to carry out such studies (14). Thus, it is desirable to establish a simple protocol for collecting skin samples that is feasible to carry out in a basic laboratory in a resource-limited country without compromising the quantity and quality of the microbial DNA collected. The development of such a protocol will lead to ensuring the consistency of techniques employed in the field and guarantee of the quality of data acquired.

To achieve this objective, this study attempted to evaluate the feasibility of collecting and processing skin samples at a hospital and university research laboratory in Yaoundé, Cameroon with basic equipment. A non-invasive sample collection method was employed by utilizing flocculated swabs (15) to confirm the presence of enough amount of bacterial DNA coding for 16S ribosomal RNA (rRNA).

2. Materials and Methods

2.1. Ethical consideration

This study was approved by the National Ethics Committee of Cameroon, (Ethical Clearance 2018/06/N°1045/CE/CNERSH/SP) and an authorization was obtained from the hospital administration before participants were recruited. Participation in the study

was voluntary and written informed consent was obtained from each participant prior to enrollment. Oral consent and signature from a guardian were provided for those who were physically unable to provide written consent. The study was performed in strict respect of the guidelines for human clinical research and all data were decoded for anonymity.

2.2. Collection site and sample population

This study was part of a larger cross-sectional study that took place from June to October 2018 at the HIV clinic of the Efoulan District Hospital in Yaoundé, Cameroon. The Efoulan District Hospital was chosen due to an existing collaboration with the hospital and university research center. In the original study, out-patients, in-patients and hospital staff were enrolled for sampling. HIV-uninfected, healthy subjects were defined by the absence of any known skin pathology and a negative HIV rapid diagnostic test (RDT) result; HIV-infected subjects were defined by a positive HIV RDT result. Pregnant women and those who had apparent skin disorders that are not associated with HIV or AIDS, such as atopic dermatitis and psoriasis, were excluded.

2.3. Sample collection

Skin swabs were collected using the Puritan HydraFlock Sterile Flocked Swabs (25-3306-H, Puritan Medical Products Company, ME, USA). Prior to swabbing, 1.5-mL microcentrifuge tubes were filled with 100 μ L of sterile 0.9% sodium chloride solution (S5815; Teknova, CA, USA) with 0.1% Tween 20 (28353-14; Nacalai Tesque, Inc., Kyoto, Japan). First the swab head was soaked in the solution in the tube (16,17). Swabbing was then performed in a 5 \times 5 cm-square on designated sites (Figure S1, <http://www.ddtjournal.com/action/getSupplementalData.php?ID=51>). The patients with Kaposi's sarcoma were additionally swabbed at lesion sites. After swabbing, each swab head was placed into the original tubes (Figure S2, <http://www.ddtjournal.com/action/getSupplementalData.php?ID=51>). Samples were stored in a cooler box and transferred to the laboratory for DNA extraction.

2.4. DNA extraction from skin swab samples

DNA was extracted from samples using the Kaneka Easy DNA Extraction Kit version 2 (KN-T110005; Kaneka Corp., Tokyo, Japan), which contains DNA extraction Solutions A and B, according to the manufacturer's instructions (Figure S2, <http://www.ddtjournal.com/action/getSupplementalData.php?ID=51>). Briefly, 200 μ L of Solution A was added into each microcentrifuge tube containing the swab head and was mixed by vortexing. Next, sample tubes were placed in a water bath and incubated for 9 min at

98 °C. The samples were cooled to room temperature, and 28 µL of Solution B was added to each tube. After mixing briefly by vortexing, samples were stored at -20°C until further analysis.

2.5. Qualitative PCR amplification of 16S rRNA gene

To confirm whether bacterial DNA was successfully obtained, qualitative PCR amplification of the 16S rRNA gene was performed using SapphireAmp Fast PCR Master Mix (RR350A, Takara Bio Inc., Shiga, Japan) and primers (forward: 341F, 5'-CCTACGGGNGGCWGCAG-3'; reverse: 806Rmod, 5'-GACTACHVGGGTATCTAAKCC-3'; targeting 460-bp V3-V4 region of the 16S rRNA gene). One microliter of the template DNA was used in the 10 µL reaction mixture. The PCR protocol was set as: 94°C for 1 min; 33 cycles of 98°C for 10 sec, 55°C for 10 sec, and 72°C for 15 sec; and 72°C for 1 min. The PCR products were then electrophoresed by using i-MyRun II (IMR2-001, CosmoBio Co., Ltd., Tokyo, Japan) with 2% Agarose S (312-01193, FUJIFILM Wako Pure Chemical Corp., Osaka, Japan) gel, stained by 0.5 µg/mL ethidium bromide (315-90051, FUJIFILM Wako Pure Chemical Corp.), and visualized using LuminoGraph I (WES-6100, ATTO Corp., Tokyo, Japan). The presence of a band at the expected size (~460 bp) for each sample was determined positive.

2.6. DNA clean up

To exclude the possibility of PCR inhibition, DNA samples were cleaned using a NucleoSpin gDNA Clean-up kit (740230, Macherey-Nagel GmbH & Co. KG, Düren, Germany) according to the manufacturer's instructions. The samples were stored at -20°C until further analysis.

2.7. Quantitative PCR

Quantitative real-time PCR (qPCR) was performed as described elsewhere (18). In brief, the DNA samples were amplified with 16S universal primer pairs (F: 5'-ACTGAGAYACGGYCCA-3'; R: 5'-CTGCTGGCACGDAGTTAGCC-3') and a 16S universal probe (5'-VIC-ACTGCTGCCTCCCGTANFQ-MGB-3') by using the Thunderbird Probe qPCR Mix (Toyobo Co., Ltd., Osaka, Japan). A standard curve was drawn from a known amount of the 16S rRNA gene. All the reactions were performed with the LightCycler 480 System (F. Hoffmann-La Roche, Ltd., Basel, Switzerland).

2.8. Statistical data analysis

Data are shown as the 25th, 50th, 75th percentile boxes

with 25th percentile - 1.5 × interquartile range (IQR) to 75th percentile + 1.5 × IQR whisker in the box plot. The box plot with dots was created using the R statistical software (version 3.6.0). The differences in the copy number of the 16S rRNA gene among groups were compared by using the Kruskal-Wallis test followed by the Steel-Dwass *post hoc* multiple comparison test using R. A *p*-value < 0.05 was considered statistically significant.

3. Results and Discussion

In Yaoundé, Cameroon, we successfully obtained skin swab samples of head, left and right arms and back from 26 HIV-negative healthy individuals (males: 7, females: 19; age 21-51, median 27) and 25 HIV-positive patients (males: 5, females: 20; age 22-61, median 39). Of all the HIV-positive patients, two patients presented with Kaposi's sarcoma, and swabs from the sarcoma lesions were also obtained from those patients.

There are multiple skin microbiome sampling methods, including swabs, biopsies, surface scrapes, cup scrubs and tape strips (18,19). Each method varies in biomass yield, human DNA contribution, sampling depth and discomfort level. Since patients with skin disorder are commonly sensitive to skin stimulation, it is difficult to tolerate even minimal pain that accompanies invasive methods. To overcome this problem, using pre-moistened skin swabs was our method of choice. As a result, no skin-related troubles were reported when collecting skin samples, even in patients who were immunosuppressed with later stages of AIDS.

Next, we attempted to confirm if the extracted DNA can be used for subsequent bacterial DNA analysis (*e.g.*, next generation sequencing [NGS]) by qualitative PCR for the bacterial 16S rRNA gene. Although crudely extracted DNA samples processed just after the DNA extraction still contain debris of skin cells, sebum, and dirt, we found that nine out of 18 representative samples were successfully amplified by PCR (Figure S3, <http://www.ddtjournal.com/action/getSupplementalData.php?ID=51>). Lack of amplicons is likely due to the presence of skin cells, sebum or other debris, which could interfere with the PCR amplification process of extracted DNA. Contamination of these objects can be explained by the lack of washing steps for the kit used in this study; which is otherwise beneficial by reducing the burden of sample processing.

To minimize any interference from heavy contamination of human cell debris and/or sebum, all crude DNA samples were cleaned with a gDNA cleaning kit. After cleaning of crude DNA samples, the targeted area of 16S rRNA gene was successfully amplified for all samples tested without any non-specific products, regardless of swabbing area (Figures 1 and S3, <http://www.ddtjournal.com/action/>

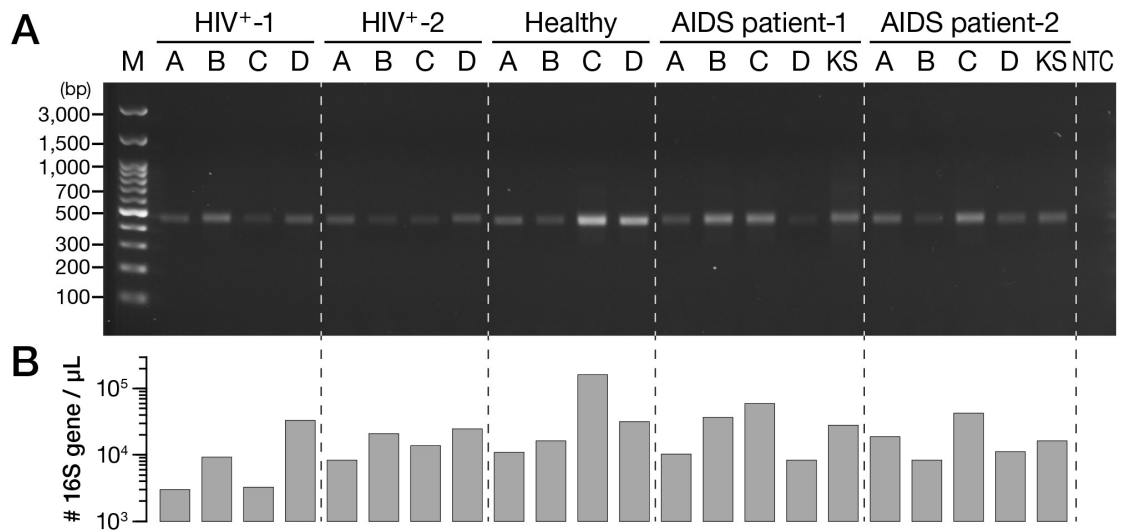


Figure 1. Successful amplification of bacterial 16S rRNA gene from skin swabs obtained from Cameroonians at the Efoulan district hospital. (A) Representative amplicons of the 16S rRNA gene (covering V3-V4 region, expected size ~ 460 bp) derived from two HIV-positive patients, one healthy individual, and two AIDS patients were electrophoresed and visualized. (B) The numbers of 16S rRNA gene in each sample. Each individual was sampled from four regions of interest, namely, the forehead (denoted as A), right forearm (B), left forearm (C), and mid-upper back (D). Skin swabs on the lesion of Kaposi's sarcoma in AIDS patients were also analyzed and visualized (KS). M: 100 bp marker, NTC: no template control.

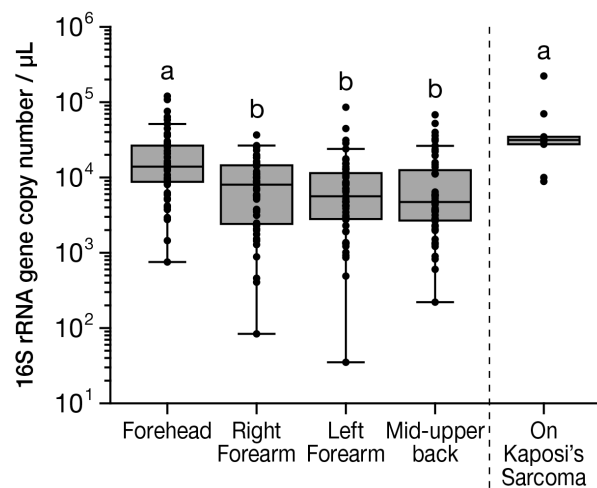


Figure 2. Copy number of obtained bacterial 16S rRNA gene. Although the amount of 16S rRNA gene varied among participants and collection sites, sufficient amount of 16S rRNA gene was successfully obtained. The same letters indicate no significant difference, whereas different letters indicate significant difference ($p < 0.05$) between the groups.

getSupplementalData.php?ID=51). Bands for two samples, 10D and 40B, were extremely faint but present as confirmed by qPCR. For samples 19C and 40B, the signals diminished after cleaning, probably due to technical error.

We next quantified the copy number of bacterial 16S rRNA gene in each sample. Copy numbers of 16S rRNA gene slightly differed depending on the individual and body parts of collection; samples collected from the forehead and the lesion of Kaposi's sarcoma showed significantly higher copy numbers of the 16S rRNA gene (Figure 2 and Table 1). Except for a few samples (2 samples showed < 100 copies/ μ L), we confirmed

Table 1. p -values of the multiple comparison in the number of 16S copy number

	Forehead	Right forearm	Left forearm	Mid-upper back
Right forearm	0.003	-	-	-
Left forearm	<0.001	0.94	-	-
Mid-upper back	<0.001	0.95	1.00	-
Kaposi's sarcoma	0.22	0.002	0.001	0.004

Please refer to Figure 2.

that the amounts of the 16S rRNA gene were sufficient enough for further analysis. The median copy number of bacterial 16S rRNA gene varied across participants and collection sites, with significantly more copies in samples collected from the forehead compared to the right forearm ($p = 0.003$), left forearm ($p < 0.001$) or back ($p < 0.001$) (Figure 2 and Table 1). This variation could be explained by the frequency of exposure to the external environment (especially for the forehead) or physiological differences across sampled skin types: such as moisture or oiliness, that could harbor groups or quantity of distinct microbes (20).

The skin microbiota can provide colonization resistance, hindering pathogenic microbes from colonizing the skin, by competing for space or metabolites and by creating a hostile environment (1,20,21). Dysbiosis in the skin could disrupt colonization resistance and introduce a niche for pathogenic microbes to thrive. Whether the dysbiosis in skin microbiota leads to worsened skin disorders or vice versa is unknown; and a longitudinal study would be necessary to provide an answer. A simple method for sample collection and processing is crucial to conduct longitudinal studies in resource-limited countries; and our study showed that sufficient quantity

and quality of bacterial 16S rRNA gene for downstream applications can be collected using a non-invasive swab method.

We conclude that skin sampling with pre-moistened cotton is the valid method for collecting skin surface bacterial samples both in healthy people and those with skin disorders in resource-limiting situation such as in developing countries.

Acknowledgements

We thank the staff of the Efulan district hospital for their collaboration and support, especially Dr Akame, the HIV clinic coordinator. We also thank the researchers and laboratory staff at the Biotechnology Centre, University of Yaoundé I, Cameroon, for processing and archiving the samples, and Ms. Ayaka Matsuoka for archiving samples, creating sample inventory, running gel electrophoresis and qPCR. Thanks to Dr. Ivo Sah Bandar and Eva ML for proofreading the manuscript. We appreciate all the participants of this study for their time and contribution. This research was supported by grants: International Research Training Program, National Institute on Minority Health and Health Disparities (T37MD008636); Global Infectious Disease Research Training, Fogarty International Center, National Institutes of Health (NIH) (D43TW009074); Centers of Biomedical Research Excellence, National Institute of General Medical Sciences, NIH (P30GM114737); National Institute of Allergy and Infectious Diseases, NIH (1R21 AI105286); Japan Society for the Promotion of Science Kakenhi (17H04428); and Kanazawa University Sakigake Project. YML's travels were supported by the Career Development Award from the American Association of University Women Hawaii Branch. KO's travel and accommodation expenses were supported in part by the Overseas Research Support for Young Scientists in Kanazawa University.

References

1. Belkaid Y, Segre JA. Dialogue between skin microbiota and immunity. *Science*. 2014; 346:954-959.
2. Belkaid Y, Tamoutounour S. The influence of skin microorganisms on cutaneous immunity. *Nat Rev Immunol*. 2016; 16:353-366.
3. Grice EA. The skin microbiome: potential for novel diagnostic and therapeutic approaches to cutaneous disease. *Semin Cutan Med Surg*. 2014; 33:98-103.
4. Bjerre RD, Bandier J, Skov L, Engstrand L, Johansen JD. The role of the skin microbiome in atopic dermatitis: a systematic review. *Br J Dermatol*. 2017; 177:1272-1278.
5. Langan EA, Griffiths CEM, Solbach W, Knobloch JK, Zillikens D, Thaci D. The role of the microbiome in psoriasis: moving from disease description to treatment selection? *Br J Dermatol*. 2018; 178:1020-1027.
6. Tanaka A, Cho O, Saito C, Saito M, Tsuboi R, Sugita T. Comprehensive pyrosequencing analysis of the bacterial microbiota of the skin of patients with seborrheic dermatitis. *Microbiol Immunol*. 2016; 60:521-526.
7. Fitz-Gibbon S, Tomida S, Chiu BH, *et al*. *Propionibacterium acnes* strain populations in the human skin microbiome associated with acne. *J Invest Dermatol*. 2013; 133:2152-2160.
8. Silva PE, Costa PS, Avila MP, Suhadolnik ML, Reis MP, Salgado AP, Lima MF, Chartone-Souza E, Nascimento AM. Leprous lesion presents enrichment of opportunistic pathogenic bacteria. *Springerplus*. 2015; 4:187.
9. Silva PES, Reis MP, Avila MP, Dias MF, Costa PS, Suhadolnik MLS, Kunzmann BG, Carmo AO, Kalapotakis E, Chartone-Souza E, Nascimento AMA. Insights into the skin microbiome dynamics of leprosy patients during multi-drug therapy and in healthy individuals from Brazil. *Sci Rep*. 2018; 8:8783.
10. Gimblet C, Meisel JS, Loesche MA, Cole SD, Horwinski J, Novais FO, Mistic AM, Bradley CW, Beiting DP, Rankin SC, Carvalho LP, Carvalho EM, Scott P, Grice EA. Cutaneous leishmaniasis induces a transmissible dysbiotic skin microbiota that promotes skin inflammation. *Cell Host Microbe*. 2017; 22:13-24.e14.
11. Salter SJ, Cox MJ, Turek EM, Calus ST, Cookson WO, Moffatt MF, Turner P, Parkhill J, Loman NJ, Walker AW. Reagent and laboratory contamination can critically impact sequence-based microbiome analyses. *BMC Biol*. 2014; 12:87.
12. Human Microbiome Project Consortium. A framework for human microbiome research. *Nature*. 2012; 486:215-221.
13. Kong HH, Andersson B, Clavel T, Common JE, Jackson SA, Olson ND, Segre JA, Traidl-Hoffmann C. Performing skin microbiome research: a method to the madness. *J Invest Dermatol*. 2017; 137:561-568.
14. Ngwarai MR, Ah Tow LE, Nicol MP, Kaba M. The human microbiome research in Africa – A systematic review. *Int J Infect Dis*. 2016; 45:143.
15. Warnke P, Warning L, Podbielski A. Some are more equal--a comparative study on swab uptake and release of bacterial suspensions. *PLoS One*. 2014; 9:e102215.
16. Grice EA, Kong HH, Conlan S, Deming CB, Davis J, Young AC, Program NCS, Bouffard GG, Blakesley RW, Murray PR, Green ED, Turner ML, Segre JA. Topographical and temporal diversity of the human skin microbiome. *Science*. 2009; 324:1190-1192.
17. Capone KA, Dowd SE, Stamatias GN, Nikolovski J. Diversity of the human skin microbiome early in life. *J Invest Dermatol*. 2011; 131:2026-2032.
18. Ogai K, Nagase S, Mukai K, Iuchi T, Mori Y, Matsue M, Sugitani K, Sugama J, Okamoto S. A comparison of techniques for collecting skin microbiome samples: swabbing versus tape-stripping. *Front Microbiol*. 2018; 9:2362.
19. Grice EA, Kong HH, Renaud G, Young AC, Program NCS, Bouffard GG, Blakesley RW, Wolfsberg TG, Turner ML, Segre JA. A diversity profile of the human skin microbiota. *Genome Res*. 2008; 18:1043-1050.
20. Grice EA, Segre JA. The skin microbiome. *Nat Rev Microbiol*. 2011; 9:244-253.
21. Sanford JA, Gallo RL. Functions of the skin microbiota in health and disease. *Semin Immunol*. 2013; 25:370-377.

(Received October 4, 2019; Revised December 19, 2019; Accepted December 21, 2019)

"4+7" city drug volume-based purchasing and using pilot program in China and its impact

Mi Tang^{1,§}, Jiangjiang He^{1,2,§}, Minxing Chen¹, Lixuan Cong¹, Yuan Xu¹, Yan Yang¹, Zhiying Hou¹, Peipei Song³, Chunlin Jin^{1,*}

¹Shanghai Health Development Research Center, Shanghai Medical Information Center, Shanghai, China;

²School of Public Health, Fudan University, Shanghai, China;

³The Institute for Global Health Policy Research, Bureau of International Health Cooperation, National Center for Global Health and Medicine, Tokyo, Japan.

Summary

In order to deepen the health system reform and improve the mechanism for the formation of drug prices, in January 2019, the General Office of the State Council of the People's Republic of China issued the "National centralized drug purchasing and using pilot program", selected 11 cities in mainland China to carry out "4+7" city drug volume based purchasing pilot work. This paper introduces the specific implementation plan, organizational structure and drug selection process of China's "4+7" city drug volume-based purchasing pilot work, and expounds the initial effects, existing problems and policy development after the implementation of the policy. After the implementation of the policy, the prices of 25 selected drugs were significantly lower, compared with the minimum purchase price of the same drugs in 11 pilot cities in 2017, the average drop was 52%. After the pilot scope was extended to the nation, compared with the minimum purchase price of the Union in 2018, the proposed price of the 25 drugs have an average price drop of 59%, compared with the selected price of the "4+7" pilot cities, the average price drop was 25%, and the price of drugs dropped further. By the end of August 2019, the implementation progress of 25 selected drugs in the "4+7" city drug volume-based purchasing was better than expected, the burden of patients' drug expenses was reduced, and the pilot work was beginning to bear fruit. The long-term influence and effect of the "4+7" city drug volume-based purchasing and policy implementation after the expansion needs to be further observed.

Keywords: Volume-based purchasing, centralized drug purchasing, pilot program

In recent years, China's total investment in health expenditures has basically increased linearly, increasing at a faster growth rate year by year (1). From 2008 to 2017, China's total health expenditures rose from 1453.54 billion yuan to 5259.83 billion yuan. The average annual compound growth rate is 13.51% (2). According to comparable prices, compared with 2016, China's total health expenditure in 2017 increased by 9.03%, higher than the GDP growth rate (6.86%) (3).

The total drug expenditure in China is also showing a growing trend. The drug expenditure for outpatients, hospitalizations and retail sales is increasing year by year. The proportion of drug expenditure to total health expenditure is still high (3), higher than the international level, and high drug price is one of the important reasons. At present, many problems still exist in the field of drug circulation in China, such as the obvious distortion of interests in the drug circulation, complicated circulation of drugs, disordered order, imperfect drug purchasing mechanisms, and the degree of marketization is not high and so on (4), all of which contribute to the high price of drugs. The burden of medicines for patients is heavier, and the problem of "expensive medical treatment" still exists.

In order to deepen the health system reform and

[§]These authors contributed equally to this work.

*Address correspondence to:

Dr. Chunlin Jin, Shanghai Health Development Research Center (Shanghai Medical Information Center), Room 807, No.1477, Beijing (W) Road, Jing'an District, Shanghai 200040, China.

E-mail: jinchunlin@shdrc.org

improve the mechanism for the formation of drug prices, in January 2019, the General Office of the State Council of the People's Republic of China issued the "National centralized drug purchasing and using pilot program" (hereinafter referred to as the "Program"), selected 11 cities (include 4 municipalities: Beijing, Tianjin, Shanghai, and Chongqing; 7 key cities: Shenyang, Dalian, Xiamen, Guangzhou, Shenzhen, Chengdu, and Xi'an) in mainland China to carry out "4+7" city drug volume-based purchasing pilot work (5). The so-called drug volume-based purchasing refers to clarify the purchase volume when the purchaser conducts bidding or negotiation in the drug centralized purchasing process, and the drug supply enterprise bids or negotiates through the centralized purchasing platform for the specific quantity, and finally determines the purchase price (6). The significance is to determine the contractual relationship between price and volume. The higher the dosage, the lower the price (7), to achieve "volume-price linkage", "volume-for-price", and "price-based volume".

The basic idea of the "Program" is that the national level formulates basic policies, scope and requirements, and organizes 11 pilot cities to form a purchasing alliance. The public medical institutions in the alliance area are the main purchasing entities, and estimate the total purchase amount according to 60-70% of the total annual drug use of all public medical institutions in the league, and conduct a cross-regional alliance mechanism for drug volume-based purchasing. The pilot work is mainly carried out by the pilot working group and the joint purchasing office. The Shanghai Pharmaceutical Centralized Bidding and Purchasing Management Office undertakes the daily work of the Joint Purchasing Office and is responsible for the specific implementation. The organizational framework for its work is shown in Figure 1.

The drug volume-based purchasing in "4+7" city

are selected from the varieties with large sales volume in the fields of cardiovascular, anti-tumor, antibiotics, and psychology. The drug needs to be the original drug, the generic drug, which passes the evaluation of the consistency of quality and efficacy by the State Drug Administration, or the corresponding reference preparation (8). The drugs of volume-based purchasing will be declared by the enterprise first, and the selected varieties will be determined after pre-selection and quasi-selection. The process is shown in Figure 2. Adopting respective bidding purchasing, bargaining purchasing and negotiation purchasing methods according to the number of production enterprises of each pre-selected drug, a total of 25 drugs were selected, of which 22 (88%) were generic drugs, and 3 (12%) were original drugs. Only one company is selected for each variety, and the purchasing cycle is 12 months (9). If the agreed purchase amount is completed ahead of the purchasing cycle, the excess will still be purchased at the selected price until the purchase cycle expires.

The direct implementation impact of the "Program" is to achieve a significant reduction in drug prices. Compared with the minimum purchase price of the same drug in 11 pilot cities in 2017, the average price drop of 25 proposed selected drugs was 52%, with a maximum drop of 96%. Among them, the price reduction of imported original drug gefitinib and fusinopril were respectively 76% and 68%, and price reduction of domestic original drug flurbiprofen ester injection was 44%. The effect of "volume-for-price" has been revealed. The sharp drop in drug prices has driven the price linkage of non-selected drugs, further amplifying the price reduction effect, reducing the burden of medication for patients, and effectively alleviating the problem of expensive medical treatment. The "4+7" pilot city's joint volume-based purchasing model clarifies the price of drugs and

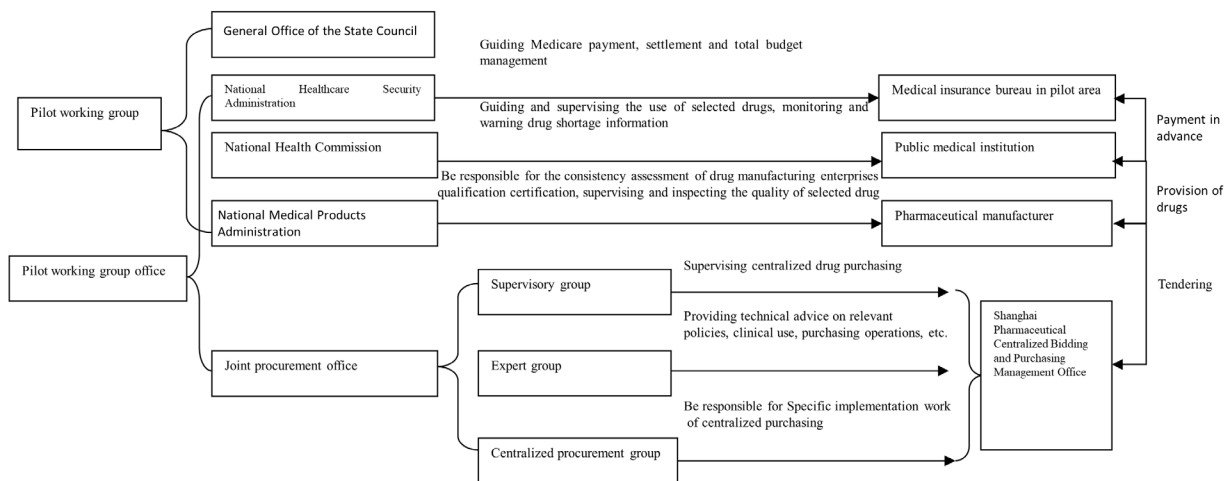


Figure 1. Organizational framework of "4+7" city drug volume-based purchasing and using pilot program.

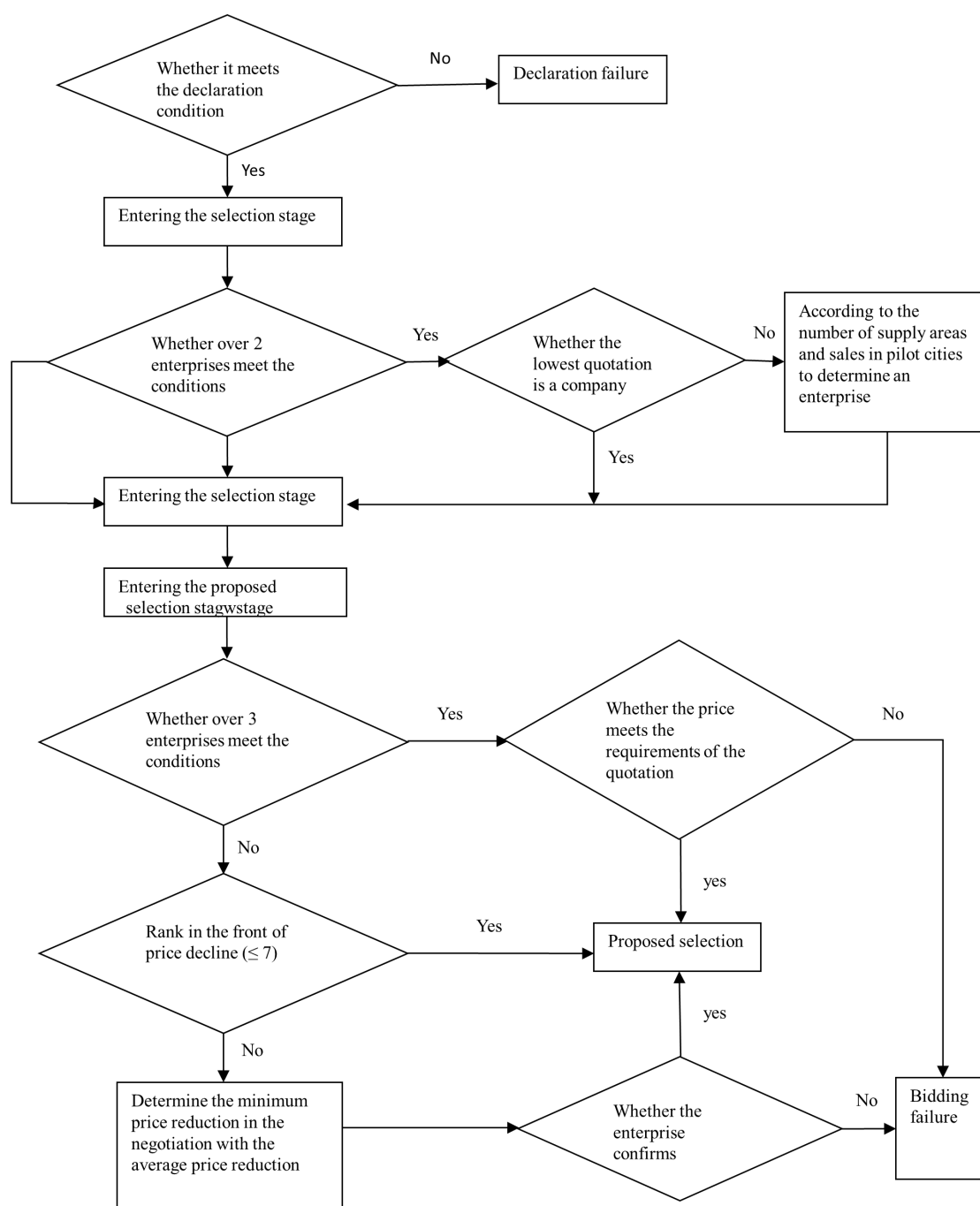


Figure 2. Selection flow chart of "4+7" city drug volume-based purchasing.

specific purchase quantity. The agreement changes the drug circulation model, cuts off the interest chain of drug circulation (10), regulates distribution behavior and purchasing behavior, and also simultaneously reduces the sales and transaction cost of the company (11). In addition, the reduction of drug prices also contributes to the achievement of the control fee index in hospital management. At the same time, the "volume-price linkage" has positive significance for the ethos construction of medical personnel. The medical insurance department also needs to realize change through volume-based purchasing and use limited

resources on a more valuable level.

There are also some potential risks and disputes in the implementation of the "Program": In terms of drug supply security, the selected drugs take the form of a "single source" supply method. It is not only easy to frustrate the enthusiasm of the unsuccessful enterprise to improve the quality and consistency of efficacy in the early stage of the trial. There is also the risk of supply shortages (7). In the clinical use of drugs, in order to implement the use of selected drugs, the use of non-selected drugs is limited, and to a certain extent, it also limits the doctor's prescription rights and

patients' drug choice. Upon drug quality, there is still a lack of authoritative data such as adverse reaction reports and defect reports related to the quality of the selected drugs. Clinicians and patients have doubts about the quality of the selected drugs at a low price. Due to the drug prices in the pilot areas, which are significantly lower than those in other areas, this forms a "price depression effect". Non-pilot patients go to the pilot areas to see doctors and buy drugs themselves, which interferes with the medical circulation order and increases the burden on patients.

In September 2019, in order to expand the "4+7" city drug volume-based purchasing pilot reform effect, based on the valuable experience accumulated in the previous pilot work, under the guidance of the China National Healthcare Security Administration and other departments, 25 provinces in mainland China and the Xinjiang Production and Construction Corps formed a new cross-regional purchasing alliance to purchase twenty five "4+7" pilot drugs, except for the "4+7" pilot city, Fujian Province, and Hebei Province that have previously been followed up. All 25 varieties were purchased successfully in this alliance purchase, 45 enterprises and 60 products are to be selected. Compared with the lowest purchase price in 2018 in the alliance area, the average decline of selected prices is 59%. Compared with the selected price of the "4+7" pilot city, the average decline is 25% (12). The expansion of the national drug centralized purchasing pilot not only promoted the policy nationwide, but also joined the military medical institutions participating in the pilot expansion of the regional scope and medical insurance designated social medical institutions, medical insurance designated retail pharmacies volunteering to participate in the pilot expansion of the regional scope. It also solved the problem of large price gap of pilot drugs in the "4+7" pilot city and other related regions, and also made the reform results benefit more people (13). In addition, the expansion has improved and adjusted the selection rules on the number of enterprises and the quotation level based on previous pilot experience, many enterprises can be allowed to win the bid. The bid price of different enterprises can be different to guide the enterprises to compete in an orderly manner. The increase in the number of selected enterprises also avoids the risk of supply shortage and monopoly of the exclusive winning bid, and guarantees the long-term stable implementation of the national drug centralized bidding purchasing policy (14).

The 25 drugs selected by "4+7" volume-based purchasing were fully implemented on April 1, 2019. As of the end of August, the purchase quantity of 25 selected drugs in the "4+7" area was 1.7 billion tablets. The progress of total purchase quantity exceeded expectations, and the purchase quantity of selected drugs accounted for 78% in the same generic name drugs (15). The pilot work achieved initial results. In

September 2019, China expanded the scope of pilot and the price of 25 drugs was decreased further. Nine central departments such as China National Healthcare Security Administration issued a document to guide the development of related work (13). In the next step, all localities and departments will focus on the implementation of the selected results, to ensure that patients gain high quality and low price for selected varieties before the end of the year and effectively reduce the drug burden of patients (12).

References

1. Ma Xinmei. Analysis of health expenditure input in recent ten years in China. *Jing Ji Shi*. 2018; 4:236-237. (in Chinese)
2. National Health Commission. *China Health Statistics Yearbook (2018)* (National Health Commission, eds.). China Union Medical University Press, Beijing, China, 2018; p. 93. (in Chinese)
3. Guo F, Zhang YH, Wan Q, Zhai TM, Chai PP, Li Y, Wang RR, Huang YX, Chen CM, Li T. China total health expenditure accounting results and analysis in 2017. *Zhong Guo Wei Sheng Jing Ji*. 2019; 38:5-8. (in Chinese)
4. Yin X, Zhang YX, Mao ZF. Review on the Reform Policies of Drug Circulation in China-from the Perspective of Stakeholder Game. *Zhong Guo Wei Sheng Zheng Ce Yan Jiu*. 2017; 10:13-19. (in Chinese)
5. The General Office of the State Council. Notice of The General Office of the State Council on Issuing National Drug Centralized Purchasing and Using Pilot. http://www.gov.cn/zhengce/content/2019-01/17/content_5358604.htm (accessed August 25, 2019). (in Chinese)
6. Chen H, Rao YH. Practice and thinking on the drug volume based purchasing in the new era. *Zhong Guo Yao Wu Jing Ji Xue*. 2019; 14:9-26. (in Chinese)
7. Hu SL. The economics theoretical basis and impact analysis of volume based purchasing. *Wei Sheng Ruan Ke Xue*. 2019; 33:5-7. (in Chinese)
8. Shanghai Sunshine Pharmaceutical Purchasing Network. 4+7 City Drug Centralized Purchasing Documents. <http://www.yyzbsw.sh.cn/gjsdgc/2018/11/15/8511.shtml> (accessed August 25, 2019). (in Chinese)
9. Shanghai Sunshine Pharmaceutical Purchasing Network. Notice on the Publication of the Selected Results of the 4+7 City Drug Centralized Purchasing. <http://www.yyzbsw.sh.cn/gjsdgc/2018/12/17/8580.shtml> (accessed August 25, 2019). (in Chinese)
10. Shu Q, Yao ZR, Wang YZ, Wang DD. Stakeholder analysis of drug volume based purchasing policy. *Wei Sheng Jing Ji Yan Jiu*. 2019; 36:8-9+12. (in Chinese)
11. Li DS, Bai XS. Analysis on the general mechanism of reducing the price of volume based purchasing and "4+7 mode". *Wei Sheng Jing Ji Yan Jiu*. 2019; 36:10-12. (in Chinese)
12. Shanghai Sunshine Pharmaceutical Purchasing Network. Nationwide Expansion to Produce the Proposed Selected Results of National Drug Centralized Purchasing and Using Pilots. <http://www.smpaa.cn/gjsdgc/2019/09/24/9014.shtml> (accessed October 01, 2019). (in Chinese)

13. National Healthcare Security Administration, Ministry of Industry and Information Technology, Ministry of Finance, etc. Implementation Opinions of Nine Departments Such As The National Health Security Administration on Nationwide Expansion of Drug Purchasing and Using Pilots. http://www.nhsa.gov.cn/art/2019/9/30/art_37_1817.html (accessed October 01, 2019). (in Chinese)
 14. Shanghai Sunshine Pharmaceutical Purchasing Network. Drug Centralized Purchasing Documents in the Alliance Area. <http://www.smpaa.cn/gjsdgc/2019/09/01/8974.shtml> (accessed October 01, 2019). (in Chinese)
 15. Shanghai Sunshine Pharmaceutical Purchasing Network. Press Briefing on the Expansion of National Drug Centralized Purchasing Scope. <http://www.smpaa.cn/gjsdgc/2019/09/25/9016.shtml> (accessed October 01, 2019). (in Chinese)
- (Received October 22, 2019; Revised December 13, 2019; Accepted December 16, 2019)*

Guide for Authors

1. Scope of Articles

Drug Discoveries & Therapeutics welcomes contributions in all fields of pharmaceutical and therapeutic research such as medicinal chemistry, pharmacology, pharmaceutical analysis, pharmaceuticals, pharmaceutical administration, and experimental and clinical studies of effects, mechanisms, or uses of various treatments. Studies in drug-related fields such as biology, biochemistry, physiology, microbiology, and immunology are also within the scope of this journal.

2. Submission Types

Original Articles should be well-documented, novel, and significant to the field as a whole. An Original Article should be arranged into the following sections: Title page, Abstract, Introduction, Materials and Methods, Results, Discussion, Acknowledgments, and References. Original articles should not exceed 5,000 words in length (excluding references) and should be limited to a maximum of 50 references. Articles may contain a maximum of 10 figures and/or tables.

Brief Reports definitively documenting either experimental results or informative clinical observations will be considered for publication in this category. Brief Reports are not intended for publication of incomplete or preliminary findings. Brief Reports should not exceed 3,000 words in length (excluding references) and should be limited to a maximum of 4 figures and/or tables and 30 references. A Brief Report contains the same sections as an Original Article, but the Results and Discussion sections should be combined.

Reviews should present a full and up-to-date account of recent developments within an area of research. Normally, reviews should not exceed 8,000 words in length (excluding references) and should be limited to a maximum of 100 references. Mini reviews are also accepted.

Policy Forum articles discuss research and policy issues in areas related to life science such as public health, the medical care system, and social science and may address governmental issues at district, national, and international levels of discourse. Policy Forum articles should not exceed 2,000 words in length (excluding references).

Case Reports should be detailed reports of the symptoms, signs, diagnosis, treatment, and follow-up of an individual patient. Case reports may contain a demographic profile of the patient but usually describe an unusual or novel occurrence. Unreported or unusual side effects or adverse interactions involving medications will also be considered. Case

Reports should not exceed 3,000 words in length (excluding references).

News articles should report the latest events in health sciences and medical research from around the world. News should not exceed 500 words in length.

Letters should present considered opinions in response to articles published in Drug Discoveries & Therapeutics in the last 6 months or issues of general interest. Letters should not exceed 800 words in length and may contain a maximum of 10 references.

3. Editorial Policies

Ethics: Drug Discoveries & Therapeutics requires that authors of reports of investigations in humans or animals indicate that those studies were formally approved by a relevant ethics committee or review board.

Conflict of Interest: All authors are required to disclose any actual or potential conflict of interest including financial interests or relationships with other people or organizations that might raise questions of bias in the work reported. If no conflict of interest exists for each author, please state "There is no conflict of interest to disclose".

Submission Declaration: When a manuscript is considered for submission to Drug Discoveries & Therapeutics, the authors should confirm that 1) no part of this manuscript is currently under consideration for publication elsewhere; 2) this manuscript does not contain the same information in whole or in part as manuscripts that have been published, accepted, or are under review elsewhere, except in the form of an abstract, a letter to the editor, or part of a published lecture or academic thesis; 3) authorization for publication has been obtained from the authors' employer or institution; and 4) all contributing authors have agreed to submit this manuscript.

Cover Letter: The manuscript must be accompanied by a cover letter signed by the corresponding author on behalf of all authors. The letter should indicate the basic findings of the work and their significance. The letter should also include a statement affirming that all authors concur with the submission and that the material submitted for publication has not been published previously or is not under consideration for publication elsewhere. The cover letter should be submitted in PDF format. For example of Cover Letter, please visit <http://www.ddtjournal.com/downloadcentre.php> (Download Centre).

Copyright: A signed JOURNAL PUBLISHING AGREEMENT (JPA) must be provided by post, fax, or as a scanned file before acceptance of the article. Only forms with a hand-written signature are accepted. This copyright will ensure the widest possible dissemination of information. A form facilitating transfer of copyright can be downloaded by clicking the appropriate link and can be returned to the e-mail address or fax number noted on the form (Please visit

Download Centre). Please note that your manuscript will not proceed to the next step in publication until the JPA form is received. In addition, if excerpts from other copyrighted works are included, the author(s) must obtain written permission from the copyright owners and credit the source(s) in the article.

Suggested Reviewers: A list of up to 3 reviewers who are qualified to assess the scientific merit of the study is welcomed. Reviewer information including names, affiliations, addresses, and e-mail should be provided at the same time the manuscript is submitted online. Please do not suggest reviewers with known conflicts of interest, including participants or anyone with a stake in the proposed research; anyone from the same institution; former students, advisors, or research collaborators (within the last three years); or close personal contacts. Please note that the Editor-in-Chief may accept one or more of the proposed reviewers or may request a review by other qualified persons.

Language Editing: Manuscripts prepared by authors whose native language is not English should have their work proofread by a native English speaker before submission. If not, this might delay the publication of your manuscript in Drug Discoveries & Therapeutics.

The Editing Support Organization can provide English proofreading, Japanese-English translation, and Chinese-English translation services to authors who want to publish in Drug Discoveries & Therapeutics and need assistance before submitting a manuscript. Authors can visit this organization directly at <http://www.iacmhr.com/iac-eso/support.php?lang=en>. IAC-ESO was established to facilitate manuscript preparation by researchers whose native language is not English and to help edit works intended for international academic journals.

4. Manuscript Preparation

Manuscripts should be written in clear, grammatically correct English and submitted as a Microsoft Word file in a single-column format. Manuscripts must be paginated and typed in 12-point Times New Roman font with 24-point line spacing. Please do not embed figures in the text. Abbreviations should be used as little as possible and should be explained at first mention unless the term is a well-known abbreviation (e.g. DNA). Single words should not be abbreviated.

Title page: The title page must include 1) the title of the paper (Please note the title should be short, informative, and contain the major key words); 2) full name(s) and affiliation(s) of the author(s); 3) abbreviated names of the author(s); 4) full name, mailing address, telephone/fax numbers, and e-mail address of the corresponding author; and 5) conflicts of interest (if you have an actual or potential conflict of interest to disclose, it must be included as a footnote on the title page of the manuscript; if no conflict of interest exists for each author, please state "There is no conflict of interest to disclose"). Please visit [Download Centre](#) and refer to the title page of the manuscript sample.

Abstract: The abstract should briefly state the purpose of the study, methods, main findings, and conclusions. For article types including Original Article, Brief Report, Review, Policy Forum, and Case Report, a one-paragraph abstract consisting of no more than 250 words must be included in the manuscript. For News and Letters, a brief summary of main content in 150 words or fewer should be included in the manuscript. Abbreviations must be kept to a minimum and non-standard abbreviations explained in brackets at first mention. References should be avoided in the abstract. Key words or phrases that do not occur in the title should be included in the Abstract page.

Introduction: The introduction should be a concise statement of the basis for the study and its scientific context.

Materials and Methods: The description should be brief but with sufficient detail to enable others to reproduce the experiments. Procedures that have been published previously should not be described in detail but appropriate references should simply be cited. Only new and significant modifications of previously published procedures require complete description. Names of products and manufacturers with their locations (city and state/country) should be given and sources of animals and cell lines should always be indicated. All clinical investigations must have been conducted in accordance with Declaration of Helsinki principles. All human and animal studies must have been approved by the appropriate institutional review board(s) and a specific declaration of approval must be made within this section.

Results: The description of the experimental results should be succinct but in sufficient detail to allow the experiments to be analyzed and interpreted by an independent reader. If necessary, subheadings may be used for an orderly presentation. All figures and tables must be referred to in the text.

Discussion: The data should be interpreted concisely without repeating material already presented in the Results section. Speculation is permissible, but it must be well-founded, and discussion of the wider implications of the findings is encouraged. Conclusions derived from the study should be included in this section.

Acknowledgments: All funding sources should be credited in the Acknowledgments section. In addition, people who contributed to the work but who do not meet the criteria for authors should be listed along with their contributions.

References: References should be numbered in the order in which they appear in the text. Citing of unpublished results, personal communications, conference abstracts, and theses in the reference list is not recommended but these sources may be mentioned in the text. In the reference list, cite the names of all authors when there are fifteen or fewer authors; if there are sixteen or more authors, list the first three followed by *et al.* Names of journals should

be abbreviated in the style used in PubMed. Authors are responsible for the accuracy of the references. Examples are given below:

Example 1 (Sample journal reference):
Nakata M, Tang W. Japan-China Joint Medical Workshop on Drug Discoveries and Therapeutics 2008: The need of Asian pharmaceutical researchers' cooperation. *Drug Discov Ther.* 2008; 2:262-263.

Example 2 (Sample journal reference with more than 15 authors):
Darby S, Hill D, Auvinen A, *et al.* Radon in homes and risk of lung cancer: Collaborative analysis of individual data from 13 European case-control studies. *BMJ.* 2005; 330:223.

Example 3 (Sample book reference):
Shalev AY. Post-traumatic stress disorder: Diagnosis, history and life course. In: *Post-traumatic Stress Disorder, Diagnosis, Management and Treatment* (Nutt DJ, Davidson JR, Zohar J, eds.). Martin Dunitz, London, UK, 2000; pp. 1-15.

Example 4 (Sample web page reference):
World Health Organization. The World Health Report 2008 – primary health care: Now more than ever. http://www.who.int/whr/2008/whr08_en.pdf (accessed September 23, 2010).

Tables: All tables should be prepared in Microsoft Word or Excel and should be arranged at the end of the manuscript after the References section. Please note that tables should not in image format. All tables should have a concise title and should be numbered consecutively with Arabic numerals. If necessary, additional information should be given below the table.

Figure Legend: The figure legend should be typed on a separate page of the main manuscript and should include a short title and explanation. The legend should be concise but comprehensive and should be understood without referring to the text. Symbols used in figures must be explained.

Figure Preparation: All figures should be clear and cited in numerical order in the text. Figures must fit a one- or two-column format on the journal page: 8.3 cm (3.3 in.) wide for a single column, 17.3 cm (6.8 in.) wide for a double column; maximum height: 24.0 cm (9.5 in.). Please make sure that artwork files are in an acceptable format (TIFF or JPEG) at minimum resolution (600 dpi for illustrations, graphs, and annotated artwork, and 300 dpi for micrographs and photographs). Please provide all figures as separate files. Please note that low-resolution images are one of the leading causes of article resubmission and schedule delays. All color figures will be reproduced in full color in the online edition of the journal at no cost to authors.

Units and Symbols: Units and symbols conforming to the International System of Units (SI) should be used for physicochemical quantities. Solidus notation (*e.g.* mg/kg, mg/mL, mol/mm²/min) should be used. Please refer to the SI Guide www.bipm.org/en/si/ for standard units.

Supplemental data: Supplemental data might be useful for supporting and enhancing your scientific research and Drug Discoveries & Therapeutics accepts the submission of these materials which will be only published online alongside the electronic version of your article. Supplemental files (figures, tables, and other text materials) should be prepared according to the above guidelines, numbered in Arabic numerals (*e.g.*, Figure S1, Figure S2, and Table S1, Table S2) and referred to in the text. All figures and tables should have titles and legends. All figure legends, tables and supplemental text materials should be placed at the end of the paper. Please note all of these supplemental data should be provided at the time of initial submission and note that the editors reserve the right to limit the size and length of Supplemental Data.

5. Submission Checklist

The Submission Checklist will be useful during the final checking of a manuscript prior to sending it to Drug Discoveries & Therapeutics for review. Please visit [Download Centre](#) and download the Submission Checklist file.

6. Online submission

Manuscripts should be submitted to Drug Discoveries & Therapeutics online at <http://www.ddtjournal.com>. The manuscript file should be smaller than 5 MB in size. If for any reason you are unable to submit a file online, please contact the Editorial Office by e-mail at office@ddtjournal.com

7. Accepted manuscripts

Proofs: Galley proofs in PDF format will be sent to the corresponding author *via* e-mail. Corrections must be returned to the editor (proof-editing@ddtjournal.com) within 3 working days.

Offprints: Authors will be provided with electronic offprints of their article. Paper offprints can be ordered at prices quoted on the order form that accompanies the proofs.

Page Charge: A page charge of \$140 will be assessed for each printed page of an accepted manuscript. The charge for printing color figures is \$340 for each page. Under exceptional circumstances, the author(s) may apply to the editorial office for a waiver of the publication charges at the time of submission.

(Revised February 2013)

Editorial and Head Office:

Pearl City Koishikawa 603
2-4-5 Kasuga, Bunkyo-ku
Tokyo 112-0003
Japan
Tel: +81-3-5840-9697
Fax: +81-3-5840-9698
E-mail: office@ddtjournal.com

JOURNAL PUBLISHING AGREEMENT (JPA)

Manuscript No.:

Title:

Corresponding author:

The International Advancement Center for Medicine & Health Research Co., Ltd. (IACMHR Co., Ltd.) is pleased to accept the above article for publication in Drug Discoveries & Therapeutics. The International Research and Cooperation Association for Bio & Socio-Sciences Advancement (IRCA-BSSA) reserves all rights to the published article. Your written acceptance of this JOURNAL PUBLISHING AGREEMENT is required before the article can be published. Please read this form carefully and sign it if you agree to its terms. The signed JOURNAL PUBLISHING AGREEMENT should be sent to the Drug Discoveries & Therapeutics office (Pearl City Koishikawa 603, 2-4-5 Kasuga, Bunkyo-ku, Tokyo 112-0003, Japan; E-mail: office@ddtjournal.com; Tel: +81-3-5840-9697; Fax: +81-3-5840-9698).

1. Authorship Criteria

As the corresponding author, I certify on behalf of all of the authors that:

- 1) The article is an original work and does not involve fraud, fabrication, or plagiarism.
- 2) The article has not been published previously and is not currently under consideration for publication elsewhere. If accepted by Drug Discoveries & Therapeutics, the article will not be submitted for publication to any other journal.
- 3) The article contains no libelous or other unlawful statements and does not contain any materials that infringes upon individual privacy or proprietary rights or any statutory copyright.
- 4) I have obtained written permission from copyright owners for any excerpts from copyrighted works that are included and have credited the sources in my article.
- 5) All authors have made significant contributions to the study including the conception and design of this work, the analysis of the data, and the writing of the manuscript.
- 6) All authors have reviewed this manuscript and take responsibility for its content and approve its publication.
- 7) I have informed all of the authors of the terms of this publishing agreement and I am signing on their behalf as their agent.

2. Copyright Transfer Agreement

I hereby assign and transfer to IACMHR Co., Ltd. all exclusive rights of copyright ownership to the above work in the journal Drug Discoveries & Therapeutics, including but not limited to the right 1) to publish, republish, derivate, distribute, transmit, sell, and otherwise use the work and other related material worldwide, in whole or in part, in all languages, in electronic, printed, or any other forms of media now known or hereafter developed and the right 2) to authorize or license third parties to do any of the above.

I understand that these exclusive rights will become the property of IACMHR Co., Ltd., from the date the article is accepted for publication in the journal Drug Discoveries & Therapeutics. I also understand that IACMHR Co., Ltd. as a copyright owner has sole authority to license and permit reproductions of the article.

I understand that except for copyright, other proprietary rights related to the Work (e.g. patent or other rights to any process or procedure) shall be retained by the authors. To reproduce any text, figures, tables, or illustrations from this Work in future works of their own, the authors must obtain written permission from IACMHR Co., Ltd.; such permission cannot be unreasonably withheld by IACMHR Co., Ltd.

3. Conflict of Interest Disclosure

I confirm that all funding sources supporting the work and all institutions or people who contributed to the work but who do not meet the criteria for authors are acknowledged. I also confirm that all commercial affiliations, stock ownership, equity interests, or patent-licensing arrangements that could be considered to pose a financial conflict of interest in connection with the article have been disclosed.

Corresponding Author's Name (Signature):

Date:

